UCSF
UC San Francisco Electronic Theses and Dissertations

Title
Enhancement of transdermal drug delivery

Permalink
https://escholarship.org/uc/item/6kg697g1

Author
Bommannan, D.,

Publication Date
1990

Peer reviewed|Thesis/dissertation

eScholarship.org Powered by the California Digital Library
University of California

ENHANCEMENT OF TRANSDERMAL DRUG DELIVERY: MECHANISMS AND METHODOLOGIES

by

D. BOMMANNAN

DISSERTATION

Submitted in partial satisfaction of the requirements for the degree of

DOCTOR OF PHILOSOPHY

in

BIOENGINEERING

in the

GRADUATE DIVISION

of the

UNIVERSITY OF CALIFORNIA

San Francisco

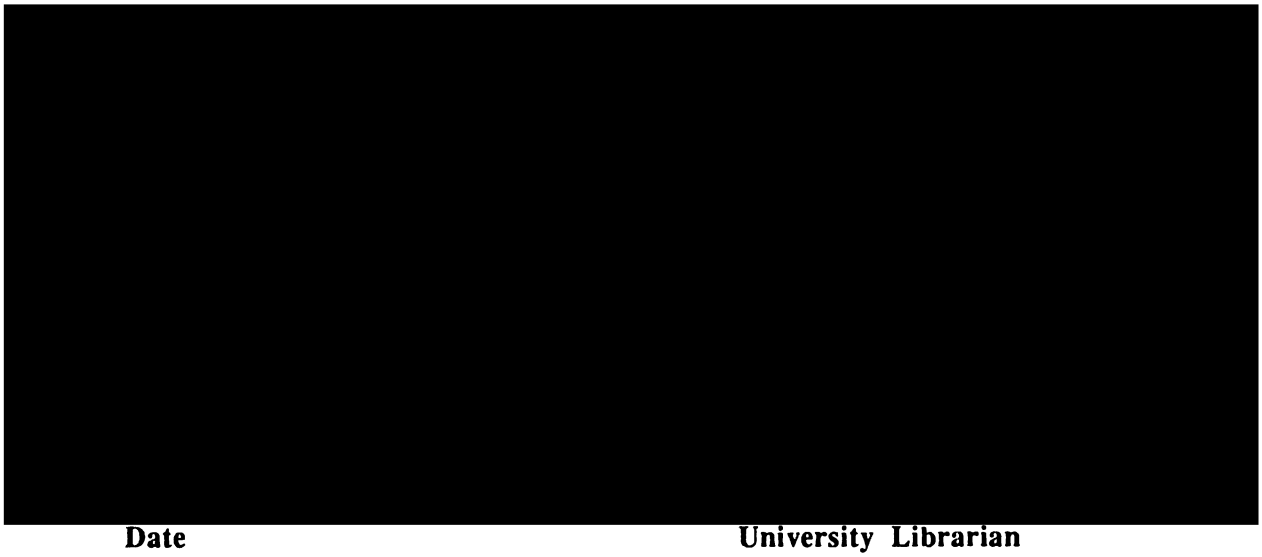

Date **University Librarian**

Degree Conferred: 12/31/90

Copyright (1990)

by

D. Bommannan

TO ALL MY FRIENDS, WHO HAVE MADE LIFE ENJOYABLE

Acknowledgements

I would like to express my gratitude to the following people:

Dr. Richard H. Guy, for being my thesis advisor and teaching me the tricks of the trade. While an ideal advisor may never exist, Richard comes close.

Dr. Ronald A. Siegel, for helping me retain my engineering roots and overseeing that I become a bioengineer. Thanks for the many stimulating discussions as well, Ron.

Dr. Robert S. Hinz, who made my stay in the lab truly enjoyable. Bob had the patience (which he has in abundance) to listen to my rambling about sundry things.

Dr. Russell O. Potts, for acting as my unofficial co-advisor and his help in various ways.

Hirohisa Okuyama, for collaborating with me on the sonophoresis project. Many thanks to Hirosan for recording those nocturnal readings.

Dr. Gopi Menon, for introducing me to the excitement and frustrations of electron microscopy.

Dr. Paul Stauffer, for his generosity with his time and equipment and for his commitment to the sonophoresis project.

Dr. Vivien Mak, for introducing me to the vagaries of the FTIR machine.

I also would like to express my appreciation to the people whom I came to know as part of the "Guy group": Dan Bucks, Chris Cullander, Carol Gay, Phil Green, Naruhito Higo, Jurij Hostynek, Connie Hodson, Vicki Knepp, Cynthia Lorence, Aarti Naik, Vikram Ramanathan, Girish Rao, Geoff Ridout, and Mathew Wang. I learnt something from each one of these people.

During my stay, I have enjoyed the company of fellow bioengineers, particularly, Pam deMoor, Murali Ramanathan and Tracy Wonnell.

The Department of Pharmacy was my second home, and I thank all those who made my second home a thoroughly enjoyable place for me.

I express my gratitude to the Schaevitz family for providing me the much needed (and much appreciated) home atmosphere.

Thanks to the many friends I have made during my stay here; they have made San Francisco unforgettable.

I would like to express my love and appreciation to my sisters, Radha and Aruna, and also for putting up with me!! I also express my thanks to my aunt, Prabha Raghavan, for influencing my early years. Finally, I am most grateful to my parents, for without them I doubt if I will be what I am.

The text of Chapter 3a is a reprint of the material as it appears in the Journal of Investigative Dermatology (1990) **95,** 403-408. Permission to reprint this material was granted by Elsevier Science Publishing Company, Inc. The co-authors listed in this publication directed and supervised the research which forms the basis for part of this dissertation.

ENHANCEMENT OF TRANSDERMAL DRUG DELIVERY: MECHANISMS AND METHODOLOGIES

by

D. Bommannan

ABSTRACT

Although methods to enhance transdermal drug delivery (TDD) are being increasingly studied, the mechanisms of action remain unclear. The first part of this thesis describes the application of Fourier Transform Infrared Spectroscopy (FTIR) (1) to examine the intercellular lipids of the stratum corneum (SC), which is generally accepted as the functional component of skin's barrier function, and (2) to study the effects of ethanol, a putative enhancer, on this lipid domain. Using adhesive tape-stripping and attenuated total reflectance (ATR)-FTIR *in vivo* in human volunteers, it was found that (a) per unit volume, the intercellular lipids are more abundant nearer to the surface than deeper within the SC, (b) the lipids are more disordered in the superficial SC layers than in those closer to the stratum granulosum (SG), and (c) SC hydration increases from the surface toward the SC-SG interface. In exploring the mechanism(s) underlying ethanol-induced enhancement of TDD in humans *in vivo* , it was discovered that pure ethanol (a) induced a transient increase in the order of SC intercellular lipids near the skin surface, and (b) extracted appreciable amounts of lipid from the SC. These findings contradict the suggestion that ethanol "disorders" the intercellular lipid bilayers of the SC. Furthermore, the changes induced by the short-term exposure of the skin to ethanol are reversed within 24 hours.

The second part of this thesis examines the use of ultrasound to enhance TDD (so-called sonophoresis). An analysis of the physics of ultrasound propagation in tissue, coupled with existing knowledge of the barrier properties of skin, suggested that high frequency ultrasound could produce effective sonophoresis. We tested this hypothesis *in vivo* using hairless guinea pigs, by comparing the passive TDD of salicylic acid with that under the influence of ultrasound at frequencies of 2, 10 and 16 MHz frequency.

While sonophoresis for 20 minutes at 2 MHz did not increase salicylic acid delivery compared to passive diffusion, ultrasound application at 10 and 16 MHz significantly elevated salicylic acid transport (by 4-fold and 2.5-fold respectively). The urinary elimination kinetics of the drug suggested, furthermore, that the diffusional lag-time associated with TDD was reduced. A shorter period (5 minutes) of sonophoresis also resulted in enhanced TDD (relative to the corresponding control) at the higher frequencies. To probe the mechanism of sonophoresis, the permeation of an electron dense tracer, lanthanum nitrate (LN), was mapped by electron microscopy (EM). Concurrently, we were also able to use EM to study the effect of ultrasound on skin morphology. The electron micrographs revealed that sonophoresis for 5 minutes, at a frequency of 10 or 16 MHz, delivers the tracer through the epidermis into the dermis, a remarkable achievement. The penetration pathway of the tracer appears to be intercellular. Longer exposure of the skin to high frequency ultrasound (20 minutes, 16 MHz) resulted in significant alterations within the cells of the stratum granulosum and stratum basale. The reversibility of these effects, and the long-term potential of sonophoresis, (and of penetration enhancement strategies, in general), warrant further investigation.

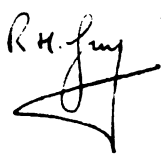

Table of Contents

	Page
Acknowledgements	iv
Abstract	vi
1. Transdermal Drug Delivery	1
1.1 Barrier Properties of Skin	3
1.2 Skin Structure	3
1.2.1 Epidermis	4
1.2.2 Stratum Corneum (SC)	4
1.2.3 Dermis	5
1.3 Enhancement Methods.	5
1.3.1 Chemical Enhancers.	6
1.3.2 Iontophoresis	7
1.3.3 Sonophoresis	8
1.4 Mechanisms of Percutaneous Absorption . . .	9
1.4.1 Evidence that the SC is the Rate Limiting Barrier .	9
1.4.2 Penetration Pathways Across the SC . . .	9
1.5 Conclusion	14
2. Infrared Spectroscopy	31
2.1 Theoretical Aspects of IR Spectroscopy. . . .	31
2.2 Biomembrane Spectroscopy	34
2.2.1 Attenuated Total Reflection (ATR) IR Spectroscopy .	35
2.3 Infrared Absorbances of Typical Biomolecules . .	36
2.3.1 Methylene Group Vibrations	36
2.3.2 Amide Group Vibrations	37
2.4 Phase Transition and Permeability Studies Using Infrared Spectroscopy	37
2.4.1 Frequency Shifts	38
2.4.2 Half-bandwidth Changes	38
2.4.3 Permeability Changes	39
2.5 IR Spectroscopy of Skin	39
3a. Examination of Stratum Corneum Barrier Function *in vivo* by Infrared Spectroscopy	50

Abstract 51
Materials and Methods 52
Attenuated Total Reflectance-Fourier Transform Infrared Spectroscopy (ATR-FTIR) 52
Experiments 52
Spectral Analyis 52
Statistical Analysis 53
Results 53
Discussion 54

3b. Examination of the Effect of Ethanol on Human Stratum Corneum *in vivo* Using Infrared Spectroscopy 57
Abstract 58
Introduction 59
Experimental 60
1. Attenuated total reflectance infrared spectroscopy (ATR-IR) 60
2. Methodology 60
3. Spectral Analysis 61
Results and Discussion 62

4. Physics of Ultrasound 75
4.1 Introduction 75
4.2 Linear Acoustics 76
4.2.1 Traveling Plane Wave in a Lossless Medium . . 76
4.3 Non-linear Acoustics 77
4.3.1 Non-linear Intensity 78
4.3.2 Radiation Force 79
4.3.2.1 Radiation Force Measurements . . . 79
4.3.3 Acoustic Streaming 80
4.3.4 Cavitation 81
4.4 Generation and Propagation of Ultrasound . . . 81
4.4.1 Transducers for Generating Ultrasound . . 81
4.4.2 Propagation of Ultrasound 82
4.4.2.1 Attenuation 83
4.5 Effects of Ultrasound 84
4.5.1 Thermal Effects 84

4.5.1.1 Transient Heat Flow 86
4.5.1.2 Steady-state Heat Flow 87
4.5.2 Mechanical and Cavitational Effects (Non-thermal Effects) 87
4.6 Conclusion 90

5. Sonophoresis: I. The Use of Ultrasound to Enhance Transdermal Drug Delivery 99
5.1 Introduction 99
5.2 Materials and Methods 102
5.2.1 Tape-stripping and Urinary Excretion . . . 103
5.2.2 Urinary Excretion 104
5.2.3 Pre-treatment Experiments 104
5.2.4 Skin Temperature Measurements . . . 105
5.2.5 Data Analysis 105
5.3 Results 105
5.4 Discussion 107
5.5 Conclusions 112

6. Sonophoresis: II. Examination of the Mechanism(s) . . 129
6.1 Ultrasound Effects on Skin 129
6.2 Thermal and Non-thermal Effects of Sonophoresis . . 129
6.3 Methods 131
6.3.1 Release Experiments 131
6.3.2 Electron Microscopy 132
6.4 Results 133
6.4.1 Effect of Ultrasound on Drug Release from the Gel . 133
6.4.2 EM Observations 133
6.4.2.1 Controls 133
6.4.2.2 Ultrasound-exposed Skin 133
6.5 Discussion 134
6.6 Conclusions 136

List of Tables

		Page
Table 1.1	Permeability Coefficients of Water and Methanol Through Biomembranes	15
Table 1.2	Estimated Transdermal Patch Size for Various Drugs	16
Table 1.3	Examples of Percutaneous Penetration Enhancement by Various Chemicals	17
Table 2.1	Infrared Band Assignments for Stratum Corneum Constituents	43
Table 4.1	Acoustic Quantities	91

List of Figures

		Page
Chapter 1		
Figure 1.1	Schematic of Drug Conentration Profile in Blood Using Different Delivery Modes	26
Figure 1.2	Schematic Cross Section of the Skin	27
Figure 1.3	Schematic of the SC	28
Figure 1.4	The Sequential Steps Involved in Transdermal Absorption	29
Figure 1.5	Putative Penetration Pathways Across the SC	30
Chapter 2		
Figure 2.1	Total Internal Reflection	44
Figure 2.2	IR Spectroscopy and Attenuated Total Reflectance	45
Figure 2.3	C-H Stretching Vibrations	46
Figure 2.4	*Trans* and *Gauche* Conformations	47
Figure 2.5	Temperature Dependence of the IR Frequency	48
Figure 2.6	ATR-FTIR Spectrum of SC *in vivo*	49
Chapter 3a		
Figure 1	Normalization of an IR Absorbance	52
Figure 2	Frequency Shift of the C-H Asymmetric Stretching Absorbance	53
Figure 3	Bandwidth at half-height of the C-H Asymmetric Stretching Absorbance	53
Figure 4	Relative Lipid Content within the SC	53
Figure 5	Frequency Shifts of the Amide I and Amide II absorbances	54
Figure 6	Relative Water Content within the SC	54
Figure 7	Sequential IR Spectra Recorded During Progressive Tape-stripping	54
Figure 8	Cumulative Weight per unit Area of SC Removed by Tape-stripping	55
Figure 9	Schematic Model of the SC	55
Chapter 3b		
Figure 1	Infrared Spectra of Ethanol, human SC *in vivo*, and human SC *in vivo* Post-ethanol Treatment	70
Figure 2	Shift in the Peak Maximum of the C-H Asymmetric Stretching Frequency	71
Figure 3	Amount of SC Lipids Present Post-ethanol Treatment	72
Figure 4	IR Spectra of Material Extracted from the SC	73
Figure 5	IR Spectra of Ethanol, human SC *in vivo*, and human SC *in vivo* post-exposure to Ethanol Vapor	74
Chapter 4		
Figure 4.1	Compressions and Rarefactions in a Longitudinal Wave	93
Figure 4.2	Plane Wave	94
Figure 4.3	Variation of Pressure with Time in a Continuous, Single-frequency Ultrasound Wave	94
Figure 4.4	Apparatus for Radiation Force Measurements	95
Figure 4.5	Deformation of a Piezoelectric Crystal	96
Figure 4.6	Resonance and Acoustic Power Output	97

Figure 4.7 Acoustic Pressure and Pressure Amplitude 98

Chapter 5

Figure 5.1 An Ultrasound Wave is Described by its Amplitude and Frequency 117
Figure 5.2 Percentage of the Applied Ultrasound Energy Lost in a 1mm Thick Tissue 118
Figure 5.3 Experimental Apparatus for the Generation of High Frequency Ultrasound 119
Figure 5.4 Experimental Apparatus for Measuring Acoustic Power Output 120
Figure 5.5 Radiation Force Measurements to Determine the Acoustic Efficiency of the Transducers 121
Figure 5.6 TDD of Salicylic Acid Following 20 minutes of Ultrasound Using 2, 10, and 16 MHz frequencies, and Passive Diffusion. 122
Figure 5.7 TDD of Salicylic Acid Following (a) sonophoresis and passive diffusion for 5 minutes. 123
Figure 5.8 Total Amount of Salicylic Acid Absorbed Transdermally 124
Figure 5.9a Radioactivity in the Urine as a Function of Time (20 minute sonophoresis) 125
Figure 5.9b Radioactivity in the Urine as a Function of Time (5 minute sonophoresis) 126
Figure 5.10 TDD of Salicylic Acid Following Pre-treatment of the Skin with Ultrasound 127
Figure 5.11 TDD of Salicylic Acid delivered in its Unionized Form 128

Chapter 6

Figure 6.1 Effect of Ultrasound on Drug Release Rate from the Gel 141
Figure 6.2 Electron Micrograph of Control Skin 142
Figure 6.3 Electron Micrograph of Control Skin 143
Figure 6.4 Electron Micrograph of the Excised Skin After 5 minute Ultrasound Treatment at 16 MHz 144
Figure 6.5 Electron Micrograph of the Excised Skin After 5 minute Ultrasound Treatment at 16 MHz 145
Figure 6.6 Alterations in the Cellular Morphology Following 20 minutes of 16 MHz Ultrasound 146
Figure 6.7 Electron Micrograph Showing the Presence of the Tracer in Large Quantities Past the Basal Lamina 147
Figure 6.8 Electron Micrograph of Dermal Tissue Below the Basal Lamina 148
Figure 6.9 10 MHz Ultrasound Treatment Also Drives the Tracer Deep into the Dermis 149
Figure 6.10 Electron Micrograph of Unstained Sections 150
Figure 6.11 Electron Micrograph of Unstained Sections 151

1. Transdermal Drug Delivery

Since the late 70s, it has been accepted that the skin can be used as an entry port for medications targeted towards the systemic circulation. This mode of drug input is known generally as transdermal drug delivery (TDD) *[Shaw, 1978; Hadgraft and Guy, 1989]*. The introduction and regulatory approval of transdermal systems, such as Transdermscop®, Nitrodur®, and Estraderm® has established the feasibility of TDD. Furthermore, these systems demonstrate many of the advantages of TDD, including:

(1) *increased patient compliance*. Since TDD is non-invasive, the acceptance level among patients is relatively high compared to IV or IM dosage forms.

(2) *controlled drug delivery*. Conventional dosage forms yield a saw-tooth profile when the plasma concentration of the drug is plotted against time. In contrast, TDD can maintain a controlled drug concentration for a prolonged period (Figure 1.1). Another shortcoming of the conventional dosage forms, such as tablets, is that patients may forget to take a dose. With an increasingly aging patient population, the ability to control the delivery rate of a drug over prolonged periods (days or even weeks) is a particularly attractive feature.

(3) *overcoming first-pass effect*. Some drugs that are administered orally can be extensively metabolized in the liver before reaching the systemic circulation and eliciting their therapeutic effect. This is the first-pass effect; nitroglycerin (GTN) is a good example of a drug that undergoes a large first-pass effect. When administered transdermally, GTN and other such drugs can substantially avoid the first-pass effect.

Despite the impressive advantages of TDD, the number of transdermal systems approved for sale is small. Currently, transdermal systems are available for only five

drugs. This is primarily due to the excellent barrier property of skin. Molecules traverse the skin by passive diffusion, and they do so very slowly. Table 1.1 lists the permeability coefficients of water and ethanol through three representative biomembranes. The skin is the least permeable by three orders of magnitude, and presents, therefore, a formidable barrier to the penetration of molecules. Simple calculations, based on the size of an acceptable transdermal patch, the permeability of the drug through skin, and the required steady-state plasma concentration, reveal that very few drugs can be candidates for TDD *[Knepp et al., 1987]*. For example, let us calculate the transdermal patch size required to deliver a therapeutic level of acetaminophen. In a 70 kg adult, the clearance (Cl) of acetaminophen is about 23,000 ml/hr the target plasma concentration (C_{ss}) is 15 μg/ml *[Benet and Sheiner, 1980]*. If we assume that a transdermal delivery rate (J) of 25 $\mu g/cm^2/hr$ is possible (a generous assumption, admittedly), then at steady state:

rate in = rate out

$$J \times A = Cl \times C_{ss} \qquad (1.1)$$

where A is the area of the transdermal patch. It follows, therefore, that

$$A = \frac{\frac{23{,}000\ ml}{hr} \times 15 \frac{\mu g}{ml}}{25 \frac{\mu g}{cm^2\ h}}$$

$$\approx 13{,}000\ cm^2$$

Considering the fact that the total skin surface area of an adult human is 20,000 cm^2 (2 m^2) *[Odland, 1983]*, a 13,800 cm^2 patch is rather impractical! One can conclude rather quickly that acetaminophen is not a viable TDD candidate. Table 1.2 tabulates the results of similar calculations for other molecules. By passive diffusion alone, very

few molecules go through the skin rapidly. Because of the limited permeation of molecules through skin, TDD has not yet become a generally applicable mode of drug administration. To exploit the benefits of TDD it is, therefore, imperative to have access to methods which can increase the flux of molecules across the skin. Many laboratories have been working on this problem, and different degrees of success have been reported. Before we review recent developments in this area, it is useful to discuss the structure of skin, and to understand how and why it is a formidable barrier.

1.1 Barrier Properties of Skin

The principal function of skin is to act as a barrier to the outward transport of water. Equally, skin provides a major resistance to the ingress of topically-contacting substances. Unlike aquatic species, humans and other land-based mammals must survive in an arid environment. Without a tough, water-impermeable skin, the body would rapidly dehydrate. Therefore, the skin has evolved primarily as a barrier to water loss from inside the body to the surrounding environment. This barrier also inhibits the entry of substances into the body, thereby providing protection from harmful organisms and molecules. In the context of TDD, the barrier to the ingress of molecules is of greatest relevance, although the water-barrier properties are essential for survival. Nevertheless, the mechanistic basis of water barrier function and TDD appears similar. Understanding the development of this barrier can facilitate attempts to enhance percutaneous absorption of drug molecules.

1.2 Skin Structure *[Odland, 1983]*

The skin has two distinct layers (shown schematically in Figure 1.2): (1) the epidermis and (2) the dermis, each of which contribute to barrier function, albeit in different ways. The epidermis can be further classified into the stratum corneum (SC) and the viable epidermis, which consists of the granular, malphigian, and basal cell layers.

While the SC presents the main barrier to permeability, the remainder of the epidermis and the dermis also contribute to the overall resistance, and, in certain circumstances, can be rate-limiting.

1.2.1 Epidermis

The epidermis is an epithelium of variable dimensions *[Whitton and Everall, 1973]*. It is thickest on frictional surfaces such as palms and soles, and thinnest over the eyelids, the lower parts of the abdomen, around the external genitalia, and the back of the ears. It is connected to the dermis along a highly convoluted surface of large area. Since the epidermis is avascular and derives its nutrients from the highly perfused dermis, the increased contact area facilitates nutrient transfer. This same arrangement allows for the facile exchange of topically absorbed compounds with the systemic circulation.

The primary biochemical events occurring in the epidermis are proliferation and differentiation. Epidermal cells, which proliferate in the basal layer, gradually differentiate and ascend to the surface, forming the SC. The cells of the basal layer of the epidermis are columnar or cuboidal, with the long axis usually oriented perpendicularly to the surface. As these cells divide and ascend to the surface, they become progressively larger and of altered shape, oriented horizontally to the surface and increasingly flattened until they reach the SC, where their appearance becomes scalelike in form. This complete process takes 3-4 weeks in humans.

1.2.2 Stratum Corneum (SC)

The endpoint of epidermal differentiation is the formation of the SC, a matrix of keratinized cells (corneocytes) surrounded by lipids (Figure 1.3). The lipids of the SC are unique in a number of ways:- (1) They consist primarily of cholesterol, free fatty acids and ceramides; no phospholipids are present, unlike other biomembranes *[Wertz*

and Downing, 1989; Lampe et al., 1983]. (2) The lipids of the SC are most abundant in the intercellular spaces. (3) The SC lipids exist in multilamellar arrays which form the only continuous medium from top to bottom of this tissue *[Williams and Elias, 1987].* Despite the apparent differences between SC lipids and those more commonly found in biomembranes, the mechanistic basis of solute permeability through all of these barriers appears to be similar *[Potts and Francoeur, 1990].* The SC, however, has an exceptionally low permeability compared to these other membranes. One explanation (at least, in part) for this low permeability may be the highly tortuous nature of the extracellular lipid domain (see below).

1.2.3 Dermis

The dermis comprises 90% of the skin. It can be likened to an aqueous gel which derives its structure from collagen fibers and elastin. Unlike the relatively rapid turnover of the epidermis, the connective tissue is slowly regenerated. The roots of the body hairs and the secretory coils of the sweat glands are situated in the dermis. In contrast to the avascular epidermis, the dermis is pervaded with a mass of arterioles, venules, and capillaries. Permeants which are transported through the SC and epidermis are ultimately removed by this dermal vasculature.

1.3 Enhancement Methods

In Section 1, the need for methods, which can reduce reversibly the barrier properties of skin and, consequently, increase penetrant flux across the skin, was outlined. In this section, we review the attempts that are being made towards this goal, and we discuss the merits and shortcomings of some of these enhancement methodologies. Increased TDD flux can be achieved by two methods: (1) Altering the composition of the formulation so that the thermodynamic activity of the drug (diffusant molecule) is increased. The augmented thermodynamic activity increases the permeant driving force

and, consequently, enhances drug flux. (2) Reducing skin barrier function. In this thesis, we will limit our discussion to enhancement achieved due to alterations in the barrier. Enhancement is typically defined as follows:

$$\text{Enhancement} = \frac{\text{Drug flux across the skin post-"treatment"}}{\text{Drug flux due to passive diffusion}} \qquad (1.2)$$

It follows from Equation 1.2 that enhancement is a dimensionless quantity. It should be pointed out that when the flux due to passive diffusion is negligible, as in the case of large and/or polar molecules such as peptides, the above definition of enhancement is of limited utility, because infinite enhancement seems possible.

Two major enhancement methods, on which researchers have focussed their attention, are: (1) chemical enhancers and (2) iontophoresis.

1.3.1 Chemical Enhancers

By definition, a chemical enhancer is a molecule which is itself pharmacologically inactive; however, when incorporated into a transdermal formulation, an enhancer can decrease skin barrier function. The attributes of an ideal enhancer include *[Barry, 1983]*:

1. The compound should not elicit any pharmacological response.

2. The compound should be non-toxic, non-allergenic, and non-irritating.

3. The onset of the effect should be immediate, and the duration of the effect should be predictable.

4. The action of the enhancer should be reversible; i.e. the skin should revert to its original state on removal of the material.

5. The enhancer should be chemically and physically compatible with a wide range of drugs and pharmaceutical adjuvants.

6. The enhancer should be inexpensive, odorless, tasteless, and colorless.

It is not surprising that enhancers exhibiting all the above properties remain undiscovered. However, a variety of molecules, ranging from water to the highly lipophilic 1-dodecylazacycloheptan-2-one (Azone®, a specifically synthesized molecule) have been cited as penetration enhancers for TDD. Table 1.3 summarizes the enhancement effects elicited by certain putative enhancers. Despite much research, the mechanism(s) of action of chemical enhancers are still unclear. In Chapter 2 we discuss methods employed to unravel the mechanism(s) of percutaneous penetration enhancement. Subsequently, we describe a specific example: namely, the use of infrared spectroscopy to decipher the mechanism of action of ethanol.

1.3.2 Iontophoresis

Iontophoresis is the process of increased permeation of solutes under an applied electrical gradient. It is a successful method to enhance the transdermal delivery of certain drugs *[Tyle, 1986]*. Iontophoretic enhancement can result from one or more mechanistic origins *[Burnette, 1989]*:

1. A charged solute, present in an applied electric field, is subject to an external force. Solute transport, then, is promoted (or retarded, depending on the field direction) relative to passive diffusion. The net flux can be described by the following Nernst-Planck equation *[Friedman, 1986]*:

$$J_i = -u_i RT \left[\frac{dc_i}{dx} + z_i \frac{F}{RT} c_i \frac{dV}{dx}\right]$$

where subscript i refers to the ion (charged solute) under consideration, J = flux, R = gas constant, T = temperature (in Kelvins), u = mobility, z = charge, F = Faraday's constant, c = concentration, x = distance along the direction of transport, and $\frac{dV}{dx}$ is the potential gradient at point x.

2. If the solute is uncharged, the movement of ions results in the "co-transport" of the uncharged solute molecules. At physiological pH, the skin is negatively charged. Therefore, under an applied potential gradient, positive ions pass through the skin preferentially compared to the negative ions. This will result in a net volume flow (electro-osmotic flow) of material in the direction of motion of the positive ions. Consequently, uncharged molecules can be transported across the skin with this induced volume flow.

3. If the applied current either "opens" new pathways and/or results in structural alterations in the skin, the barrier property can be compromised, and this can result in enhanced transport. The application of current can cause irreversible damage to the skin. Recent experiments *[Burnette and Ongpipattanakul, 1988; Green et al., 1990]* have suggested that, even at low current densities, irreversible alterations may be induced. (Note: these were *in vitro* experiments, which imply that the "repair" mechanism of the *in vivo* system was absent)

Which of these mechanisms is/are more important? The answer requires knowledge of the routes of solute penetration through the SC, a subject discussed in more detail below (Section 1.4).

1.3.3 Sonophoresis

Sonophoresis is the enhanced flux of molecules due to an ultrasonic perturbation. Sonophoresis as applied to TDD will be discussed fully in Chapter 4.

1.4 Mechanisms of Percutaneous Absorption

Percutaneous absorption involves the following sequence of events (Figure 1.4):

1. Partitioning of the molecule into the stratum corneum from the applied vehicle phase.
2. Diffusion through the stratum corneum.
3. Partitioning from the SC into the viable epidermis.
4. Diffusion through the epidermis and upper dermis.
5. Capillary uptake.

Hence, the movement of molecules through the skin involves transport through a number of resistances in series. It follows that the overall rate of transport is dictated by the least permeable barrier.

1.4.1 Evidence that the SC is the Rate Limiting Barrier

The results of several elegant experiments *[Scheuplein, 1965; 1976; 1978]* have shown that the SC is the rate limiting barrier to the penetration of many chemicals through the skin. Scheuplein *[1976]* tape-stripped the skin, thereby removing the SC, and compared the resulting permeability with that of unstripped skin. Removal of the SC increased the permeabilities of many solutes by orders of magnitude, strongly implicating the SC as the primary rate-limiting barrier.

1.4.2 Penetration Pathways Across the SC

For all but the most lipophilic compounds, the SC is the least permeable layer of the skin. Although the SC is a biomembrane, its function and its composition distinguish

it from other membranes in the body. While most epithelia have evolved to exchange material, the SC has evolved to prevent or strictly control the transport of molecules. The primary difference between the morphology of SC and that of other epithelia is that the SC comprises a matrix of proteinaceous material surrounded by extracellular, multilamellar bilayers of lipid. The distinct morphology of the SC has frequently been likened to a brick wall, with the keratinocytes corresponding to the bricks, and the intercellular lipids analogous to the mortar *[Michaels et al., 1975]*. From the description of the SC components and morphology, and following the classic work of Scheuplein *[1976]*, one can envisage that a diffusing molecule can take one or more of the following routes of penetration (Figure 1.5):

(1) The transcellular path, indicating that the molecules transfer sequentially and repeatedly through the "bricks" and "mortar",

(2) The intercellular path--*via* the tortuous but continuous intercellular lipids, and

(3) The transappendageal path *via* hair follicles, etc.

It has been deduced that, at passive steady-state, appendageal transport makes a negligible contribution to the overall percutaneous flux across human skin *[Scheuplein, 1967; Flynn, 1981; Keister and Kasting, 1986]*. Furthermore, there is a poor correlation between appendageal density and percutaneous absorption when different anatomical sites are compared *[Rougier et al., 1986, 1987, 1988]*. However, transport through the appendageal route has been shown to be significant during the initial (non-steady state) period of percutaneous penetration *[Scheuplein, 1967; Keister and Kasting, 1986]*. The minimal capacity (i.e small relative surface density of follicles, etc.) of this route would appear to offset the higher apparent permeability such that at steady state, the contribution to total transport becomes rather insignificant. Nevertheless, discussion of the issue is not completely closed: recent research has once

again raised the question of the participation of the follicles in percutaneous absorption *[Schaefer et al., 1989]*.

Debate over the major permeation pathway through the SC remains controversial. One school of thought proposes the co-existence of polar (hydrophilic) and non-polar (lipophilic) routes. A second opinion finds little evidence for the so-called polar pathway and suggests that most data are compatible with the SC lipid milieu as the medium through which percutaneous absorption occurs. What are the facts and the arguments?

The intercellular lipid pathway is the only continuous phase in the SC *[Williams and Elias, 1987]*. While the corneocytes with their desmosomal connections could be cited as another continuous path, the gradual disappearance of desmosomes towards the surface weakens this hypothesis. Thus, whether the permeant goes around or through the corneocytes, it must traverse the intercellular lipids during its passage from the top to the bottom of the SC. Hence, there would appear to be at least circumstantial evidence that the intercellular lipids of the SC represent the rate determining component. This hypothesis is strongly supported by several biophysical studies the results of which show that measures of SC lipid structure are highly correlated with the permeability of water and other solutes *[Potts and Francouer, 1990]*. It is logical, therefore, that much effort has focussed on understanding the intercellular lipids of the SC.

Support for the co-existence of a "polar" or "pore" pathway across the SC is, again, based upon inferences rather than direct experimental evidence. Recent work by Guy and Hadgraft *[Guy and Hadgraft, 1988]*, based on reanalysis of the data used to promote the "pore" pathway, challenges the existence of the "pore pathway".

Furthermore, other, indirect evidence supports the lipid pathway. For example, regional variations in skin permeability are correlated with quantitative differences in lipid content rather than stratum corneum thickness or cell number *[Lampe et al., 1983]*. If the transcellular route were a major permeation pathway, corneocyte cell number should be correlated with permeability. The extraction of SC lipids by chloroform:methanol dramatically increases water permeability *[Scheuplein and Blank, 1971]*, supporting the importance of the lipids to barrier function. In addition, the temperature dependence of water permeability through SC suggests that the intercellular lipids are primarily responsible for the barrier to water loss *[Potts and Francouer, 1990; Blank, 1952; Blank et al., 1984]*. Interestingly, recent studies have shown that SC water permeability is highly correlated with the transport of benzoic acid *[Lotte et al., 1987]*. This correlation suggests that these lipophilic compounds and water share a common lipid pathway through the SC. Finally, using very different experimental approaches, independent investigators have shown that the diffusion pathlengths for water *[Potts and Francoeur, 1990a]* and nicotinic acid esters *[Albery and Hadgraft, 1979]* are significantly (10 times and more) greater than the thickness of the SC. Hence, for permeants with very different physicochemical properties, a tortuous pathway through the SC is strongly implicated.

Deductions have also been made about the permeation pathway from studies of SC barrier alterations in different disease states. Feingold and co-workers *[Feingold et al., 1986]* showed an impaired barrier function in fatty acid deficient rats. Furthermore, the fatty acid deficiency was manifested as an abnormal organization of the intercellular lipids of the SC suggesting that the SC intercellular lipids play a vital role in the maintenance of a normal barrier. That abnormality in the intercellular lipids leads to increased water permeability provides at least circumstantial evidence that the lipid domain represents the penetration pathway for this molecule.

The evidence cited thus far in support of the SC lipid pathway is primarily inferential. There have been significant attempts towards the direct visualization of SC transport pathways: in these experiments, the skin is exposed to a tracer molecule, and then frozen, sectioned, and visualized microscopically *[Boddé et al., 1989, 1990]*. Superficially, at least, the results of this work localize the penetrants in the intercellular spaces. However, the data remain equivocal to a certain extent because:

(1) It is not established that the tracer molecules follow the same pathway as that traversed by pharmacologically-active molecules.

(2) It is not possible to determine unambiguously if the treatment and the subsequent tissue processing influence the results.

Autoradiography has been successfully used to replace the use of electron dense tracer molecules *[Schaefer et al., 1978]*. However, the issue of considerable tissue processing still remains unresolved. Newer techniques such as confocal microscopy, which employs minimal tissue processing, may offer useful alternate approaches to examine penetration pathway(s) *[Cullander et al., 1990]*.

In summary, then, we find compelling evidence for a tortuous lipid route across the SC, but, at this time, little experimental support for the so-called "pore" pathway. The elongated shape of the corneocytes imposes upon the intercellular route a considerably lengthened diffusion pathlength, and this physical constraint accounts significantly, therefore, for the low permeability of water through the SC membrane. Thus, although biophysical measurements of water transport across the SC and across other biomembranes indicate a similar mechanism, the relatively large resistance of the SC is, at least partly, a consequence of the tortuous diffusion path. No doubt, the unique SC lipid composition also has a role in determining the magnitude of the permeability coefficient, K_p, *[Williams and Elias, 1987]* but it seems clear from the relative

magnitude of the permeability, that this cannot be the only influencing factor. Studies with model biomembranes *[Hadgraft and Ridout, 1987]* designed to mimic SC barrier function have led to similar conclusions. There is, furthermore, theoretical justification to predict a significant impact of elongated corneocyte size on the retardation of SC transport *[Cussler et al., 1988]*. The inclusion of "brick"-shaped corneocytes into a homogeneous matrix lowers transport to an extent proportional to the length/width ratio of the "brick". Interestingly, recent human percutaneous absorption data *[Rougier et al., 1988]* indicate that the permeabilities of water and benzoic acid are inversely related to corneocyte size.

1.5 Conclusion

In this chapter, we began by establishing the need for enhancement strategies to make TDD viable. Then, we discussed the structure of skin to gain insight about its barrier properties. Reviewing the literature for enhancement methodologies led us to the analysis of penetration pathways in the skin. Existing data in the literature suggest that the intercellular lipid pathway is the major route for penetration. For polar compounds, the lipid barrier turns out to be the major rate-limiting step in their percutaneous penetration. Hence, methods that can report on alterations in the membrane, and the status of the intercellular lipids in particular, can help to decipher the mechanisms of enhancement. We now address this issue in the next two chapters.

Table 1.1 Permeability Coefficients of Water and Methanol Through Biomembranes.

Membrane	Water	Ethanol
	(Permeability (cm/sec)	
[1]Red blood cell	1.2×10^{-3}	2.1×10^{-3}
[1]Toad urinary bladder	1×10^{-4}	8×10^{-5}
[2]Human skin	1.4×10^{-7}	2×10^{-7}

[1] Data from *Stein, 1986*

[2] Data from *Scheuplein, 1976*

Table 1.2 *[Knepp et al., 1987].* **Estimated Transdermal Patch Size for Various Drugs**

Drug	Cl (ml/hr)[a]	C_{ss}	Area (cm^2)[b]
Acetaminophen	23,076	15	13,846
Aspirin	29,085	150	174,510
Cimetidine	48,510	1	1,940
Clonazepam	4,032	0.025	4.0
Clonidine	12,054	0.001	0.48
Digoxin	6,800	0.002	0.54
Estradiol	66,859	0.0001	0.27
Indomethacin	9,049	0.5	181
Isosorbide dinitrate	174,636	0.001	7.0
Nitroglycerin	4,213,440	0.0001	17
Propranolol	48,594	0.02	39
Scopolamine	43,330	0.0002	0.35
Theophylline	138	5	28

[a] Calculated for a 70 kg adult except in the case of theophylline, the assessment of which is for a 2.5 kg pre-term infant

[b] The values in this column are calculated using J = 25 $\mu g/cm^2/hr$ and Equation 1.1.

Table 1.3 Examples of Percutaneous Penetration Enhancement by Various Chemicals.

Enhancer	Extent of Enhancement	Skin	Permeant
a. (EtOH- Ethanol)			
0.25 % oleic acid+0% EtOH+buffer	1.1	Hairless mouse	Piroxicam
0.25 % oleic acid+10% EtOH+buffer	12.1	Hairless mouse	Piroxicam
0.25 % oleic acid+20% EtOH+buffer	48.7	Hairless mouse	Piroxicam
0.25 % oleic acid+30% EtOH+buffer	106	Hairless mouse	Piroxicam
0.25 % oleic acid+40% EtOH+buffer	200	Hairless mouse	Piroxicam
0.25 % oleic acid+50% EtOH+buffer	132	Hairless mouse	Piroxicam
0.25 % oleic acid+100% EtOH+buffer	8.7	Hairless mouse	Piroxicam
b.			
Decylmethyl Sulfoxide	689	Hairless Rat	Azidothymidine
	894	Fuzzy Rat	Azidothymidine
	77	Human Cadaver skin	Azidothymidine
c.			
Propylene Glycol (PG)	1	Hairless mouse	Acyclovir
PG+Azone	41.4	Hairless mouse	Acyclovir
PG+1-farnesylazacycloheptan-2-one (7FU)	14.14	Hairless mouse	Acyclovir
PG+1-Geranylazacycloheptan-2-one (7GU)	12.82	Hairless mouse	Acyclovir
PG+1-Geranylazacyclopentan-2-one (5GU)	1.6	Hairless mouse	Acyclovir
Ethanol (EtOH)	1	Hairless mouse	Acyclovir
EtOH+Azone	11.24	Hairless mouse	Acyclovir
EtOH+7FU	10.1	Hairless mouse	Acyclovir
EtOH+7GU	13.6	Hairless mouse	Acyclovir

EtOH+5GU	8.65	Hairless mouse	Acyclovir
Isopropanol (IPA)	1	Hairless mouse	Acyclovir
IPA+Azone	1.543	Hairless mouse	Acyclovir
IPA+7FU	5.1	Hairless mouse	Acyclovir
IPA+7GU	6.8	Hairless mouse	Acyclovir
IPA+5GU	0.52	Hairless mouse	Acyclovir
Isopropyl Myristate (IPM)	1	Hairless mouse	Acyclovir
IPM+Azone	0.71	Hairless mouse	Acyclovir
IPM+7FU	0.97	Hairless mouse	Acyclovir
IPM+7GU	0.66	Hairless mouse	Acyclovir
IPM+5GU	0.82	Hairless mouse	Acyclovir

---

a. *Francoeur et al., 1990*

b. *Wearley and Chien, 1990*

c. *Okamoto et al., 1990*

References

Albery, W.J., and Hadgraft, J., 1979, Percutaneous Absorption: Theoretical Description, **Journal of Pharmacy and Pharmacology,** 31: 129-139.

Barry, B.W., 1983, **Dermatological Formulations,** Marcel Dekker, New York, pp. 160-161.

Benet, L.Z., and Sheiner, L.B., 1980, Design and Optimization of Dosage Regimens: Pharmacokinetic Data, in **The Pharmacological Basis of Therapeutics,** eds.: Gilman, A.G., Goodman, L.S., and Gilman, A., Macmillan, New York, pp. 1675-1737.

Blank, I. H., 1952, Factors Which Influence the Water Content of the Stratum Corneum, **Journal of Investigative Dermatology,** 18: 433-440.

Blank, I. H., Moloney, J., Emslie, A. G., Simon, I., and Apt, C. J., 1984, The Diffusion of Water Across the Stratum Corneum as a Function of Water Content, **Journal of Investigative Dermatology,** 82: 188-194.

Boddé, H. E., Kruithof, M. A. M., Brussee, J., and Koerten, H. K., 1989, Visualization of Normal and Enhanced $HgCl_2$ Transport Through Human Skin *in vitro*, **International Journal of Pharmaceutics,** 53: 13-24.

Boddé, H. E., Holman, B., Spies, F., Weerheim, A., Kempenaar, J., Mommaas, M., and Ponec, M., 1990, Freeze-fracture Electron Microscopy of In Vitro Reconstructed Human Epidermis, **Journal of Investigative Dermatology,** 95: 108-116.

Burnette, R.R., 1989, Iontophoresis, in **Transdermal Drug Delivery: Developmental Issues and Research Initiatives,** eds. Hadgraft, J., and Guy, R.H., Marcel Dekker, New York, pp. 247-291.

Burnette, R.R., and Ongpipattanakul, B., 1988, Characterization of the Pore Transport Properties of Excised Human Skin During Iontophoresis, **Journal of Pharmaceutical Sciences,** 77: 132-138.

Cullander, C., Menon, G.K., Guy, R.H., and Elias, P.M., 1990, In Situ Visualization of the Lamellar Body Secretory System by Confocal Microscopy, **Journal of Investigative Dermatology,** 94: 517.

Cussler, E.L., Hughes, S.E., Ward, W.J., and Aris, R., 1988, Barrier Membranes, **Journal of Membrane Science,** 38: 161-174.

Feingold, K.R., Brown, B.R., Lear, S.R., Moser, A.H., and Elias, P.M., 1986, The Effect of Essential Fatty Acid Deficiency on Cutaneous Sterol Synthesis, **Journal of Investigative Dermatology,** 87: 588-591.

Flynn, G.L., 1981, Topical Drug Absorption and Topical Pharmaceutical Systems, in **Modern Pharmaceutics**, Banker, G. L., Rhodes, C. T., Eds., Marcel Dekker, Inc., New York, pp. 272-305.

Francoeur, M.L., Golden, G.M., and Potts, R.O., 1990, Oleic Acid: Its Effects on Stratum Corneum in Relation to (Trans)dermal Drug Delivery, **Pharmaceutical Research,** 7: 621-627.

Friedman, M.H., 1986, **Principles and Models of Biological Transport,** Springer Verlag, Berlin.

Green, P.G., Hinz, R.S., Kim A., Szoka, Jr., F.C., and Guy, R.H., 1990, Iontophoretic Delivery of a Series of Tripeptides Across the Skin *in vitro,* in press.

Guy, R.H., and Hadgraft, J., 1988, Physicochemical Aspects of Percutaneous Penetration and its Enhancement, **Pharmaceutical Research,** 5: 753-758.

Hadgraft, J., and Guy, R.H., 1989, eds., **Transdermal Drug Delivery: Developmental Issues and Research Initiatives,** Marcel Dekker, New York.

Hadgraft, J., Ridout, G., 1987, Development of Model Membranes for Percutaneous Absorption Measurements. I. Isopropyl Myristate, **International Journal of Pharmaceutics,** 39: 149-156.

Keister, J.C., and Kasting, G.B., 1986, The Use of Transient Diffusion to Investigate Transport Pathways through Skin, **Journal of Controlled Release,** 4: 111-117.

Knepp, V.M., Hadgraft, J., and Guy, R.H., 1987, Transdermal Drug Delivery: Problems and Possibilities, **Critical Reviews in Therapeutic Drug Carrier Systems,** 4: 13-37.

Lampe, M.A., Burlingame, A.L., Whitney, J., and Williams, M.L., 1983, Human Stratum Corneum Lipids: Characterization and Regional Variations, **Journal of Lipid Research,** 24: 120-130.

Lotte, C., Rougier, A., Wilson, D.R., and Maibach, H.I., 1987, In Vivo Relationship Between Transepidermal Water Loss and Percutaneous Penetration of Some

Organic Compounds In Man: Effect of Anatomic Site, **Archives of Dermatological Research,** 279: 351-356.

Michaels, A.S., Chandrasekaran, S.K., and Shaw, J.E., 1975, Drug Permeation through Human Skin: Theory and *In Vitro* Experimental Measurement, **American Institute of Chemical Engineers' Journal,** 21: 985-996.

Odland, G.F., 1983, Structure of the Skin, in **Biochemistry and Physiology of the Skin,** Goldsmith, L. A., ed., Oxford University Press, New York, pp. 3-36.

Okamoto, H., Muta, K., Hashida, M., and Sezaki, H., 1990, Percutaneous Penetration of Acyclovir Through Excised Hairless Mouse and Rat Skin: Effect of Vehicle and Percutaneous Penetration Enhancer, **Pharmaceutical Research,** 7: 64-68.

Potts, R.O., and Francoeur, M.L., 1990, Lipid Biophysics of Water Loss through the Skin, **Proceedings of the National Academy of Sciences,** 87: 3871-3873.

Potts, R.O., and Francoeur, M.L., 1990a, The Influence of Stratum Corneum Morphology on Water Permeability, **Journal of Investigative Dermatology,** in press.

Rougier, A., Dupuis, D., Lotte, C., Roguet, R., Wester, R.C., and Maibach, H.I., 1986, Regional Variation in Percutaneous Absorption in Man: Measurement by the Stripping Method, **Archives of Dermatological Research,** 278: 465-469.

Rougier, A., Lotte, C., and Maibach, H.I., 1987, In Vivo Percutaneous Penetration of Some Organic Compounds Related to Anatomic Site in Humans: Predictive Assessment by the Stripping Method, **Journal of Pharmaceutical Sciences,** 76: 451-454, 1987.

Rougier, A., Lotte, C., and Corcuff, P., 1988, Relationship Between Skin Permeability and Corneocyte Size According to Anatomic Site, Age, and Sex in Man, **Journal of the Society of Cosmetic Chemists,** 39: 15-26.

Schaefer, H., Stuttgen, G., Zesch, A., Schalla, W., and Gazith, J., 1978, Quantitative Determination of Percutaneous Absorption of Radiolabeled Drugs *In Vitro* and *In Vivo* by Human Skin, **Current Problems in Dermatology,** 7: 80-94.

Schaefer, H., Watts, F., Brod, J., and Illel, B., 1989, Follicular Penetration, in **Prediction of Percutaneous Penetration. Methods, Measurements, Modelling,** Scott, R.C., Guy, R.H., and Hadgraft, J., eds., IBC Technical Services Ltd., Great Britain, pp. 163-173.

Scheuplein, R.J., 1965, Mechanism of Percutaneous Absorption I. Routes of Penetration and the Influence of Solubility, **Journal of Investigative Dermatology,** 45: 334-346.

Scheuplein, R.J., 1966, Analysis of Permeability Data for the Case of Parallel Diffusion Pathways, **Biophysical Journal,** 6: 1-17.

Scheuplein, R.J., 1967, Mechanism of Percutaneous Absorption II. Transient Diffusion and the Relative Importance of Various Routes of Skin Penetration, **Journal of Investigative Dermatology,** 48: 79-88.

Scheuplein, R.J., 1976, Permeability of the Skin: A Review of Major Concepts and Some New Developments, **Journal of Investigative Dermatology,** 67: 672-676.

Scheuplein, R.J., 1978, Permeability of the Skin: A Review of Major Concepts, **Current Problems in Dermatology,** 7: 172-186.

Scheuplein, R. J. and Blank, I. H., 1971, Permeability of the Skin, **Physiological Reviews,** 51: 702-747.

Shaw, J.E., 1978, Controlled Topical Delivery of Drugs for Systemic Action, **Drug Metabolism Reviews,** 8: 223-233.

Stein, W.D., 1986, **Transport and Diffusion Across Cell Membranes,** Academic Press, New York, p. 76.

Tyle, P., 1986, Iontophoretic Devices for Drug Delivery, **Pharmaceutical Research,** 3: 318-324.

Wearley, L., and Chien, Y.W., 1990, Enhancement of the *in vitro* Skin Permeability of Azidothymidine (AZT) via Iontophoresis and Chemical Enhancer, **Pharmaceutical Research,** 7: 34-40.

Wertz, P.W., and Downing, D.T., 1989, Stratum Corneum: Biological and Biochemical Considerations, in **Transdermal Drug Delivery: Developmental Issues and Research Initiatives,** eds. Hadgraft, J., and Guy, R.H., Marcel Dekker, New York, pp. 1-22.

Whitton, J.T., and Everall, J.D., 1973, The Thickness of the Epidermis, **British Journal of Dermatology,** 89: 467-476.

Williams, M.L., and Elias, P.M., 1987, The Extracellular Matrix of Stratum Corneum: Role of Lipids in Normal and Pathologic Function, **CRC Critical Reviews In Therapeutics and Drug Carrier Systems,** 3: 95-112.

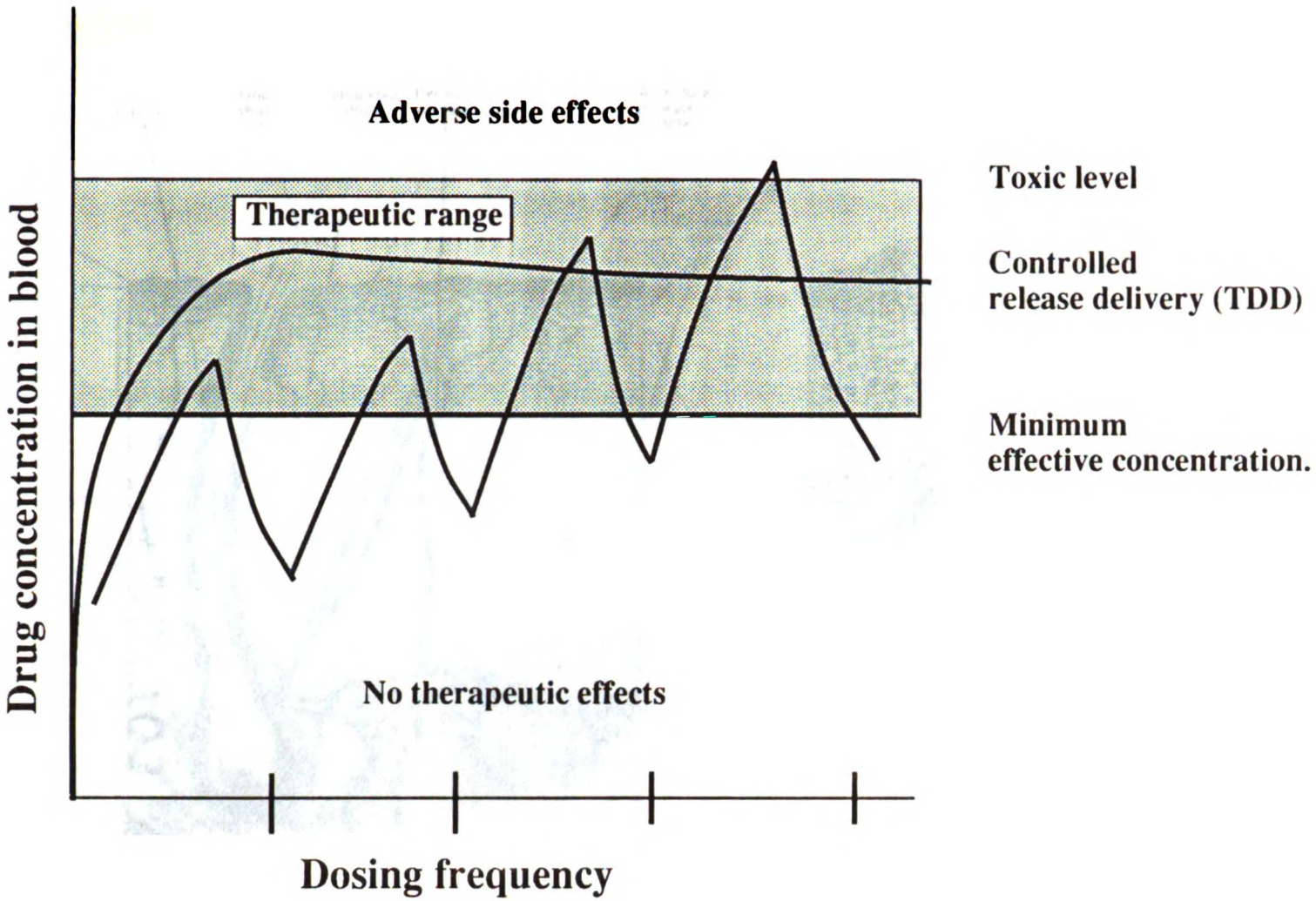

Figure 1.1. Schematic of drug concentration in blood as a function of time (dosing frequency) following conventional (e.g., oral) multiple dosing (saw-tooth profile) and controlled (e.g., transdermal) drug delivery.

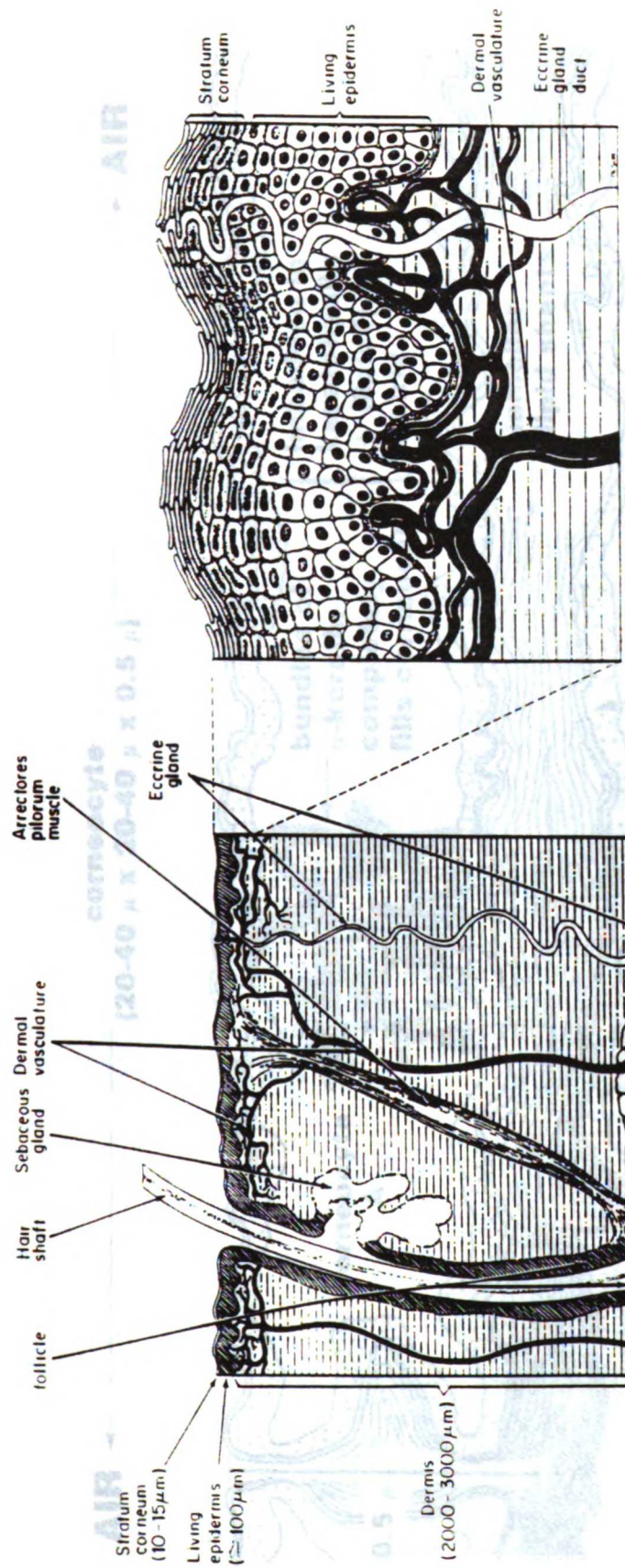

Figure 1.2 Schematic cross-sections of the skin. The full-thickness skin is shown on the left (a), and an expansion of the upper 200-μm thickness (the epidermis) is shown on the right (b). (From *Flynn, 1981*).

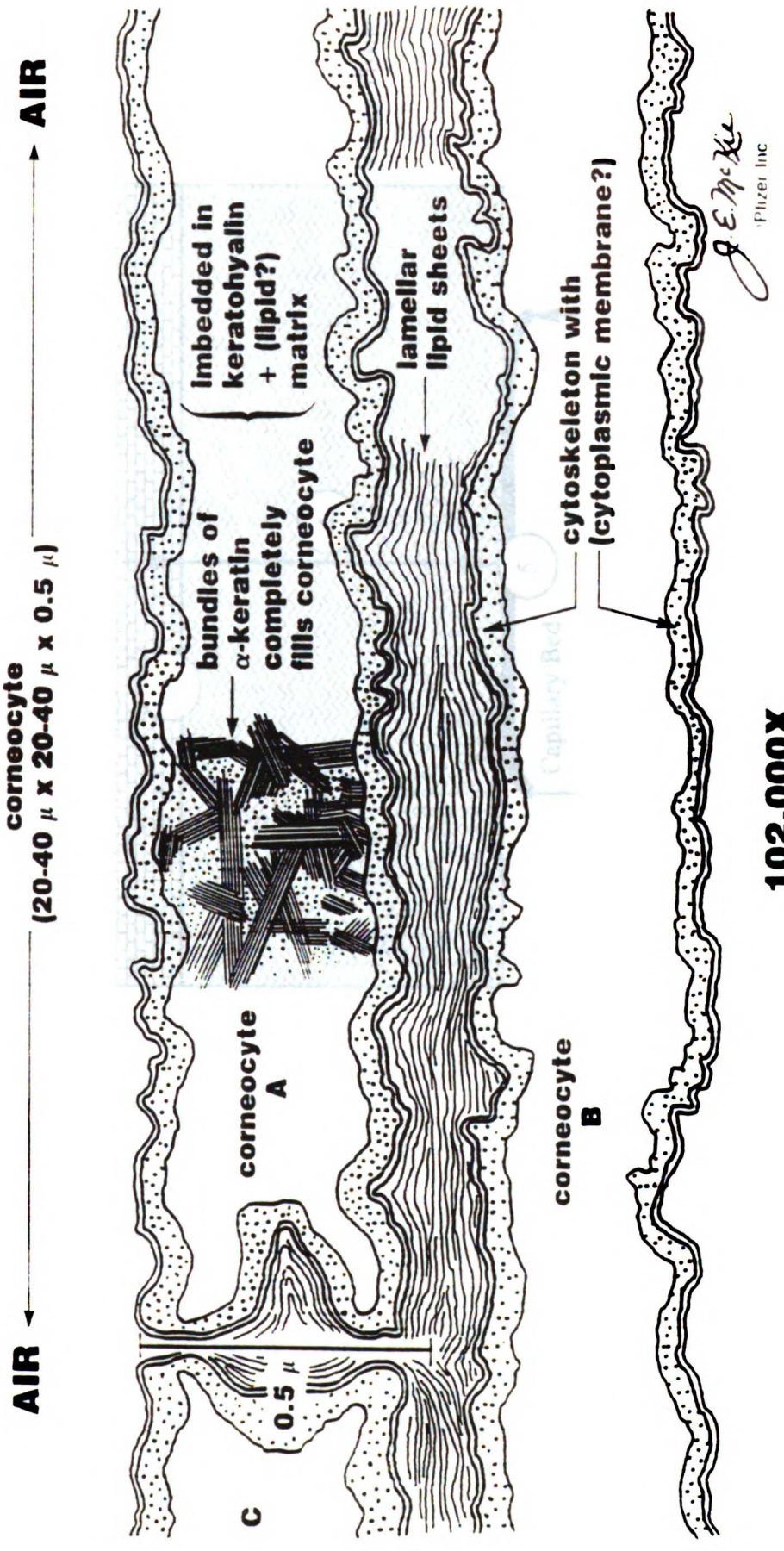

Figure 1.3 An artist's conception of the stratum corneum (SC).

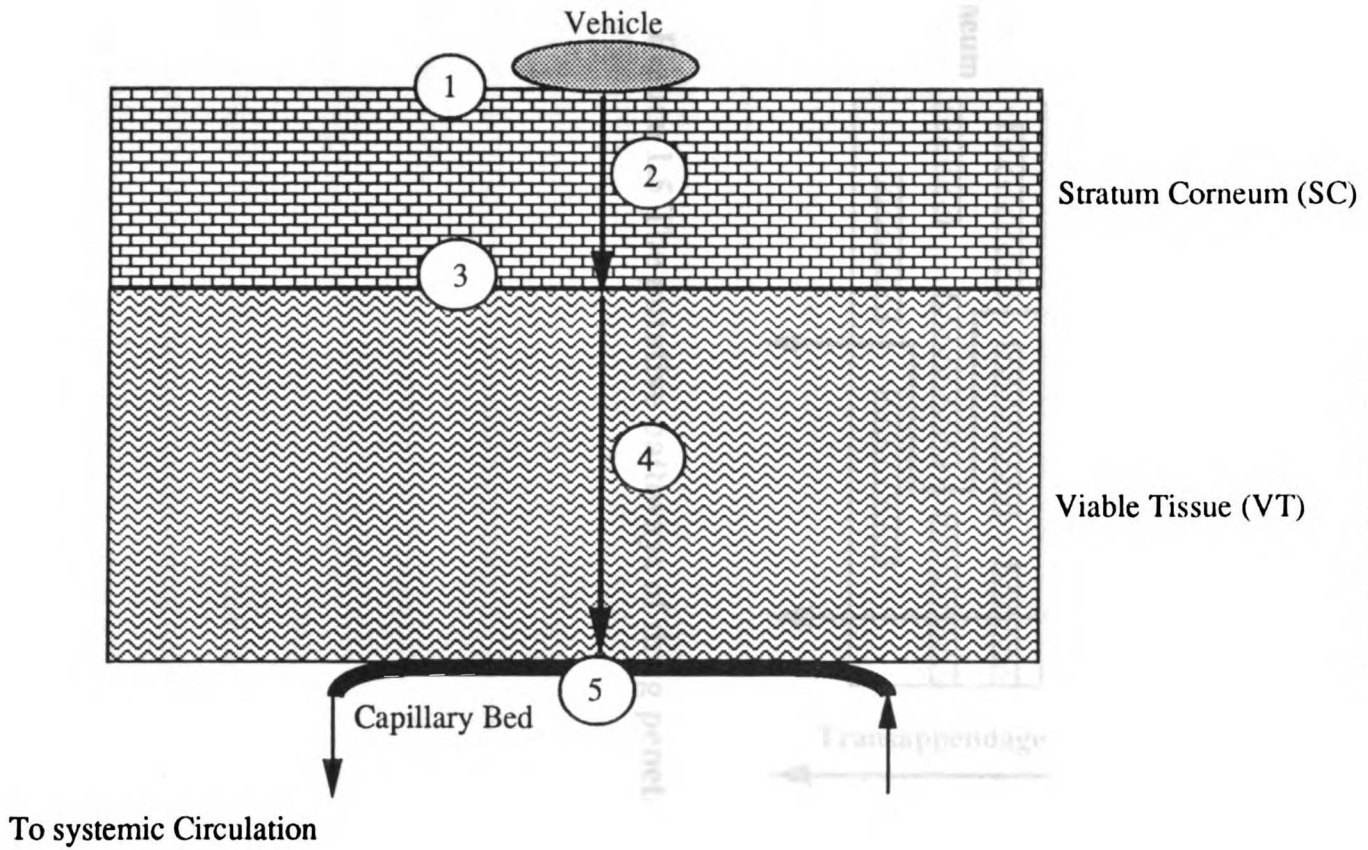

Figure 1.4 The sequential steps involved in transdermal absorption.

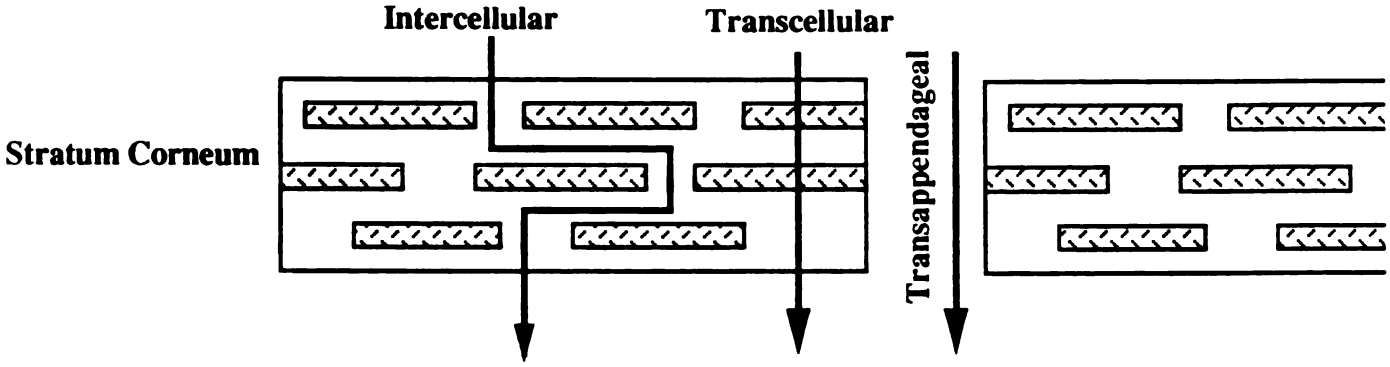

Figure 1.5 The putative pathways of drug penetration across the SC.

2. Infrared Spectroscopy

In Chapter 1, we showed that enhancement methods are necessary, if TDD is to become a viable drug delivery concept. We also argued that the permeation rate of most molecules is limited by the intercellular lipids of the SC for the following reason: the paracellular pathway, comprising the SC intercellular lipids, forms the only, significant, continuous path for diffusion. Methods employed to enhance TDD, therefore, have to focus on compromising the barrier by acting on the SC intercellular lipids. It follows that tools employed to decipher the mechanism(s) of enhancement should be capable of reporting on changes in the SC intercellular lipids, and, possibly, the other component of the SC, namely proteins. In this chapter, we discuss such a biophysical tool, namely Fourier Transform Infrared Spectroscopy (FTIR), and its application to decipher the mechanism(s) involved in the enhancement of TDD by chemical enhancers.

2.1 Theoretical Aspects of IR Spectroscopy

The total energy of a molecule arises from its rotational, translational, vibrational and electronic motions. Electronic motions, or transitions, are associated with the absorption and emission of radiation in the ultraviolet and visible regions of the electromagnetic spectrum, while molecular rotations and vibrations give rise to absorptions and emissions of radiation at characteristic frequencies in the far and near regions of the infrared (IR).

The energy, E, of a quantum radiation is given by

$$E = h\nu \qquad (2.1)$$

where h is Planck's constant, ν is the frequency of the absorbed radiation, and is related to the wavelength, λ, by the equation

$$\nu = c\,\lambda \qquad (2.2)$$

where c is the velocity of light. In IR, the absolute frequency, ν, is generally replaced by wavenumber, $\tilde{\nu}$, which has units of cm^{-1} and is defined

$$\tilde{\nu} = \frac{1}{\lambda} \qquad (2.3)$$

where λ is measured in cm. Hence,

$$E = h\,c\,\tilde{\nu} \qquad (2.4)$$

For a diatomic molecule or a chemical bond to absorb IR radiation, it must possess an electric dipole moment which changes during the motion. Thus, H_2 and Cl_2 do not absorb IR radiation, whereas HCl molecules, which consist of two atoms of different electronegativities, will give rise to absorption owing to the inherent polarity of the system.

Infrared spectroscopy is nondestructive and nonperturbing. Spectra can be obtained relatively rapidly, frequently with little or no sample preparation, and both qualitative and quantitative results can be obtained. For a detailed technical description of the hardware, the reader is referred to the literature *(Nakamishi and Solomon [1977], Griffiths and de Haseth [1986], Amey and Chapman [1983], Fringeli and Günthard [1981], and Keighley [1976])*.

The basic apparatus necessary for the technique is a spectrometer. A spectrometer is an instrument which records variations in intensity of radiation when some other parameter, such as frequency or magnetic field, is varied. An IR spectrometer,

therefore, plots a graph of light intensity against frequency in cm^{-1}. A spectrometer comprises (a) a source of radiation, (b) a radiation detector, and (c) a device to select the conditions (e.g., frequency) at which the detector gives a measure of the intensity of the radiation incident upon it. A more sophisticated, but now standard technique is Fourier Transform Infrared (FT-IR) spectroscopy. An FT-IR spectrometer consists of two parts: (1) an interferometer-based optical system; and (2) a dedicated computer which controls the optical system and all aspects of data collection and analysis. An interferometer basically consists of two plane mirrors at right angles to each other. One mirror is stationary, while the other can travel along a path perpendicular to its plane. A beamsplitter, consisting of a semi-reflecting film, is situated between the two mirrors. A collimated beam of infrared radiation from a source passes to the beamsplitter where the beam is divided, part being transmitted to the movable mirror and part being reflected to the stationary mirror. Interference occurs when the return beams recombine at the beamsplitter. From there a portion of the beam passes through the sample and on to the detector. The travelling mirror yields a sinusoidal signal at the detector which is digitized by an A/D converter and computer-stored. The interferogram of this scan, or the sum of many such scans, is then converted, by means of a fast Fourier transform (FFT) into a conventional absorbance (or percent transmission) versus wavenumber spectrum. This brings us to the definitions of absorbance and transmission.

The absorption of light by a material may be defined by the Beer-Lambert relation

$$D = \log_{10}\left(\frac{I_0}{I}\right) = \varepsilon .C. \ell \qquad (2.5)$$

where, at a given frequency,

D is the absorbance

I_0 is the intensity of light entering the sample;

I is the intensity of light leaving the sample;

ε is the molar extinction coefficient;

C is the concentration of the absorbing material in the sample;

ℓ is the pathlength through the sample.

The absorption of light by a sample plotted against the frequency can be expressed in terms of its absorbance (D), or in terms of transmission (T) or absorption (A) where

$$T = \frac{I}{I_0}$$

$$A = \frac{(I_0 - I)}{I_0} = 1 - T \qquad (2.6)$$

Hence, $D = \log_{10} \frac{1}{T}$

2.2 Biomembrane Spectroscopy

In conventional transmission spectroscopy, the sample is prepared as a thin film or pellet and is placed in the path of the infrared beam. The film or pellet should be thin enough to allow transmission of the beam. It follows that the use of transmission spectroscopy *in vivo* is necessarily limited (see Section 2.2.1 and Chapter 3). Analysis of the transmitted portion of the beam reveals the characteristics of the absorbing sample. However, certain factors complicate the spectroscopic analysis of biological molecules and biomembranes. In particular:

1. Complexity of molecules

A molecule with N atoms exhibits 3N-6 normal vibrations. A lipid molecule consisting of 100 atoms will, therefore, exhibit 294 normal vibrations. Furthermore, this number may be enlarged by overtones, combination tones, and band splitting due to intermolecular interactions. This leads to the overlapping of absorption bands and complicates, therefore, the identification and assignment of spectral features.

2. Influence of water

Water in the liquid phase absorbs strongly in the IR spectral range. Most biomembranes contain considerable amounts of water, the absorbance of which overlaps the absorption bands resulting from other constituents of the membrane.

In order to overcome some of the above mentioned difficulties, advanced infrared techniques, such as attenuated total reflection (ATR) are employed.

2.2.1 Attenuated Total Reflection (ATR) IR Spectroscopy

When electromagnetic waves (e.g., those comprising light) travel from a denser medium to a rarer medium, they can undergo (a) reflection and/or (b) refraction (Figure 2.1). As the incident angle is changed, there is a point called the critical angle, θ_c, at which all the incident light is reflected, so-called total-internal reflection. The critical angle is defined as

$$\theta_c = \sin^{-1} \frac{n_2}{n_1} \qquad (2.7)$$

where n_2 and n_1 are the refractive indices of the denser and rarer media. Total-internal reflection has been exploited in the use of IR spectroscopy *in vivo*.

Figure 2.2 compares conventional transmission IR spectroscopy with the so-called ATR technique. The latter involves placing the sample material in close contact with the optically transparent internal reflection element of higher refractive index, and working above the critical angle θ_c. An evanescent wave exists in the rarer medium beyond the reflecting interface, even under conditions of total reflection. This wave exhibits the frequency of the incoming light, but the amplitude falls off exponentially with distance from the surface. The depth of penetration, d_p, is given by

$$d_p = \frac{\lambda_1}{2\pi\,(\sin^2\nu - n_{21}^2)^{1/2}} \qquad (2.8)$$

where n_{21} equals the ratio n_2/n_1 of the refractive index of the rarer medium, n_2, to that of the internal reflection element (IRE), n_1. λ_1 denotes the wavelength λ_{vacuum}/n_1 in the IRE. According to Equation 2.8, the penetration depth approximately equals the wavelength λ_1 of the infrared radiation. This allows IR absorption measurements of thin layers (microns thick), provided optical contact between the rarer medium (sample) and the IRE may be established, e.g., by direct deposition of mono- or multilayers or by methods described in Chapter 3. Under this condition

$$\left(\frac{A_{sample}}{A_{H_2O}}\right)_{ATR} >> \left(\frac{A_{sample}}{A_{H_2O}}\right)_{Transmission} \qquad (2.9)$$

This means that ATR measurements of aqueous systems are less impeded by water absorption than transmission experiments.

2.3 Infrared Absorbances of Typical Biomolecules

2.3.1 Methylene Group Vibrations

The vibrations of the methylene group (CH_2) are shown in Figure 2.3. The symmetrical and asymmetrical stretching and deformation vibrations are the three modes (in a group containing N atoms, there are 3N-6 vibrations) originating from the individual methylene groups . When the methylene groups comprise part of a hydrocarbon chain, rotational motions (wagging, twisting and rocking) occur in relation to the axis of the chain. The characteristic frequency, $\tilde{\nu}$, (in cm^{-1}) of a vibrator with unequal masses m_1 and m_2 at the ends (assuming linear elastic interaction according to Hooke's law) is given by:

$$\tilde{\nu} = \frac{1}{2\pi c}\sqrt{\frac{k}{\left(\frac{m_1 m_2}{m_1+m_2}\right)}} = \frac{1}{2\pi c}\sqrt{\frac{k}{\mu}} \qquad (2.10)$$

$\tilde{\nu}$ is proportional to the strength of the spring (force constant k of the bond in dynes per centimeter) and inversely proportional to the reduced mass (μ). c is the velocity of light.

2.3.2 Amide Group Vibrations

The amide group gives rise to a number of amide bands characteristic of both simple peptides and fibrous proteins. The following are the principal assignments of the major amide bands;

	Approximate wavenumber (cm^{-1})	Assignment
Amide I	1660	C = O stretch
Amide II	1570	N-H in-plane bend and C-N stretch

2.4 Phase Transition and Permeability Studies Using Infrared Spectroscopy

The frequency (ν) and the half bandwidths ($\Delta\nu_{1/2}$) of the individual vibrational modes relate to specific phenomena at the molecular level and can be used to discriminate between different motions of the absorbing groups. Using synthetic lipid systems, researchers have examined the effects of temperature and/or the inclusion of other molecule(s) in the model systems on the two parameters, ν and $\Delta\nu_{1/2}$ *[Amey and*

Chapman, 1983]. Since the intercellular lipids of the SC play a crucial role in determining the barrier property of skin, the following observations, which have been obtained using model lipid systems, are relevant.

2.4.1 Frequency Shifts

The frequency of a vibrational absorption is determined by the nature of both the vibrational mode and the vibrating group. The C-H stretching vibrations in acyl chains are decoupled from other vibrations occurring within the molecule; the bulk of the acyl groups are electronically decoupled from the polar head groups. Consequently, in the all-*trans* conformational state (Figure 2.4), each of these absorbances is observed at its characteristic frequency, regardless of the terminal functional groups, and is shifted only slightly as a result of interactions with molecules of a different class (for example, proteins). However, the effects of changes in conformation, specifically the introduction of *gauche* conformers (Figure 2.4), are large, producing shifts to higher frequencies. These shifts can be used to determine the introduction of *gauche* conformers or chain melting, the magnitudes of shifts being related to the number of *gauche* bonds *[Mantsch et al., 1985]*.

2.4.2 Half-bandwidth Changes

The width of the band contour results from rotational, translational and/or collisional effects. Thus, the half-bandwidth monitors the freedom of motion of the absorbing group, i.e., the amplitudes and rates of motion within its immediate environment. The half-bandwidths will, therefore, reflect the main gel to liquid crystalline phase transition (of the lipids), at which a considerable change in this environment occurs. It is also sensitive to other changes which do not introduce *gauche* conformers, such as a decreased freedom of vibrational or torsional motion of the chains.

Lipids in the gel state are primarily in the all *trans* configuration. As they go through the melting transition, there is a mixed population of both the *trans and gauche* states. However, once the transition is complete, the molecules are primarily in the all *gauche* conformation. From Figure 2.4, which shows the *trans* and *gauche* conformations of acyl side chains of a lipid, it is apparent that the methylene side chains of the *gauche* conformers have increased freedom of motion due to repulsion. To illustrate this point, the frequency of the C-H asymmetric stretching vibration for dimyristoyl-phophatidylcholine (DMPC) is plotted as a function of temperature in Figure 2.5. Introduction of the *gauche* conformers along the acyl chains of the lipid causes increased steric hindrance and the C-H absorbance frequency shifts to higher energy. It follows that the shift in the C-H absorbance is a measure of the level of disorder in the lipid system under consideration.

2.4.3 Permeability Studies

The biophysics literature contains many reports documenting the relationship between the permeability of a biomembrane and its lipid acyl chain conformation *[Crowe et al., 1989]*. Recently, Potts and Francoeur *[Potts and Francoeur, 1990]* have shown a strong correlation between the permeability of water through SC and SC lipid disorder. These studies suggest that it may be possible to predict the relative permeability of a biomembrane based on the spectroscopically determined disorder of the lipids comprising the biomembrane.

2.5 IR Spectroscopy of Skin

Figure 2.6 shows an IR spectrum of SC *in vivo* obtained using the ATR technique. The spectrum is identical to transmission spectra obtained from isolated SC sheets. Because our objective was to study the effects of chemical enhancers on skin *in vivo* (and because transmission spectroscopy cannot be used *in vivo)*, all measurements described

in this thesis have employed ATR-FTIR. The assignments of the different absorbances in Figure 2.6 have already been reported (see Table 2.1). For example, the C-H asymmetric and symmetric stretching absorbances arise primarily from the lipids of the SC. This has been demonstrated by lipid extraction studies. An IR spectrum obtained post-extraction of the lipids reveals a significant diminution of the C-H stretching absorbances, thereby proving that these absorbances are predominantly of lipid origin. Modifications that occur in the SC constituents (lipids and proteins) due to perturbants, e.g. chemical enhancers, can, therefore, be studied by following the changes in the IR spectrum of the SC. The next chapter illustrates this strategy.

References

Amey, R.L., and Chapman, D., 1983, Infrared Spectroscopic Studies of Model and Natural Biomembranes, in **Biomembrane Structure and Function**, Chapman, D., (ed.), Macmillan, London, 199-256.

Cortijo, M. Alanso, A., Gomez-Fernandez, J.C., and Chapman, D., 1982, Intrinsic Protein-lipid Interactions. Infrared Spectroscopic Studies of Gramicidin A, Bacteriorhodopsin and Ca-ATPase in Biomembranes and Reconstituted Systems, **Journal of Molecular Biology,** 157: 597-618.

Crowe, J.H., Crowe, L.M., and Hoekstra, F.A., 1989, Phase Transitions and Permeability Changes in Dry Membranes During Rehydration, **Journal of Bioenergetics and Biomembranes,** 21: 77-91.

Fringeli, U.P., and Günthard, Hs.H., 1981, Infrared Membrane Spectroscopy, in **Membrane Spectroscopy**, Grell, E. (ed.), Springer, Berlin, 270-332.

Griffiths, P.R., and de Haseth, J.A., 1986, **Fourier Transform Infrared Spectroscopy,** Wiley, New York.

Keighley, J.H., 1976, Infra-red Spectroscopy, in **Introduction to the Spectroscopy of Biological Polymers**, Jones (ed.), Academic Press, New York, 17-80.

Knutson, K., Potts, R.O., Guzek, D.B., Golden, G.M., McKie, J.E., Lambert, W.J., and Higuchi, W.I., 1986, Macro- and Molecular Physical-chemical Considerations in Understanding Drug Transport in the Stratum Corneum, **Journal of Controlled Release,** 2: 67-87.

Mantsch, H.H., Madec, C., Lewis, R.N.A.H., and McElhaney, R.N., 1985, Thermotropic Phase Behavior of Model Membranes Composed of Phosphatidylcholines Containing Iso-branched Fatty Acids. 2. Infrared and ^{31}P NMR Spectroscopic Studies, **Biochemistry,** 24: 2440-2446.

Nakamishi, K., and Solomon, P.H., 1977, **Infrared Absorption Spectroscopy** (2nd edition), Holden-Day, San Francisco.

Potts, R.O., and Francoeur, M.L., 1990, Lipid Biophysics of Water Loss through the Skin, **Proceedings of the National Academy of Science,** 87: 3871-3873.

Table 2.1 Infrared Band Assignments for Stratum Corneum Constituents *[Knutson et al., 1986]*.

Vibrational Motion	Origin	Frequency (cm^{-1})
O-H stretching	lipid	3500-3400
N-H stretching	protein, lipid	3400-3300
C-H stretching (asymmetric)	lipid (CH_2 acyl side chain)	2920
C-H stretching (symmetric)	lipid (CH_2 acyl side chain)	2850
C=O stretching	lipid	1740
C=O stretching (Amide I)	protein, lipid (amide linkage)	1640
N-H bending (Amide II)	protein, lipid (amide linkage)	1565
C-H bending and twisting	lipid, protein	1470-1400

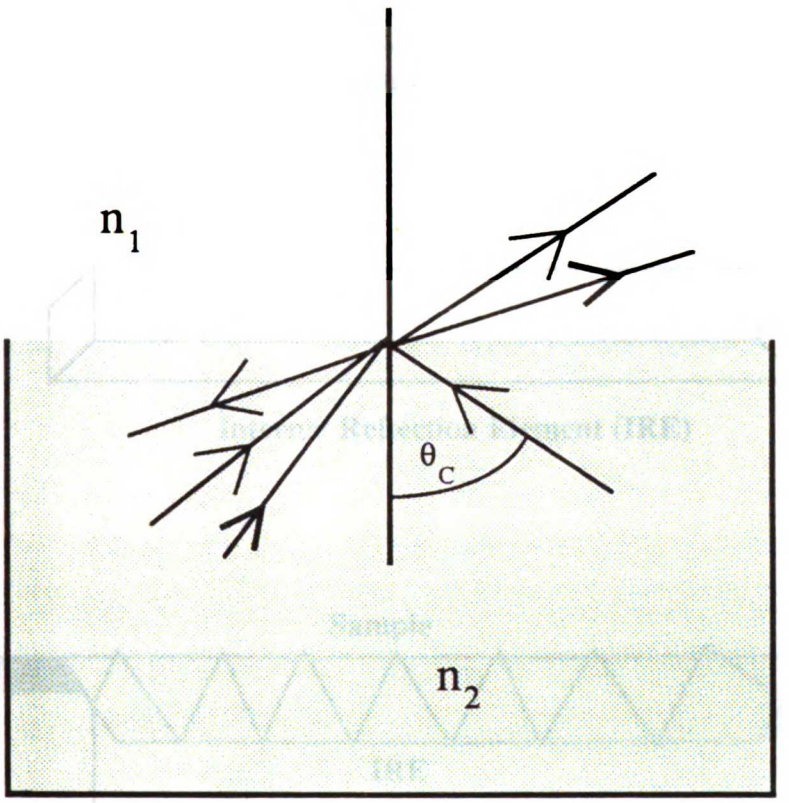

Figure 2.1 Refraction and reflection (total internal) at the interface of two media with refractive indices n_2 and n_1.

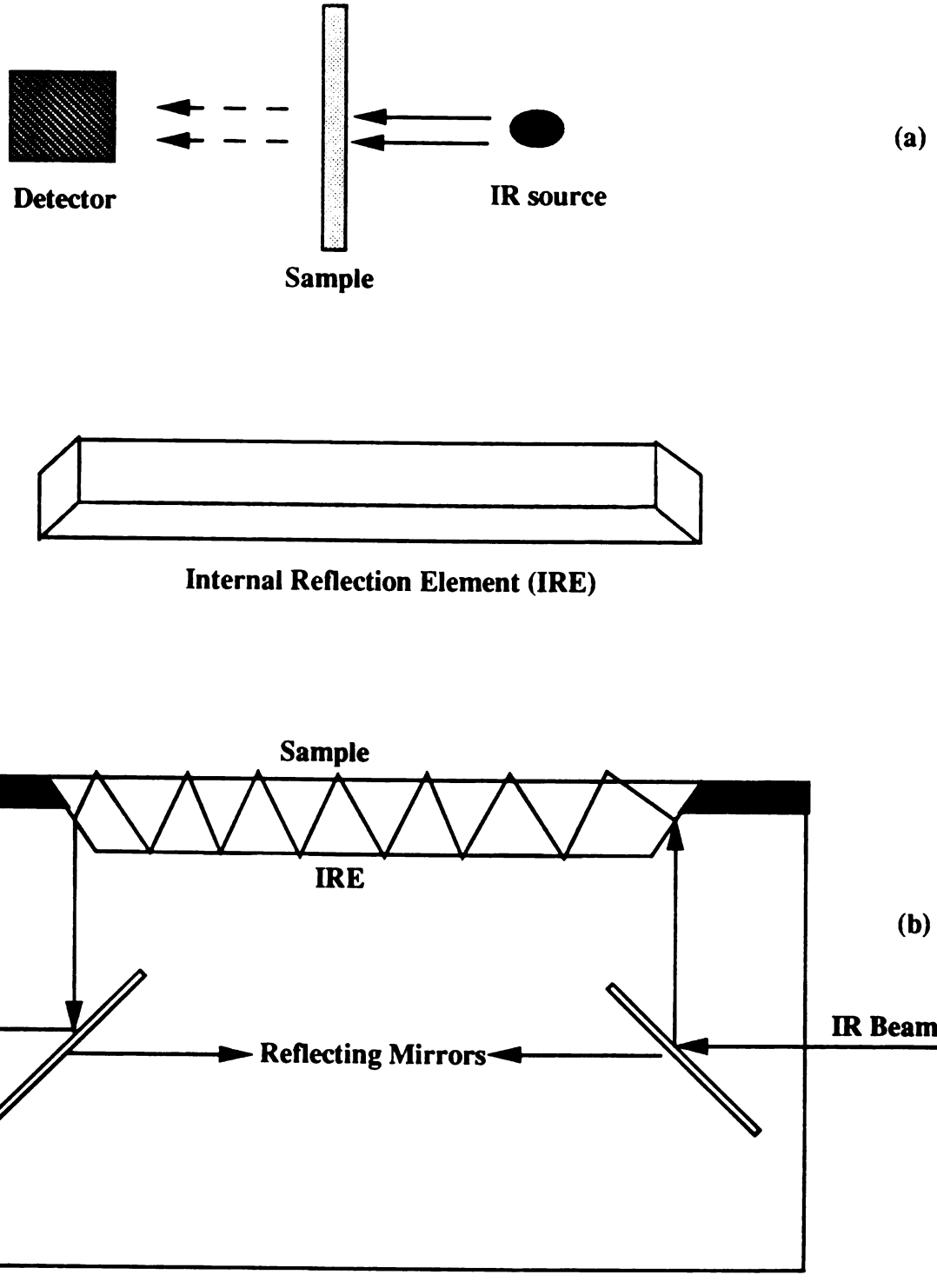

Figure 2.2 IR spectroscopy: (a) conventional transmission, and (b) attenuated total reflectance (ATR)

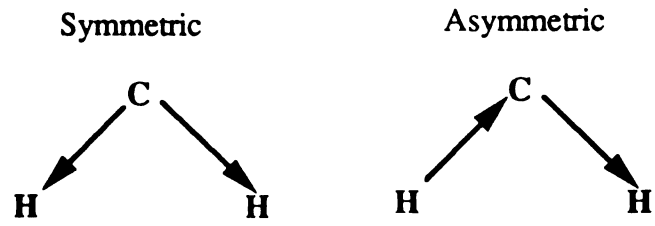

Figure 2.3 C-H stretching vibrations of the methylene alkyl side chains.

Figure 2.4 *Trans* and *gauche* conformations.

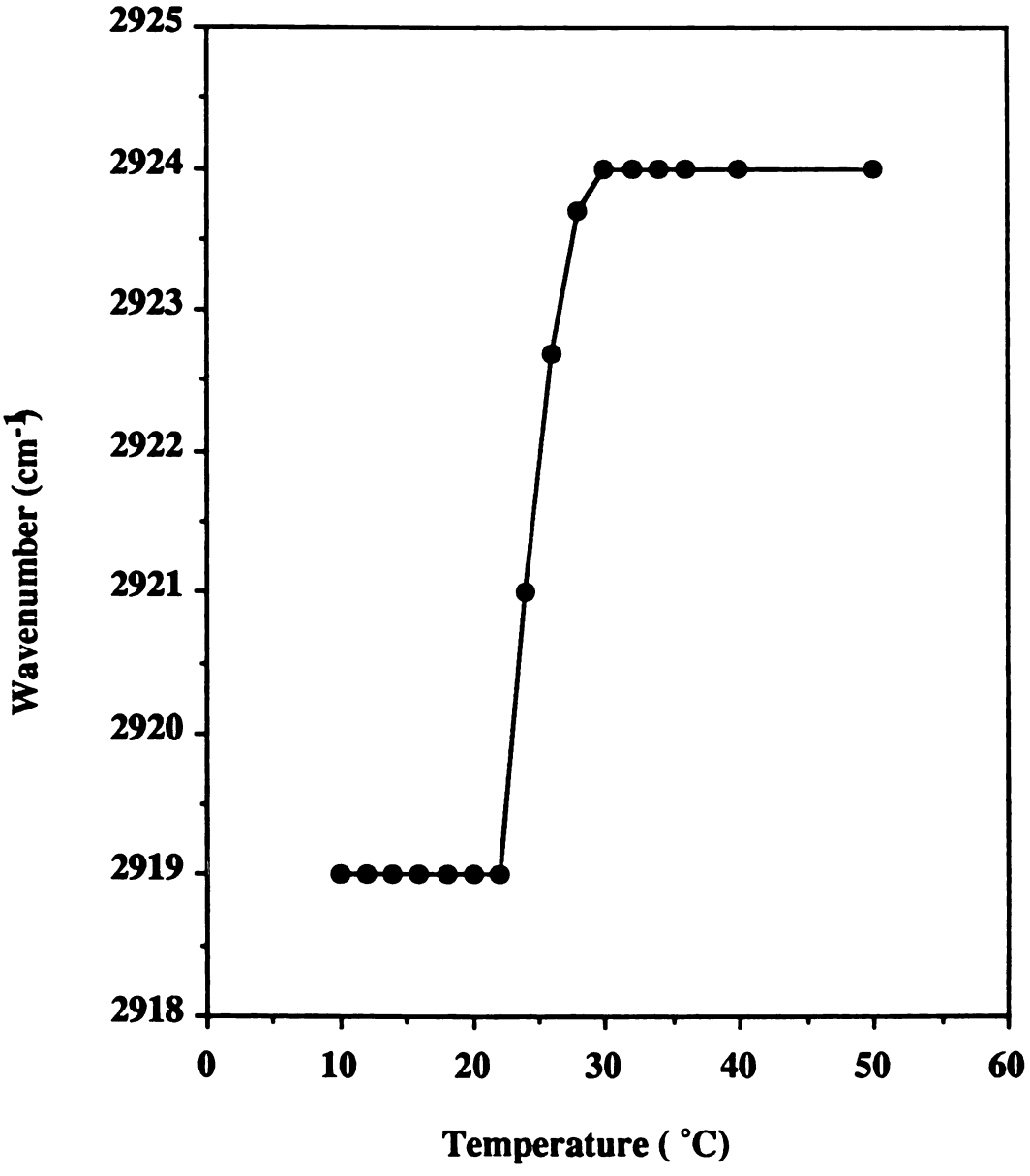

Figure 2.5 Temperature dependence of the infrared frequency of the methylene asymmetric stretching vibration in DMPC (from Cortijo et al., 1982).

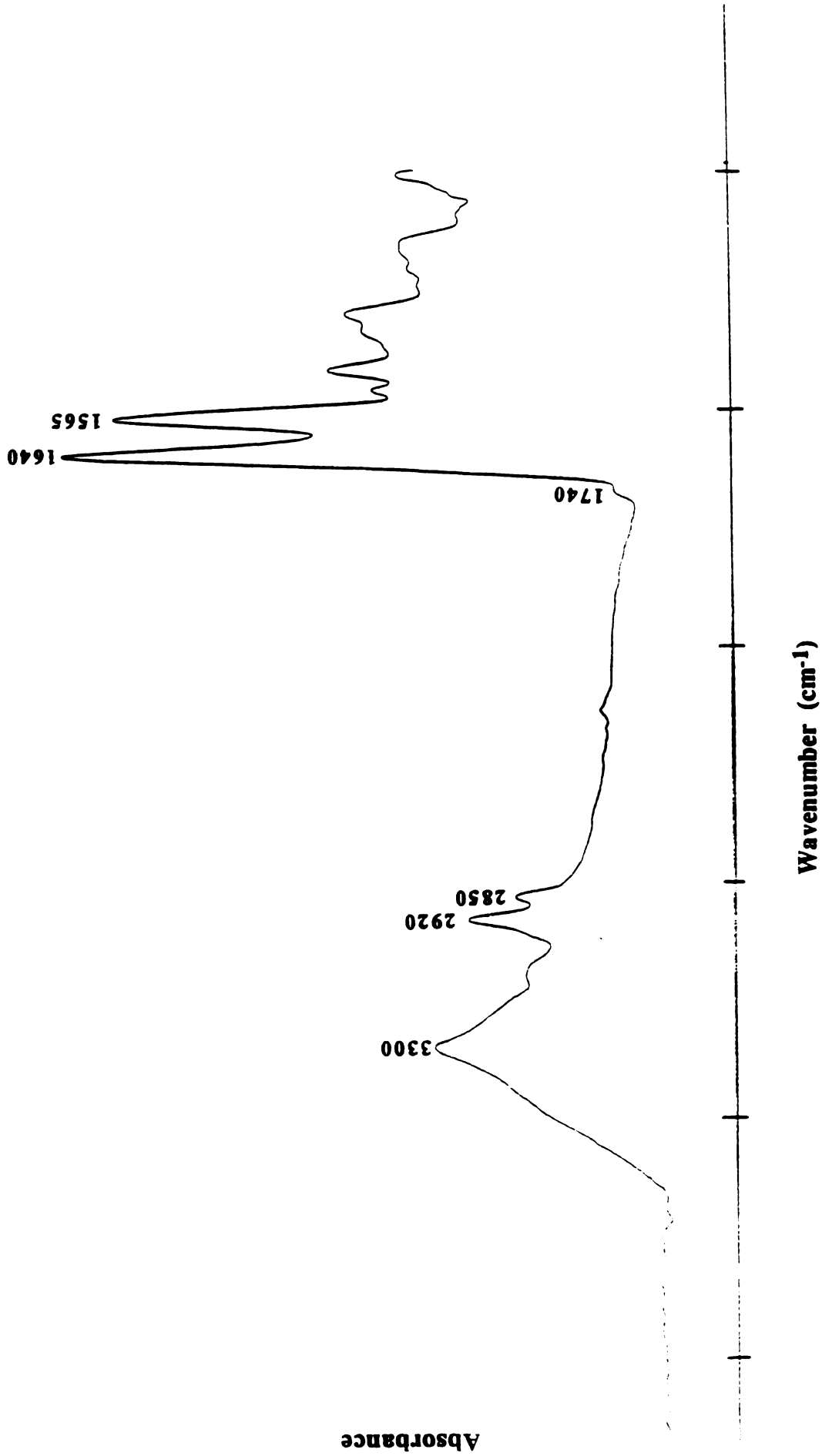

Figure 2.6 ATR-FTIR spectrum of SC *in vivo*.

Chapter 3a. Examination of Stratum Corneum Barrier Function *in vivo* by Infrared Spectroscopy

Examination of Stratum Corneum Barrier Function In Vivo by Infrared Spectroscopy

D. Bommannan, Russell O. Potts, and Richard H. Guy

Graduate Group in Bioengineering (DB, RHG), University of California, Berkeley, and University of California, San Francisco; Dermal Therapeutics Group (ROP), Pfizer Central Research, Groton, Connecticut; and Departments of Pharmacy and Pharmaceutical Chemistry (RHG), University of California, San Francisco, California, U.S.A.

It is generally accepted that the stratum corneum (SC) is the least permeable layer of the epidermis. Histologically, though, the SC is a non-uniform, inhomogeneous membrane, and the question "Is barrier function distributed uniformly across the SC thickness?" has been posed. To address this issue, human ventral forearm SC has been studied in vivo by attenuated-total-reflectance Fourier-transform infrared spectroscopy during the course of sequential tape-stripping. Because the intercellular lipids of the SC and the degree of hydration of the membrane have been shown to be crucial determinants of barrier function, attention has been focused on the spectral features, which report specifically on these parameters. The degree of disorder of the SC intercellular lipids has been found to decrease over the outer cell layers (up to three tape-strips) and then to remain essentially constant. The amount of lipids decreases similarly such that a 60% reduction (relative to the "no-strip" baseline) is observed after about four tape-strips. A plausible explanation for these measurements is that the lipids near the surface are a mixture of (a) "true" intercellular lipid (which is expected to be highly ordered), and (b) sebaceous lipid (which contains much greater amounts of low-melting components, such as fatty acids). The sequential infrared (IR) spectra provide at least circumstantial evidence to support this hypothesis. As expected, the IR spectra show that SC hydration increases from the surface towards the SC-stratum granulosum interface. Taken together, the results imply that the SC is indeed non-uniform. The properties of the outer layers (those removed by the first 3–4 tape-strips) change significantly with increasing depth. Subsequently accessed layers (those revealed by tape-strips 5 through 14) imply that this deeper part of the barrier is relatively consistent throughout its thickness, with no evidence for a single, particularly resistant, component. *J Invest Dermatol 95:403–408, 1990*

It is now established that the stratum corneum (SC) is the least permeable layer of mammalian skin [1–4]. This thin, outermost membrane is a formidable barrier to transepidermal water loss and to the percutaneous absorption of topically applied drugs. The SC is typically 10–20-μm thick and is often schematically represented as a brick wall [4–6]. The terminally differentiated, keratin-filled corneocytes are the "bricks," while the lamellar, intercellular lipid domains represent the "mortar." That the properties of the brick wall are not uniform throughout its thickness is obvious from a number of simple observations. For example, the continuous turnover of the cells of the skin means that, on average, the SC sloughs a layer of corneocytes per day; it is difficult to reconcile this desquamation process with the argument that the SC properties are essentially invariant with depth. Lipid metabolism within the SC has been documented [7–11] and has been suggested as a key step in normal SC turnover. An inhomogeneity in lipid distribution in the SC is, therefore, implicated.

Given the primary role of the SC, namely, barrier function, it is not surprising that previous research has been directed to answer the question of where, in the SC, the actual barrier resides. There have been claims that the "true barrier layer" is situated at the base of the SC [12,13]. This deduction is primarily based upon an interpretation of the effect of sequential adhesive tape-stripping of the SC on transepidermal water loss. Others have analyzed this dependence more appropriately [1,14] and have come to the contrary conclusion that the barrier properties are more evenly distributed across the entire thickness of the SC.

An improved understanding of the make-up of the SC barrier is of interest per se, and is relevant both to the design of percutaneous penetration enhancement strategy [15] and to the optimization of topical therapy for the treatment of damaged skin. The experiments in this paper are biophysical measurements of human SC in vivo. The technique of attenuated total-reflectance Fourier-transform infrared (ATR-FTIR) spectroscopy [16] has been used to examine certain features of the SC as a function of sequential tape-stripping. The properties of the intercellular lipids and the level of hydration have been studied. The results show that the SC is a non-uniform membrane, characterized by gradients of the measured properties. Using the single procedure of ATR-FTIR spectroscopy, therefore, a gross structural model of the SC has been constructed on the basis of

Manuscript received November 7, 1989; accepted for publication April 21, 1990.

This research was supported by a grant (HD-23010) from the U.S. National Institutes of Health. D. Bommannan was the recipient of a Chancellor's fellowship and a Graduate Student Research award from the University of California.

Reprint requests to: Dr. Richard H. Guy, School of Pharmacy, University of California, San Francisco, San Francisco, CA 94143-0446.

Abbreviations:
ANOVA: analysis of variance
ATR-FTIR: attenuated total reflectance-fourier transform infrared
IR: infrared
IRE: internal reflection element
n: refractive index
SC: stratum corneum
ν: wavenumber

0022-202X/90/$03.50 Copyright ©1990 by The Society for Investigative Dermatology, Inc.

the recorded observations. The model is consistent with basic SC morphology and it can account for the overall distribution of barrier function deduced by other experiments.

MATERIALS AND METHODS

Attenuated Total Reflectance-Fourier Transform Infrared Spectroscopy (ATR-FTIR) The application of ATR-FTIR to study the biophysical properties of the stratum corneum (SC) has been reported [17–19]. In contrast to classic transmission spectroscopy, where the sample intercepts the path of the IR beam, in ATR the sample is placed on an IR transparent crystal, the geometry of which permits almost total internal reflection. Thus, the IR beam is directed to the crystal [the internal reflection element (IRE)], from which an evanescent wave exits and penetrates into the sample that is in contact with the IRE. The symmetric, trapezoidal geometry of the optics then guides the beam back to the detector of the spectrophotometer. In this way, a spectrum of human SC in vivo can be obtained; the general features of the spectrum are identical to those observed in a transmission measurement using an excised sheet of the membrane [18].

In this study, an Analect FX-6200 Fourier-transform infrared spectrophotometer (Laser Precision Devices, Irvine, CA) was used to record the in vivo measurements. The spectrophotometer was equipped with an ATR accessory (Skin Analyzer, Spectra Tech, Stamford, CT), which supported a zinc sulfide IRE ($7.5 \times 1 \times 0.2$ cm, with a 60° incident angle). This ATR configuration results in a penetration depth of the IR beam of approximately 2 μm [16]. All spectra reported were the average of 50 scans (requiring a data collection period of about 90 sec). Location of the IR absorbance-peak maxima was determined to an accuracy of 0.1 cm^{-1} using a center-of-gravity algorithm [20].

Experiments The goal of these studies was to examine the IR spectral properties of human SC in vivo as a function of position within the barrier. Because it is not technically possible at this time to focus the IR beam to different depths in the SC, the optically inaccessible layers were revealed by the acquisition of multiple spectra during sequential tape-stripping of the membrane.

The experimental subjects were healthy volunteers (ages 23–30 years) with no history of dermatologic disease. The skin site examined was the ventral forearm; other than daily washing, this region of skin received no self-administered application of any topical product (lotion, cream, emollient, etc.).

At the beginning of the experiment, the skin site was cleaned by gentle wiping with dry Q-tips. An IR spectrum was then recorded. Using Scotch brand 600 transparent tape (3M, St. Paul, MN), the first tape-strip was removed from the SC. The IR spectrum was again recorded. This sequence was repeated for six tape-strips. Subsequently, spectra were recorded every two strips up to a total of 14. In all, therefore, 10 spectra plus the initial pre-treatment control were acquired.

In a separate series of measurements on the same subjects, in order to quantify the amount of SC removed by the tape-stripping procedure, the pieces of tape used were weighed before and after stripping.

Spectral Analysis FTIR spectra were collected in the frequency range 4400–400 cm^{-1}. The following features of the spectra, and the rationale for their evaluation, were examined as a function of tape-strip number: (a) the frequency shift, and the bandwidth at half-height, of the C-H asymmetric stretching absorbance observed at approximately 2920 cm^{-1}. The membrane biophysics literature [21,22] contains many examples in which permeability is correlated with lipid disorder (in this context, disorder is correlated with the reciprocal of viscosity, and indicates the degree of freedom of motion of the lipid acyl side chains). Whereas the SC is not a simple biomembrane, a relationship between permeability and intercellular lipid disorder has been demonstrated [23,24]. IR spectroscopy can be used to report on biomembrane lipid ordering through the C-H stretching absorbances from the methylene groups of the lipid acyl chains. For example, as the degree of disorder of the lipid acyl chains increases, the C-H stretching absorbances undergo a blue shift, i.e., shift to higher wavenumber [25,26]. It has been found that the C-H asymmetric stretching absorbance is sensitive to these changes in the SC [26], and the shift in the peak of this band has been used, therefore, to monitor lipid freedom in this study. Equally, the bandwidth at half-height of the C-H stretching absorbance also reflects the relative lipid acyl chain ordering: the greater the disorder of the acyl chains, i.e., the larger the number of gauche conformers [24–26], the greater the bandwidth.

(b) The area under the C-H asymmetric stretching absorbance (over the frequency range 2945–2875 cm^{-1}). The integrated intensity (area under the curve) of an infrared absorbance is directly proportional to the amount of the absorbing species [27,28]. The area under the C-H asymmetric stretching absorbance was computed to report on the relative amount of lipid present as a function of depth into the SC. Earlier work [29] has shown that the C-H asymmetric stretching absorbance originates almost entirely from the SC intercellular lipids. In ATR-IR, however, integrated intensity measurements are complicated by the fact that the intensity of an absorbance is related to the degree of contact established between the sample (in this case, the forearm) and the IRE [16]. In vivo, it is very difficult to ensure reproducible contact both within and between subjects. Consequently, to obtain meaningful results, a normalization procedure was employed (Fig 1). With increasing contact between sample and IRE, there is enhanced light scattering, leading to an enhancement in the area between the signal and the baseline. This affects both areas A and B in Fig 1. The ratio A/B, however, is degree-of-contact independent, and this is the parameter calculated. The relative nature of this quotient means, of course, that absolute measurements of the lipids as a function of SC position are not possible. Nevertheless, the proportional change with respect to the level at the surface can be accurately deduced.

(c) The frequency shift of the amide I (~1640 cm^{-1}) and amide II (~1565 cm^{-1}) stretching absorbances [26,27]. The behavior of these peak maxima report on the level of hydrogen bonding of the amide linkages within the SC. They do not, however, distinguish between the amide linkages in proteins (primarily keratin) and amide bonds in lipids (for example, ceramides). The amide I corresponds to the carbonyl stretch in the –CO–NH– group. If the C=O bond is involved in increased hydrogen bonding, stretching is easier and the absorbance occurs at a lower wavenumber. On the other hand, the amide II absorbance reflects the amide N–H in-plane bending mode. Now, if the amide hydrogen is influenced by increased H-bonding to an adjacent oxygen, e.g., from H_2O, bending of the N–H bond becomes more difficult, resulting in a shift in the amide II absorbance to higher wavenumber.

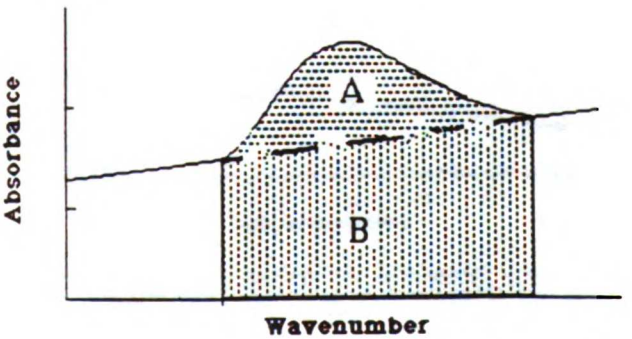

Figure 1. Normalization of an IR absorbance to permit relative quantitation of the absorbing species corrected for variations in skin-IRE contact. The area above the *dashed baseline* is proportional to the amount of the absorbing species. The area *below the line* is proportional to the degree of skin contact with the IRE, a variable which also impacts upon the IR absorbance *above the line*. The ratio of areas *(above:below)* provides an appropriate, normalized estimation of the relative amount of the absorbing species.

(d) The area under the secondary O–H stretching (water) absorbance at 2100 cm^{-1}. Potts et al [18] showed that the normalized area under the secondary O–H band centered around 2100 cm^{-1} could be used to estimate the SC water concentration. The same procedure was employed in this work for the identical purpose.

Statistical Analysis Weights of SC removed, and spectroscopic parameters determined, as a function of tape-strip number, were compared using a repeated measures analysis of variance (ANOVA, 95% confidence limits), followed, if necessary, by Scheffe's F-test [36].

RESULTS

The spectral analyses undertaken in this work primarily focus upon the content and organization of the SC intercellular lipids, and the degree of hydrogen bonding (or hydration) as a function of position. Figure 2 shows the shift in the peak of the C-H asymmetric stretching absorbance as a function of tape-stripping. The control, no-strip (pre-treatment) measurement is assigned a shift of zero. Relative to this baseline, the maximum shift, on average, is approximately $-2.5\ cm^{-1}$, that is, a decrease in frequency, which occurs after the removal of about four tape-strips. Subsequent stripping of the SC layers induces no further significant changes in the ν (C-H). The bandwidth at half-height of the C-H asymmetric stretching absorbance demonstrates entirely comparable behavior (Fig 3), as expected. By way of comparison, recent ATR-FTIR experiments from our laboratories [31] have shown that a penetration enhancer (oleic acid) causes a blue shift of approximately $+3\ cm^{-1}$ in the peak ν (C-H), and, concomitantly, reduces the barrier function to drug penetration. The SC lipids were further examined by determining the relative amounts present as a function of depth into the membrane (Fig 4). Compared to the initial amount, there is a 60% reduction by the time 4 strips have been removed; thereafter, there is a much less dramatic decline with tape-strip number. Hence, there are more, but less ordered, lipids near to the skin surface.

The shifts in the peak frequencies of the amide I and amide II absorbances as a function of tape-stripping are shown in Fig 5. Relative to the baseline (no strip) values, the amide I absorbance red-shifts (moves to lower wavenumber), whereas the amide II undergoes a blue-shift (to higher wavenumber). Figure 6 reports the relative water content of the SC as a function of depth. As expected, as the number of tape-strips increases, the level of SC hydration also increases, consistent with the results of Fig 5, which indicate progressively increasing H-bonding further and further into the SC (reflecting, presumably, therefore, the increasing availability of water). However, statistical analysis of the data in Fig 6 reveals significant differences ($p < 0.05$) only between the measurements following (a) the no-strip control and tape-strips 2 through 14, and (b) tape-strip 1, and tape-strips 4 and 10 through 14.

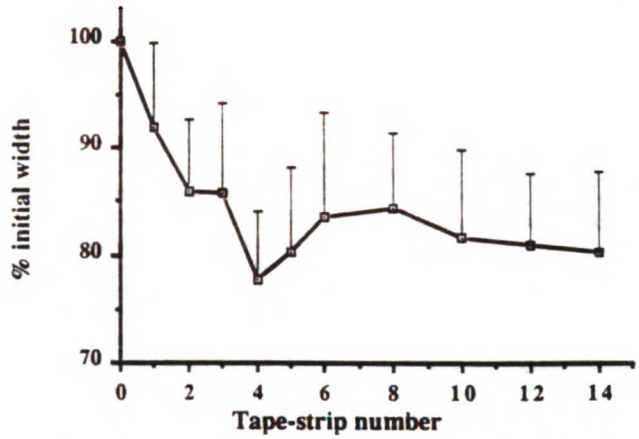

Figure 3. Bandwidth at half-height of the C–H asymmetric stretching absorbance (expressed as % of the baseline, no-strip bandwidth) as a function of tape-strip number (mean ± SD; n = 13). An analysis of variance followed by Scheffe's F-test shows that: (a) all bandwidths are significantly different ($p < 0.05$) from the pre–tape-strip (no strip) control; (b) the bandwidth after one tape-strip is significantly different ($p < 0.05$) from those after 2, 4, 5, 10, 12, and 14 tape-strips; (c) the bandwidth after 2 tape-strips is significantly different ($p < 0.05$) from that after 4 tape-strips; and (d) all other comparisons between bandwidths as a function of tape-strip number are not significantly different ($p > 0.05$).

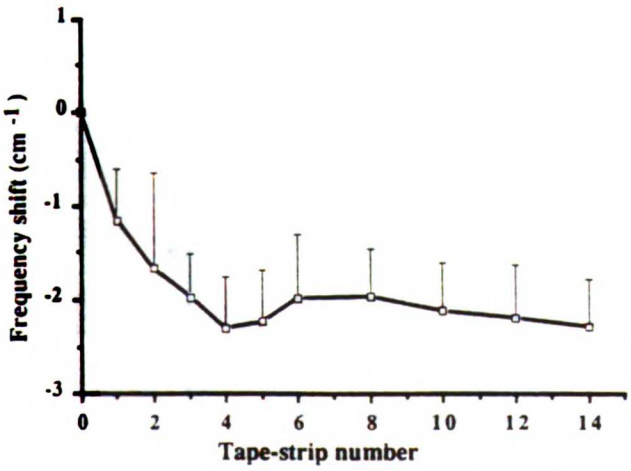

Figure 2. Frequency shift of the C-H asymmetric stretching absorbance as a function of tape-strip number (mean ± SD; n = 13). An analysis of variance followed by Scheffe's F-test shows that: (a) all frequency shifts are significantly different ($p < 0.05$) from the pre–tape-strip (no-strip) control; (b) the frequency shift after one tape-strip is significantly different ($p < 0.05$) from those after two through 14 tape-strips; (c) the frequency shift after two tape-strips is significantly different ($p < 0.05$) from that after three tape-strips; and (d) all other comparisons between frequency shifts as a function of tape-strip number are not significantly different ($p > 0.05$).

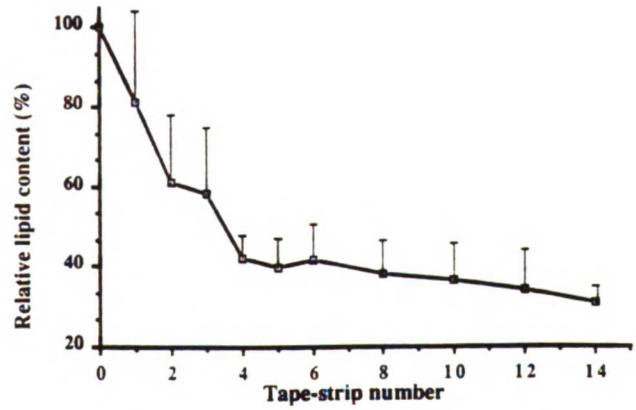

Figure 4. Relative lipid content within the SC (expressed as % of the baseline no-strip estimation) as a function of tape-strip number (mean ± SD; n = 13). An analysis of variance followed by Scheffe's F-test shows that: (a) all lipid contents are significantly different ($p < 0.05$) from the pre–tape-strip (no-strip) control; (b) the lipid content after one tape-strip is significantly different ($p < 0.05$) from those after two through 14 tape-strips; (c) the lipid content after two tape-strips is significantly different ($p < 0.05$) from that after four tape-strips; (d) the lipid content after three tape-strips is significantly different ($p < 0.05$) from that after four tape-strips; and (e) all other comparisons between lipid content as a function of tape-strip number are not significantly different ($p > 0.05$).

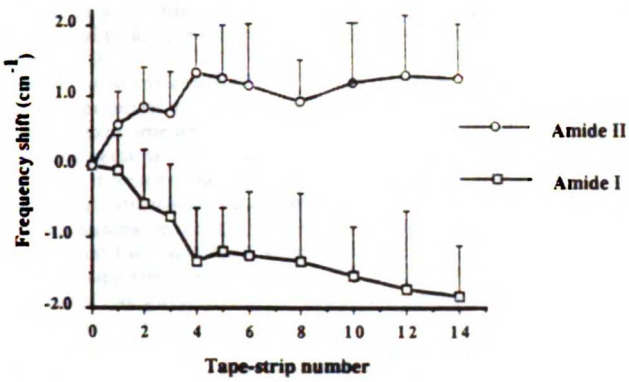

Figure 5. Frequency shifts of the amide I and amide II absorbances as a function of tape-strip number (mean ± SD; n = 13). An analysis of variance followed by Scheffe's F-test shows that for the amide I shifts: (a) all frequency shifts from four through 14 tape-strips are significantly different ($p < 0.05$) from the pre-tape-strip (no-strip) control; (b) the frequency shift after one tape-strip is significantly different ($p < 0.05$) from those after four through 14 tape-strips; (c) the frequency shift after two tape-strips is significantly different ($p < 0.05$) from those after 12 and 14 tape-strips; and (d) all other comparisons between frequency shifts as a function of tape-strip number are not significantly different ($p > 0.05$). For the amide II shifts, (a) all frequency shifts from four through 14 tape-strips are significantly different ($p < 0.05$) from the pre-tape-strip (no-strip) control; and (b) all other comparisons between frequency shifts as a function of tape-strip number are not significantly different ($p > 0.05$).

DISCUSSION

The literature has established the essential role of the intercellular lipids in SC barrier function [4,7,32], and the hydration gradient across the SC (and its maintenance) is now recognized as a fundamental signal of the state (the health) of the barrier [7,32]. With respect to the latter, for example, recent work has shown how the increase in transepidermal water loss caused by SC damage very quickly provokes lipid biosynthetic pathways in the epidermis [7,33].

The measurements in Fig 2 imply that, whereas the SC lipids are consistently (and well) ordered throughout the bulk of the membrane, the intercellular domains near the surface are significantly less structured. A possible deduction from these observations is that the outer SC layers represent somewhat less of a barrier than the interior. The "mortar" appears to be less sticky, a hypothesis supported by the fact that the outer layers are those which will desquamate in the near future.

An explanation for the decreased amounts of lipids in the deeper layers (Fig 4) is that the lipids near the surface represent a mixture of true intercellular lipids and sebaceous lipids. Whereas the intercellular lipids of the SC are expected to form ordered domains (and, indeed, do so in the deeper layers), sebaceous lipids contain large quantities of relatively low-melting-point fatty acids [9,34]. Because the sebaceous lipids are delivered to the skin surface, their impact on the order and composition of the overall SC lipid domain is attenuated quite quickly as one proceeds (through the sequential tape-stripping) into the membrane. Some support for this interpretation of the data (Figs 2, 3, and 4) is provided by the spectra in Fig 7. The shoulder (at ~ 1740 cm^{-1}) on the amide I absorbance occurs at a frequency characteristic of the carbonyl stretching of the fatty-acid carboxylic functional group. The sequential spectra show that this absorbance is large when only a few layers of SC have been removed, but diminishes to a small and relatively constant value by the time four or five tape-strips have been taken.

The change in relative water content as a function of tape-strip number is small. Similar findings, also using ATR-IR, have been reported previously [35,36], although in these latter studies, water content was measured by the ratio of the amide I to amide II absorbances. The value of these spectroscopic measurements has been called into question by the more recent work of Warner et al [37], who used electron-probe analysis to assess the water concentration profile across the SC. The latter experiments reveal a steeper change

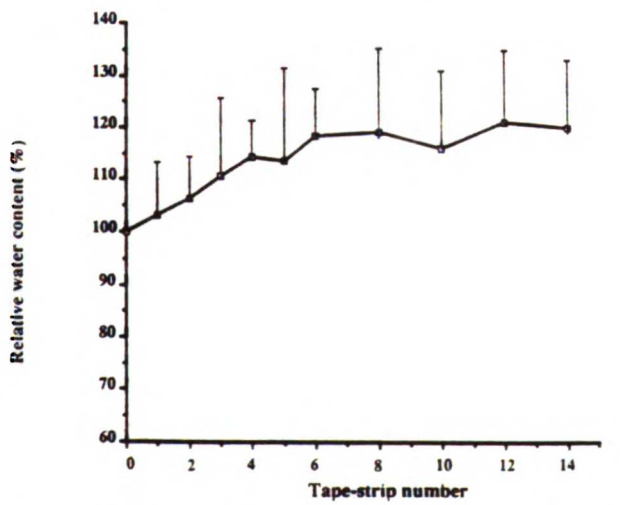

Figure 6. Relative water content within the SC (expressed as % of the baseline, no-strip estimation) as a function of tape-strip number (mean ± SD; n = 13). An analysis of variance followed by Scheffe's F-test shows that: (a) all water content values following two through 14 tape-strips are significantly different ($p < 0.05$) from the pre-tape-strip (no-strip) control; (b) the water content after one tape-strip is significantly different ($p < 0.05$) from those after four 10, 12, and 14 tape-strips; (c) all other comparisons between water content as a function of tape-strip number are not significantly different ($p < 0.05$).

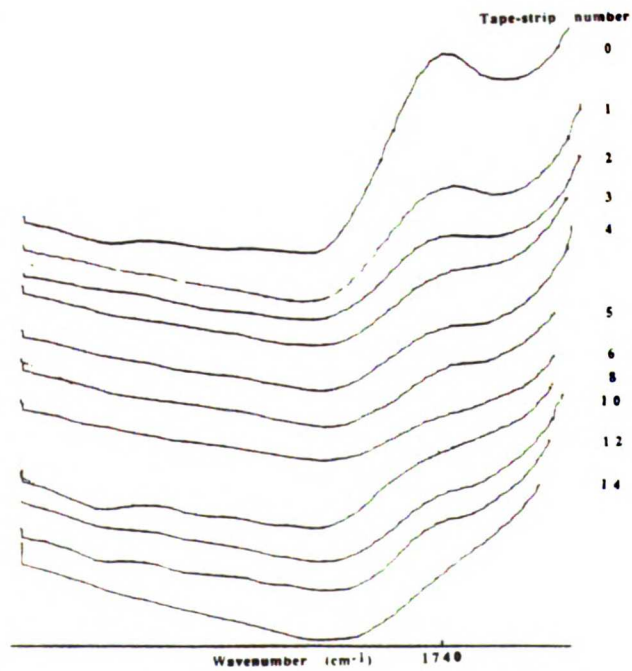

Figure 7. Sequential IR spectra recorded during progressive tape-stripping in the frequency range (1700–1850 cm^{-1}). The significant shoulder at 1740 cm^{-1} (a characteristic fatty acid absorption frequency) diminishes rapidly to a relatively small, constant value within the first few tape-strips.

in water content as a function of depth, and suggest that IR is probably not an ideal technique for the evaluation of relative water content within the SC.

Before proceeding to the conclusions that may be drawn from this work, it is appropriate to discuss the potential artifacts and limitations of the experimental procedures adopted. An obvious series of questions pertains to the tape-stripping technique: Is it reproducible? Does it remove one cell-layer per strip? Does it contaminate the spectral information subsequently obtained due to residual adhesive remaining on the skin? With respect to the first two issues, we found that the cumulative weight per unit area of SC removed by the 14 tape-strips performed was $275 \pm 25\ \mu g/cm^2$. A plot of cumulative SC weight removed per unit area as a function of tape-strip number is shown in Fig 8. ANOVA ($p < 0.05$) indicated that the weight of SC removed per strip is independent of tape-strip number. The average weight per unit area of SC removed by one tape-strip was $20 \pm 5\ \mu g/cm^2$.

From the above, we can deduce that the tape-strip procedure is quite reproducible. Previous methods have reported that the number of tape-strips necessary to remove the SC of the flexor aspect of the forearm typically falls in the range 10 to 30 [38]. Similarly, the number of SC cell-layers has been determined to be about the same. Thus, we may conclude that the tape-stripping procedure is indeed removing, on average, one SC layer per strip. The 14 strips taken in the experiments described here, therefore, must correspond to the removal of at least half of the SC, and more likely, to 75% or more removal. Based on this conclusion, and the published ranges of SC thickness on the flexor forearm (average 10 μm) [39,40], we may calculate that we have tape-stripped to a depth of between 5 and 8 μm (ranging from, minimally, 3–7 μm to, maximally, 5–12 μm).

The adhesive tape used absorbs significantly in a region of the IR spectrum (2700–1800 cm^{-1}) where the SC is transparent. Contamination of the SC spectrum by the adhesive would be clearly obvious, therefore, were it to occur. However, no such absorbance was observed in any of the recorded spectra, leading us to conclude that no IR-detectable residue remained on the SC surface post-stripping.

The depth of IR beam penetration should also be remarked upon. First, the SC spectra are not a pure reflection of the outermost layer. Indeed, they represent a weighted average over the outermost few layers. Nevertheless, the trends in the data and the general nature of the behavior deduced remain unchanged. Second, and potentially more important, is the issue that, because skin hydration changes with SC position, so too does the refractive index (n) of the skin,

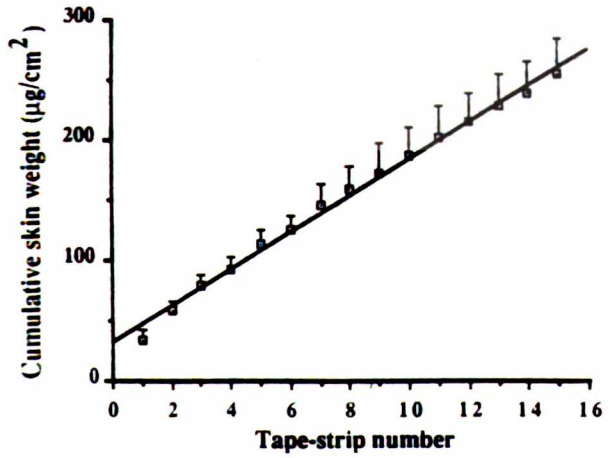

Figure 8. Cumulative weight per unit area of SC removed by sequential tape-stripping (mean ± SD; n = 8). An analysis of variance followed by Scheffe's F-test shows that the weight of the SC removed per strip is independent of the tape-strip number.

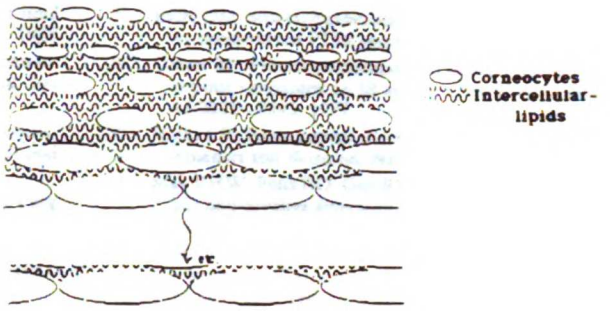

Figure 9. Schematic model of the SC based on the spectroscopic measurements reported in this paper.

and hence this will change the IR beam penetration depth [16]. The refractive index of dry, scaly SC is about 1.55 [41,42], whereas n of water is 1.33. The refractive index of SC in vivo is very likely, therefore, to fall in the range 1.33–1.55. If the maximum error is introduced into the calculation of beam penetration we use $n_{(skin)} = 1.33$ instead of 1.55), the impact is less than a 20% correction, a factor which cannot significantly affect the deductions presented above.

The results obtained support the schematic model of the SC shown in Fig 9. There is a decrease in the amount of intercellular lipid per layer as distance into the SC from the surface increases. Thus, the fractional volume occupied by the corneocytes increases with increasing depth. This may also be reflected in the greater anticipated hydration of the lower SC layers. The crude interpretation of the SC in Fig 9 is consistent with microscopic histology [43–45], which reveals dense corneocytes surrounded by relatively large amounts of lipid near the skin surface, and larger corneocytes with smaller intercellular spaces deeper in the membrane.

In conclusion, therefore, this ATR-FTIR study has permitted a novel examination of the SC (in particular, the intercellular lipid domains and the degree of hydration) to be performed in vivo in humans. It appears that the SC barrier is not uniform across its entire thickness: the outer few layers appear to be less cohesive, and the intercellular lipids more disordered, than the deeper, remainder of the membrane. There is no evidence to support a single, high-resistance component responsible for the major part of barrier function.

We thank our fearless volunteers, and the advice and criticism of our colleagues in California and Connecticut; in particular, we appreciate the input of Drs. Robert Hinz, Vivien Mak, and Michael Francoeur.

REFERENCES

1. Blank IH, Scheuplein RJ: Transport into and within the skin. Br J Dermatol 81:4–10, 1969
2. Scheuplein RJ: Percutaneous absorption after twenty-five years: or "old wine in new wineskins." J Invest Dermatol 76:31–38, 1976
3. Behl CR, Barrett M, Flynn GL, Kurihara T, Walters K, Gatmaitan O, Harper N, Higuchi W, Ho NF, Pierson C: Hydration and percutaneous absorption III: Influences of stripping and scalding on hydration alteration of the permeability of hairless mouse skin to water and n-alcohols. J Pharm Sci 71:229–234, 1982
4. Elias PM: Epidermal lipids, barrier function and desquamation. J Invest Dermatol 80:44s–49s, 1983
5. Michaels AS, Chandrasekaran SK, Shaw JE: Drug permeation through human skin: theory and in vitro experimental measurement. J Am Inst Chem Eng 21:985–996, 1975
6. Landmann L: The epidermal permeability barrier. Anat Embryol 178:1–13, 1988
7. Grubauer G, Feingold KR, Elias PM: Relationship of epidermal lipogenesis to cutaneous barrier function. J Lipid Res 28:746–752, 1987

8. Hedberg CL, Wertz PW, Downing DT: The time course of lipid biosynthesis in pig epidermis. J Invest Dermatol 91:169–174, 1988
9. Lampe MA, Williams ML, Elias PM: Human epidermal lipids: characterization and modulation during differentiation. J Lipid Res 24:131–140, 1983
10. Monger DJ, Williams ML, Feingold KR, Brown BE, Elias PM: Localization of sites of lipid biosynthesis in mammalian epidermis. J Lipid Res 29:603–612, 1988
11. Ziboh VA, Chapkin RS: Metabolism and function of skin lipids. Prog Lipid Res 27:81–105, 1988
12. Eriksson G, Lamke L: Regeneration of human epidermal surface and water barrier function after stripping. Acta Derm Venereol 51:169–178, 1971
13. Bowser PA, White RJ: Isolation, barrier properties and lipid analysis of stratum compactum, a discrete region of the stratum corneum. Br J Dermat 112:1–14, 1985
14. Idson B: Percutaneous absorption. J Pharm Sci 64:901–923, 1975
15. Walters KA: Penetration enhancers and their use in transdermal therapeutic systems. In: Hadgraft J, Guy RH (eds.). Transdermal Drug Delivery, Developmental Issues and Research Initiatives. Marcel Dekker, New York, 1988, pp 197–246
16. Mirabella Jr. FM, Harrick NJ: Internal reflection spectroscopy: review and supplement. Harrick Scientific Corporation, Ossining, New York, 1985
17. Putnam NA: Attenuated total reflectance studies of skin. J Soc Cosmet Chem 23:209–226, 1979
18. Potts RO, Guzek DB, Harris RR, McKie JE: A non-invasive, in vivo technique to quantitatively measure water concentration of the stratum corneum using attenuated total-reflectance infrared spectroscopy. Arch Dermatol Res 277:489–495, 1985
19. Bommannan D, Potts RO, Guy RH: Examination of the intercellular lipids of the stratum corneum. J Invest Dermatol 92:405, 1989
20. Cameron DG, Kauppinen JK, Mantsch H: Precision in condensed phase vibrational spectroscopy. Appl Spec 36:245–250, 1982
21. Amey RL, Chapman D: IR spectroscopic studies of model and natural biomembranes. In: Chapman D (ed.). Biomembrane Structure and Function. Macmillan, London, 1983, pp 199–256
22. Casal HL, Mantsch H: Polymorphic phase behavior of phospholipid membranes studied by IR spectroscopy. Biochim Biophys Acta 779:381–401, 1984
23. Golden GM, McKie JE, Potts RO: The role of stratum corneum lipid fluidity in transdermal drug flux. J Pharm Sci 76:25–28, 1986
24. Knutson K, Krill SL, Lambert WJ, Higuchi WI: Physicochemical aspects of transdermal permeation. J Control Rel 6:59–74, 1987
25. Lee DC, Chapman D: IR spectroscopic studies of biomembranes and model membranes. Bioscience Reports 6, 1986, pp 235–256
26. Fringeli UP, Gunthard HsH: Infrared Membrane Spectroscopy. In: Grell E (ed.). Membrane Spectroscopy. Springer, Berlin, 1981, pp 270–332
27. Keighley JH: Infra-red spectroscopy. In: Jones (ed.). Introduction to the Spectroscopy of Biological Polymers. Academic Press, New York, 1976, pp 17–80
28. Byler DM, Susi H: Examination of the secondary structure of proteins by deconvolved FTIR spectra. Biopolymers 25:469–487, 1986
29. Oertel RP: Protein conformational changes induced in human SC by organic sulfoxides: an IR spectroscopic investigation. Biopolymers 16:2329–2345, 1977
30. Hicks CR: Fundamental concepts in the design of experiments. Holt, Rinehart and Winston, New York, 1982, pp 52–53
31. Mak VHW, Potts RO, Guy RH: Oleic acid concentration and effect in SC: non-invasive determination by attenuated total reflectance infrared spectroscopy. J Control Rel 12:67–75, 1990
32. Elias PM, Cooper E, Korc A, Brown A: Percutaneous transport in relation to SC structure and lipid composition. J Invest Dermatol 76:297–301, 1981
33. Elias PM, Brown B: The mammalian cutaneous permeability barrier. Laboratory Investigation 39:574–583, 1978
34. Imokawa G, Akasaki S, Hattori M, Yoshizuka N: Selective recovery of deranged water-holding properties by stratum corneum lipids. J Invest Dermatol 87:758–761, 1986
35. Gloor M, Hirsch G, Willebrandt U: On the use of infrared spectroscopy for the *in vivo* measurement of the water content of the horny layer after application of dermatologic ointments. Arch Dermatol Res 271:305–313, 1981
36. Gloor M, Hevmann B, Stuhlerth T: Infrared spectroscopic determination of the water content of the horny layer in healthy subjects and in patients suffering from atopic dermatitis. Arch Dermatol Res 271:429–436
37. Warner R, Myer MC, Taylor DA: Electron probe analysis of human skin: Determination of the water concentration profile. J Invest Dermatol 90:218–224, 1988
38. Weigand DA, Gaylor JR: Removal of SC *in vivo*: an improvement on the cellophane tape stripping technique. J Invest Dermatol 60:84–86, 1973
39. Holbrook KA, Odland GF: Regional differences in the thickness (cell layers) of the human stratum corneum: an ultrastructural analysis. J Invest Dermatol 62:415–422, 1974
40. Plewig G, Scheuber E, Reuter B, Waidelich W: Thickness of corneocytes in Stratum Corneum. In: Marks R, Plewig G (eds.). Stratum Corneum. Springer-Verlag, Berlin, 1983, pp 171–174
41. Scheuplein RJ: A survey of some fundamental aspects of the absorption and reflection of light by tissue. J Soc Cosmet Chem 15:111–122, 1964
42. Pugliese RT, Milligan AJ: Ellipsometric measurement of skin refractive index *in vivo*. In: Marks R, Payne PA (eds.). Bioengineering and the Skin. MTP Press Limited, Boston, 1981, pp 291–302
43. Mackenzie IC, Linder JE: An examination of cellular organization within the SC by a silver staining method. J Invest Dermatol 61:245–250, 1973
44. Brody I: A light and electron microscopy study of normal human stratum corneum with particular reference to the intercellular space. Upsala J Med Sci 94:29–45, 1989
45. Menton DN, Eisen AZ: Structure and organization of mammalian stratum corneum. J Ultrastruct Res 35:247–264, 1971

3b. EXAMINATION OF THE EFFECT OF ETHANOL ON HUMAN STRATUM CORNEUM *IN VIVO* USING INFRARED SPECTROSCOPY

D. Bommannan[1], Russell O. Potts[2], and Richard H. Guy[1,3,4]

[1] Graduate Group in Bioengineering
University of California, Berkeley, and
University of California, San Francisco
San Francisco, CA 94143

[2] Dermal Therapeutics Group
Pfizer Central Research
Groton, CT 06340

[3] Departments of Pharmacy and Pharmaceutical Chemistry
University of California, San Francisco
San Francisco, CA 94143-0446

[4] Correspondence

ABSTRACT

Ethanol is generally believed to be a chemical capable of enhancing drug penetration across the skin. However, the mechanism by which ethanol achieves this effect has remained unclear. We have used Attenuated Total Reflectance Infrared (ATR-IR) spectroscopy to determine the action of ethanol on human stratum corneum (skin's barrier layer) *in vivo*. Treatment of the skin for thirty minutes with pure ethanol liquid (a) induced a transient decrease in the intensity and frequency of the C-H asymmetric stretching vibration (which originates from the acyl chains of the intercellular lipid domains of the stratum corneum), (b) caused observable increases in spectral absorbances associated with ethanol, and (c) extracted appreciable amounts of lipid from the stratum corneum. These findings contradict the suggestion that ethanol "disorders" the intercellular lipid bilayers of the stratum corneum, and reveal that ethanol enters the skin and removes measurable quantities of the barrier material. The changes induced by the short contact with ethanol are reversed within 24 hours. Exposure of the stratum corneum to ethanol-saturated vapor again led to detectable partitioning of the alcohol into the stratum corneum. However, while no lipid extraction would occur in this experiment, there was, once more, no evidence for the induction of lipid disordering. We conclude that ethanol's ability to enhance drug penetration across the skin is the result, at least in part, of stratum corneum intercellular lipid removal.

INTRODUCTION

Certain chemicals, known as penetration enhancers, can significantly lower the diffusional resistance of the stratum corneum (SC, skin's outermost and least permeable layer) and thereby enhance the flux of a concurrently, or subsequently, administered drug [1]. Ethanol is a frequently quoted example of a penetration enhancer [2-3], and is believed to act as such in the commercially available estradiol transdermal delivery system (Estraderm®, Ciba-Geigy, NY) [4-7]. Despite this important application, the mechanism, by which ethanol promotes increased drug flux across the SC, is poorly understood. The model biomembrane literature reveals that ethanol disorders the acyl chain regions of DMPC and DPPC bilayers, and that this effect causes an increase in permeability [8-9]. Because it is now well-established (a) that the intercellular regions of the SC contain multiple ordered bilayers, and (b) that these lipid-rich domains provide a significant permeation pathway through the SC, it has been suggested that ethanol acts on the SC *via* a lipid-disordering mechanism.

The objective of this study, therefore, was to test this hypothesis. Experiments were conducted *in vivo*, in normal human volunteers, using the technique of attenuated total reflectance infrared spectroscopy (ATR-IR) to evaluate the action of ethanol on the SC. The spectroscopic features of the membrane were examined prior to, and following (as a function of time) SC treatment with ethanol in both liquid and vapor phases. The results imply that lipid extraction, rather than disruption of lipid order, may be the predominant mechanism of action of ethanol on the SC *in vivo*.

EXPERIMENTAL

1. Attenuated total reflectance infrared spectroscopy (ATR-IR)

Application of ATR-IR to study the biophysical properties of human SC *in vivo* has been fully described [10]. Measurements in this study were recorded with an Analect FX-6200 Fourier transform IR spectrophotometer (Laser Precision, Irvine, CA) equipped with an ATR accessory (Skin Analyzer, Spectra-Tech, Stamford, CT), which supported a zinc sulfide internal reflection element (7.5 x 1 x 0.2 cm, cut at a 60° incident angle). This ATR configuration results in the IR radiation penetrating to a depth of about 2 μm when the human forearm is placed on the ZnS crystal [10]. All FTIR spectra recorded were the average of 50 scans, which required a data collection period of 2 minutes. The frequency of the IR absorbance peak maxima were determined to an accuracy of 0.1 cm^{-1} using a center-of-gravity algorithm [10].

2. Methodology

The volunteers were healthy adults (aged 23-30 years) with no history of skin disease. The site examined in this study was the ventral forearm. Subjects were instructed to follow their normal, daily washing routine but to apply no topical formulation (cream, lotion, etc.) to the experimental site. On arrival in the laboratory, the forearm surface was wiped with a dry cotton swab (Q-tip, Johnson & Johnson, NJ), and was then placed onto the ATR configuration to record a baseline spectrum. Immediately thereafter, the measurement site was tape-stripped four times using Scotch Magic Tape (3M Co., St. Paul, MN). The purpose of this step was to prevent "contamination" of the IR signal originating from the SC intercellular lipids with that originating from sebaceous lipids. In a recent publication [10], we have shown that

the IR lipid signal from the upper layers of the SC is a mixture of signals coming from 'true' intercellular lipids and from sebaceous lipids which have been secreted at the skin surface and have then mixed with the intercellular material. Tape-stripping the SC 4 times effectively eliminates the sebaceous contribution. Immediately post-stripping, another IR spectrum was recorded. The examination site (area ≈ 20 cm^2) was then treated by either maintaining contact (a) for 30 minutes with 10 cm^3 of spectroscopic grade absolute ethanol (Goldshield Chemical Co., Hayward, CA), or (b) for 1 hour with saturated ethanol vapor above the pure liquid. At the end of the treatment period, any excess ethanol on the skin surface was wiped away, and after leaving the arm air-exposed for 2 minutes, spectra were recorded at 30 minute intervals for 2 hours, then hourly for the next 4 hours, and, finally, at 24 hours post-treatment. Thus, in all, a total of 9 *in vivo* spectra were collected. In addition, the ethanol treatment liquid was preserved and analyzed spectroscopically as described below.

3. Spectral Analysis

FTIR spectra were recorded in the frequency range 4400-400 cm^{-1}. The following spectral features were examined as a function of time post-ethanol treatment:

(a) The frequency shift, and the band-width at half-height, of the C-H asymmetric stretching absorbance at *ca.* 2920 cm^{-1}. This absorbance originates essentially exclusively from the SC lipids. It has been shown that an increase in the frequency of this absorbance, and a broadening of the peak, is indicative of an increase in SC lipid acyl chain disorder (often referred to as "fluidization") [11].

(b) The area under the C-H anti-symmetric stretching absorbance (over the frequency range 2945-2875 cm^{-1}). The integrated intensity (area under the curve) of an IR absorbance is directly proportional to the observed amount of the absorbing

species. Thus, the measured integrated intensity was computed to evaluate the amount of SC lipid present after ethanol treatment relative to the baseline level. The procedure used to determine the integrated intensity, so that different degrees of contact between the skin and the reflection element were correctly taken into account, is described elsewhere [10].

(c) The enhanced absorbances at 880 and 1050 cm^{-1}. Ethanol shows a major absorbance, due to C-O stretching, at 1050 cm^{-1}, and a minor absorbance at 880 cm^{-1}, due to the C-C skeletal vibration [12], in this region of the IR spectrum. Thus, augmentation of these peaks could be used to confirm, after surface evaporation, the presence of dissolved ethanol in the outer microns of the SC.

RESULTS AND DISCUSSION

The principal objective of this study was to test the hypothesis that ethanol increases SC permeability *in vivo* by disordering the intercellular lipid domains. Substantiation of the hypothesis would provide strong circumstantial evidence for the mechanism of ethanol action.

It was first established that skin pretreatment with ethanol did indeed lead to significant levels of the solvent in the region of the SC "visible" to the IR spectrophotometer. Figure 1 shows *in vivo* SC spectra, in the frequency range 800 - 1300 cm^{-1}, before and after treatment with liquid ethanol for 30 minutes, and a spectrum of ethanol for comparison. The treated SC shows significant increase in the absorbances at *ca.* 880 and 1050 cm^{-1} compared to the control. The absorbances originate from the ethanol which has partitioned into the SC. The C-O stretching frequency also shifts to higher wavenumber post-ethanol treatment, an effect that may be explained in part by reduced hydrogen bonding between water and SC structural components [13].

Figure 2 shows the shift in the maximum frequency of the C-H asymmetric stretching absorbance during and following the treatment protocol with liquid ethanol. The baseline (pre-treatment) spectrum was first recorded, and the maximum frequency of the C-H asymmetric stretching absorbance was assigned a shift of 0 cm^{-1}. The site was then tape-stripped four times and, as previously reported [10], the peak frequency of the C-H asymmetric stretching absorbance (υ_{CH}) decreased significantly (by about -2 cm^{-1}). The skin was then treated for 30 minutes with ethanol, and after removal of excess liquid from the skin surface, another IR spectrum was obtained. Although the resulting values were variable, there was, on average, a further net decrease (by ~1 cm^{-1}) in the peak frequency of υ_{CH}. Such a change indicates a slight **ordering**, rather than a disordering, of the intercellular lipid acyl chains. Furthermore, because the ethanol which has partitioned into the SC also contributes to the C-H absorbances, and because υ_{CH} for ethanol occurs at ≈10 cm^{-1} higher than that from the SC lipids, the change observed following ethanol treatment may represent an underestimate of the ordering effect perceived.

The bandwidth at half-height of the C-H asymmetric stretching absorbance (which is an alternative parameter that can be used to assess lipid "fluidity") indicated the identical ordering pattern (data not shown). Subsequent spectra over the next several hours revealed that the υ_{CH} returned quickly to the "4-tape strip" value and then more gradually to the pre-treatment frequency.

No disordering effect of ethanol on the SC lipids was therefore observed; in fact, the opposite result was obtained. Inspection of the literature reveals that similar findings were reported by Lewis *et al.* [13], who studied ethanol-induced changes on plasma membranes from the rat liver. Compared to the appropriate controls, they found a statistically significant reduction in υ_{CH} following ethanol treatment. They suggested that a plausible explanation for the apparent "ordering" is that ethanol

promotes interdigitation of the hydrocarbon chains by displacement of bound water molecules at the lipid headgroup/membrane interface region.

The question remains, though, as to the mechanism of ethanol action on the SC. As it had been reported [14] that SC lipids can be extracted for analysis by ethanol, we next examined the possibility that lipid removal could explain the ethanol-mediated lowering of skin barrier function. Figure 3 shows the IR-determined, relative SC lipid content during and following the liquid ethanol treatment protocol. The pretreatment, baseline level was assigned arbitrarily a value of 100%, and all further measurements were reported relative to this value. Tape-stripping caused a decrease in the lipid content, as previously noted [10]; ethanol treatment elicited a further, highly significant, decrease, which recovered to the pretreatment value in a manner very similar to that shown by υ_{CH} (Figure 2). The results imply, therefore, that ethanol had indeed extracted an appreciable amount of SC lipid. Once again, because the ethanol present in the SC contributes to the C-H stretching absorbance, the perception of reduced lipid content may be an underestimate of the total effect. Confirmation of this conclusion was obtained by evaporation of the ethanol-treatment liquid and subsequent IR analysis of the residue (Figure 4). The representative spectra from three volunteers all show large lipid-associated absorbances in the 3000-2750 cm^{-1} region (i.e., from the C-H symmetric and asymmetric stretching vibrations).

It is noteworthy that the time-course of lipid recovery is consistent with the results of Grubauer *et al.* [15-16], who measured SC barrier function by transepidermal water loss following skin treatment with acetone and other solvents, and Imokawa *et al.* [17], who measured the water-holding capacity of the SC following acetone/ether treatment. We have found that the lipids recover quickly in the initial phase, and then completely within 24 hours following the ethanol liquid

treatment protocol. The concomitant recovery of intercellular lipid and of lipids of sebaceous origin is implicated.

Finally, to be absolutely certain that the lipid extraction phenomena was not masking a true disordering action (i.e., there was not sufficient lipid remaining for the effect to be "seen" by the IR), experiments were conducted in which the SC was treated with ethanol-saturated vapor. In this case, no lipids could be extracted into the solvent phase. Once again, ethanol uptake into the SC was apparent (see Figure 5), but no disordering effects were observed, and results indistinguishable from those in Figure 2 were obtained.

In summary, therefore, these experiments show that *in vivo*, in humans, ethanol does not disorder SC lipid domains. Relatively short-term exposure with the liquid solvent, however, causes significant lipid extraction, an effect that can be expected to lower skin barrier function. Ethanol may replace the extracted lipids and this can increase the partitioning of hydrophilic molecules, and, consequently, increase their flux across the skin.

ACKNOWLEDGEMENT

We thank our volunteers for their participation, Dr. Robert Hinz for his help and advice, and the U.S. National Institutes of Health (HD-23010) for financial support. DB is the recipient of a Graduate Student Research Award from the University of California, San Francisco.

REFERENCES

1. K.A. Walters, Penetration enhancers and their use in transdermal therapeutic systems, in : J. Hadgraft and R.H. Guy (Eds.), Transdermal Drug Delivery. Developmental Issues and Research Initiatives, Marcel Dekker, Inc., New York, NY, 1989, pp. 197-246.

2. B. Berner, G.C. Mazzenga, J.H. Otte, R.J. Steffens, R.H. Juang, C.D. Ebert, Ethanol: water mutually enhanced transdermal therapeutic system II: skin permeation of ethanol and nitroglycerin, Journal of Pharmaceutical Sciences, 78 (1989) 402-407.

3. T. Sekine, Y. Machida, T. Nagai, Gel ointment of verapamil for percutaneous absorption, Drug Design and Delivery, 1(1987) 245-252.

4. L.K. Pershing, W.J. Lambert , K. Knutson, Mechanism of ethanol-enhanced estradiol permeation across human skin in vivo, Pharmaceutical Research, 7 (1990) 170-175.

5. K. Knutson, S. L. Krill, W. J. Lambert, W. I. Higuchi, Physicochemical aspects of transdermal permeation, J. Control. Rel., 6 (1987) 59-74.

6. W.R. Good, M.S. Powers, P. Campbell, and L. Schenkel, A new transdermal delivery system for estradiol, J. Control. Rel., 2 (1985) 89-97.

7. A. Ghanem, H. Mahmoud, W.I. Higuchi, U.D. Rohr, S. Borsadia, P. Liu, J.L. Fox and W.R. Good, The effects of ethanol on the transport of β-estradiol and other permeants in hairless mouse skin. II. A new quantitative approach, J. Control. Rel., 6 (1987) 75-83.

8. R. C. Lyon, J.A. McComb, J. Schreurs and D.B. Goldstein, A relationship between alcohol intoxication and the disordering of brain membranes by a series of short-chain alcohols, J. of Pharmacology and Experimental Therapeutics, 218 (1981) 669-675.

9. E.S. Rowe, Thermodynamic reversibility of phase transitions. Specific effects of alcohols on phosphatidylcholines, Biochim. Biophys. Acta, 813 (1985) 321-330.

10. D. Bommannan, R.O. Potts and R.H. Guy, Examination of stratum corneum barrier function *in vivo* by infrared spectroscopy, J. Invest. Dermatol., in press.

11. R.L. Amey , D. Chapman : IR spectroscopic studies of model and natural biomembranes. In: Chapman D (ed.). Biomembrane structure and function. Macmillan, London, 1983, pp. 199-256.

12. G. Herzberg: Infrared and Raman Spectra of Polyatomic Molecules, Van Nostrand, Princeton, 1954, p. 361.

13. E.N. Lewis, I.W. Levin and C.J. Steer, Infrared spectroscopic study of ethanol-induced changes in rat liver plasma membrane, Biochimica et Biophysica Acta, 986 (1989) 161-166.

14. L.B. Goldsmith, S.E. Friberg, and J.E. Wahlberg, The effect of solvent extraction on the lipids of the stratum corneum in relation to observed immediate whitening of the skin, Contact Dermatitis, 19 (1988) 348-350.

15. G. Grubauer, P.M. Elias and K.R. Feingold, Transepidermal water loss: the signal for recovery of barrier structure and function, J. Lipid Res., 30 (1989) 323-333.

16. G. Grubauer, K.R. Feingold, R.M. Harris, P.M. Elias, Lipid content and lipid type as determinants of the epidermal permeability barrier, J. Lipid Res., 30 (1989) 89-96.

17. G. Imokawa, S. Akasaki, M. Hattori, N. Yoshizuka, Selective recovery of deranged water-holding properties by stratum corneum lipids, J. Invest. Derm., 87 (1986) 758-761.

FIGURE LEGENDS

Figure 1 : Infrared spectra of (A) ethanol, (B) human SC *in vivo,* and (C) human SC *in vivo* immediately after 30 minutes treatment with pure ethanol liquid. Note the enhanced absorbances in (C) at 880 and 1050 cm^{-1} indicating the presence of ethanol in the SC.

Figure 2 : Average values (n=6, error bars = SD) of the shift in the peak maximum of the
C-H asymmetric stretching absorbance plotted as a function of time during the ethanol liquid treatment protocol. ANOVA followed by Scheffe's F-test revealed a statistically significant difference ($p<0.05$) between the location of the peak maximum before and after the 30 minutes ethanol exposure. There was no statistically significant difference between the baseline value and and that at 24 hrs.

Figure 3 : Average values (n=6, error bars = SD) of the amount of ATR-IR detected SC lipids plotted as a function of time during the ethanol liquid treatment protocol. ANOVA followed by Scheffe's F-test revealed a statistically significant difference ($p<0.05$) between the amount of lipids before and after the 30 minutes ethanol exposure. There was no statistically significant difference between the baseline value and that at 24 hrs.

Figure 4 : IR spectra of material extracted from the SC of three individuals by ethanol treatment. These reflectance spectra were obtained following evaporation of the ethanolic solutions on the ATR element.

Figure 5 : IR spectrum of (A) ethanol, (B) human SC *in vivo*, and (C) human SC *in vivo* immediately after 1 hour exposure to ethanol-saturated vapor. Note the enhanced absorbances in (C) at 800 and 1050 cm^{-1} indicating the presence of ethanol in the SC.

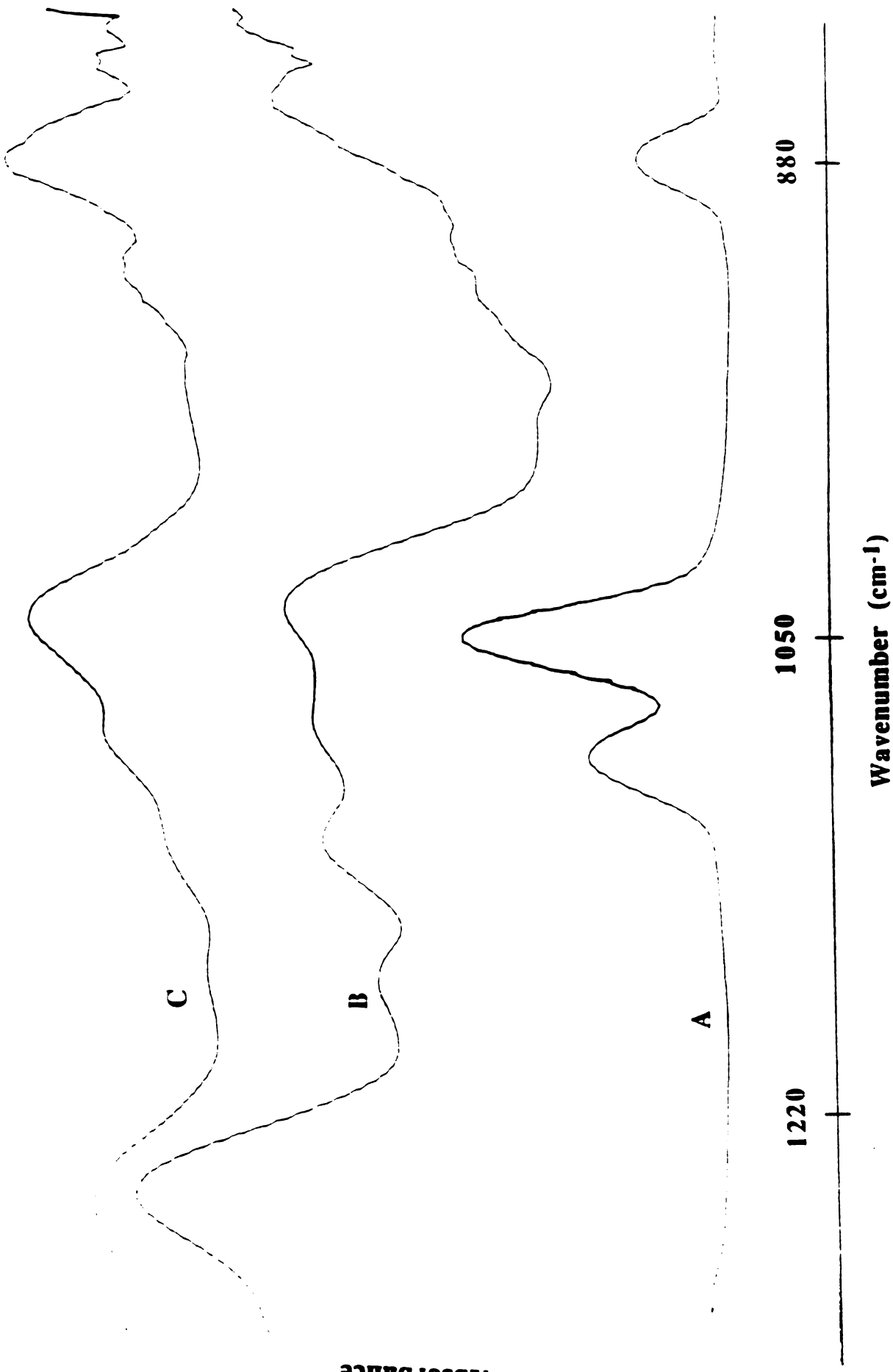
C
B
A
1220
1050
880
Wavenumber (cm-1)
Absorbance

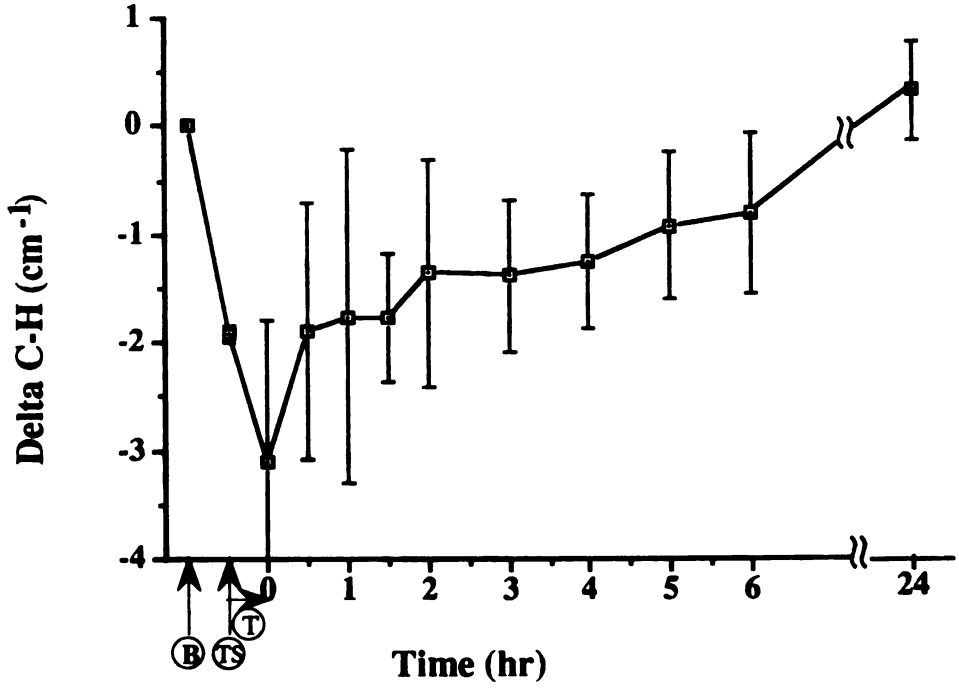
Delta C-H (cm-1)
1
0
-1
-2
-3
-4
0
1
2
3
4
5
6
24
B
TS
T
Time (hr)
B - baseline value
TS - after 4 tape-strips
T - 30 min. ethanol treatment

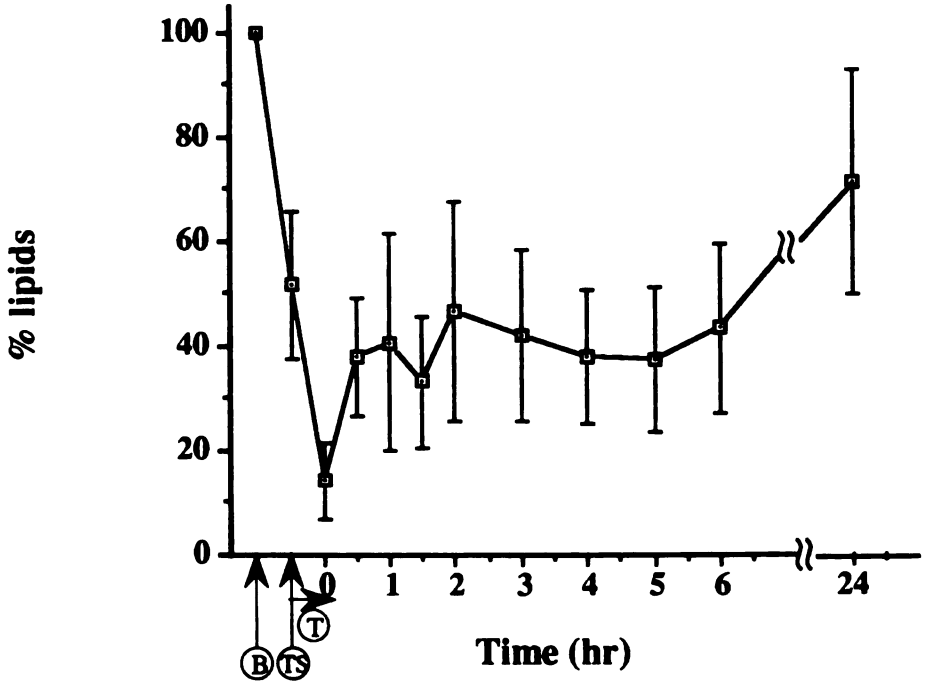

B - baseline value
TS - after 4 tape-strips
T - 30 min. ethanol treatment

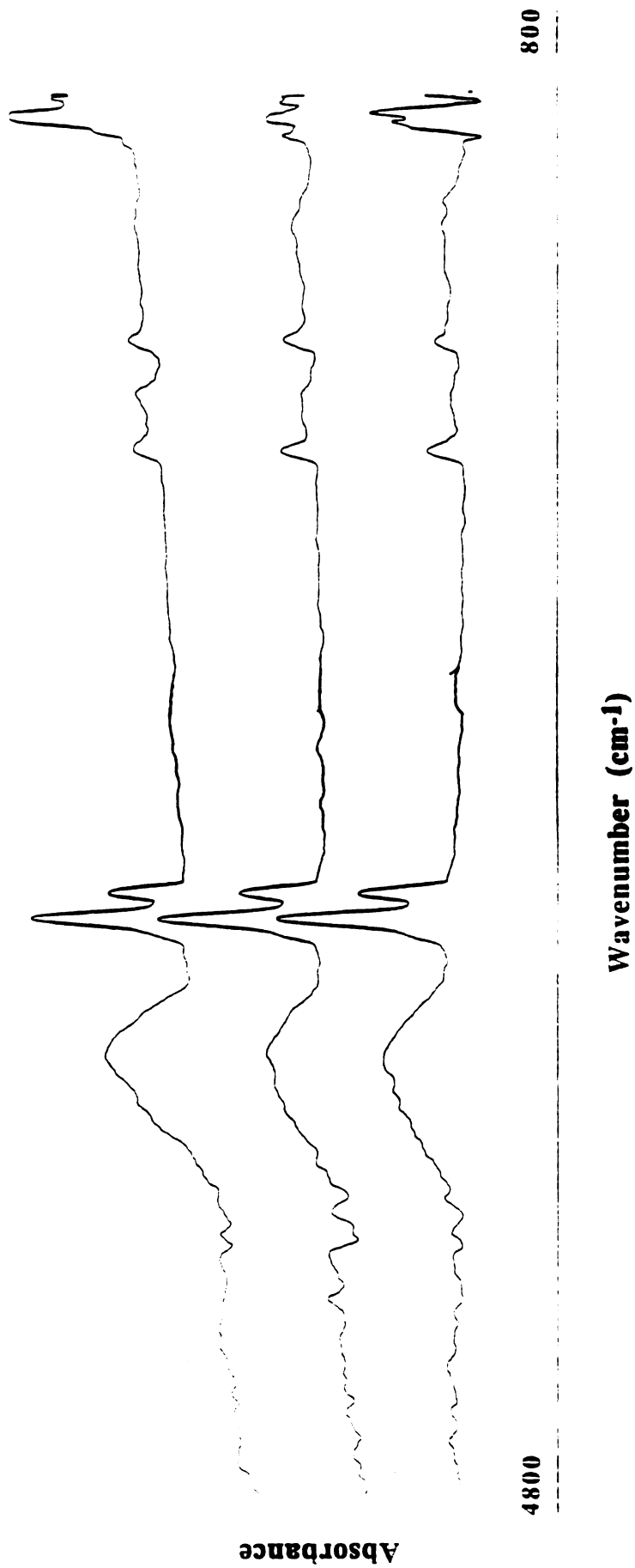
800
4800
Wavenumber (cm-1)
Absorbance

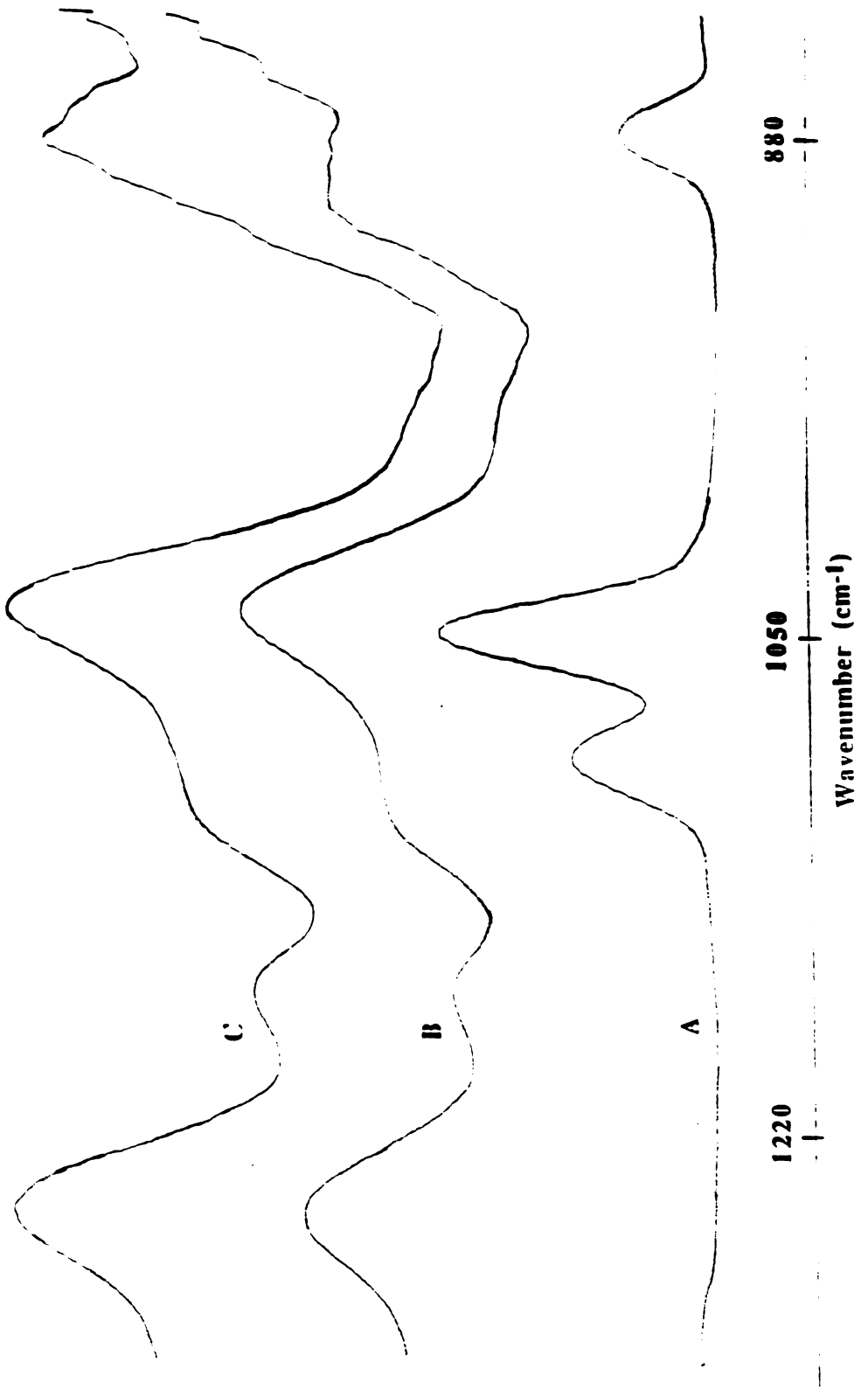
C
B
A
1220
1050
880
Wavenumber (cm-1)
Absorbance

4. Physics of Ultrasound

4.1 Introduction

We hear sound due to the mechanical disturbance set up by oscillatory movements of particles in a medium. Humans may be able to hear, if the medium is air and the frequency of oscillation is below 20,000 cycles per second (20,000 Hz or 20 kHz). At frequencies higher than 20 kHz, sound is usually inaudible to humans and it is called **ultrasound**. Ultrasound follows exactly the same laws as audible sound.

Ultrasound is typically generated by alternate compressions and relaxations of a piezoelectric crystal (see Section 4.4 on generation of ultrasound). Hence, an ultrasound wave is composed of regions which are alternately compressed and stretched (Figure 4.1). Particles in the medium, in which ultrasound propagates, oscillate back and forth. The maximum distance a particle is displaced from its equilibrium position is called the displacement amplitude. In a longitudinal wave, the particle motion is along a line parallel to the direction of ultrasound propagation.

Another type of sound propagation is by transverse waves, where the particles travel in a direction normal to the direction of ultrasound propagation. The following situation can give rise to transverse waves: If a rope is fixed at its ends and gently tugged at the center, a sinusoidal wave transmission can be observed. However, the rope itself moves in a direction normal to the propagation of the sinusoidal wave. Transverse waves are damped out extremely rapidly in liquids and soft tissues, and do not constitute a major mode of propagation in soft tissues. Since we will be dealing with ultrasound propagation in tissue, particularly skin, we shall limit our discussion to the physics of longitudinal waves.

4.2 Linear Acoustics

For a transducer, the radiating surface of which vibrates sinusoidally in time with frequency f and amplitude A, linear acoustics predicts that the pressure, particle velocity and other related quantities vary sinusoidally in time with the same frequency f and with amplitude proportional to A.

4.2.1 Traveling Plane Wave in a Lossless Medium

The pressure in this type of a wave is plotted in Figure 4.2 as a function of distance along the direction of wave propagation. Curve 1 represents the wave at a time t_1 and the other curve represents the wave at a slightly later time t_2. The distance along the z direction between any two consecutive identical points on the wave (such as the peaks) is the wavelength, λ. At any position z in the region through which the wave passes, the pressure oscillates as high and low pressure regions pass by. This oscillation of the pressure as a function of time is plotted in Figure 4.3. The acoustic pressure, p, is the difference between the actual pressure and the time-averaged pressure.

The acoustic pressure, p, and the particle velocity, u, of a single frequency wave traveling in the positive z direction, in a medium with no attenuation, are expressed by the following equations:

$$p = p_0 \sin(\omega t - kz) \qquad (4.1)$$

$$u = \frac{p_0}{\rho c} \sin(\omega t - kz) \qquad (4.2)$$

(ρ is the density of the medium and c is the velocity of ultrasound in that medium). The instantaneous intensity, i, and the (time-averaged) intensity, I are given by:

$$i = pu = \frac{p_0^2}{\rho c} \sin^2(\omega t - kz) = \frac{p_0^2}{\rho c}[1 - \cos 2(\omega t - kz)] \qquad (4.3)$$

$$I = \frac{1}{T}\int_0^T i(t)\,dt$$

where $T = \frac{2\pi}{\omega}$ is the period of the wave.

$$I = \frac{p_0^2}{\rho c} \qquad (4.4)$$

The maximum deviation of the pressure from its mean value during a cycle is the pressure amplitude, p_0; the velocity amplitude, $u_0 = p_0 / \rho c$, is the greatest magnitude of u during a cycle. The instantaneous intensity has a constant part (equal to the time-averaged intensity I) and a second harmonic part. In the above equations, the pressure amplitude, p_0, the velocity amplitude, $p_0 / \rho c$, and the intensity I, are independent of position. Most (if not all) ultrasonic fields are spatially nonuniform, but the above relationships are nevertheless often applicable locally.

For an ultrasound beam of intensity 1 W/cm^2 traveling through water ($\rho = 10^3$ kg/m^3 and c = 1500 m/sec), the pressure amplitude calculated using Equation 4.4 is $\approx$ 0.4 atm., and the velocity amplitude u_0 = 25.5 cm/sec.

4.3 Nonlinear Acoustics

The basic differential equations of acoustics are nonlinear. In the previous section, we described the linear approximation of these equations, which is adequate at low amplitudes. Under conditions commonly employed in the medical field, the acoustic field can not be explained by linear theory alone. Even if the transducer vibrates sinusoidally, the ultrasound generated may not be sinusoidal for one or more of the following reasons:

a) The mean pressure point is raised or lowered.

b) Objects in the field are acted on by steady forces.

c) Particles suspended in a fluid are set into steady translatory or rotary motion.

d) Steady circulatory flow is set up in fluid media.

e) Harmonics are generated, so that the waveform becomes distorted and the attenuation becomes intensity-dependent.

f) Cavitation phenomena appear.

Nonlinear theory is required for the explanation and quantitative description of these phenomena. This can be achieved by the method of successive approximations. Each variable, such as the density, is considered to consist of a series of terms:

$$\rho = \rho_0 + \rho_1 + \rho_2 + \ldots \qquad (4.5)$$

The quantities with subscripts "0", "1", "2", etc. are called zero-order, first-order, second-order, etc. contributions respectively. Zero-order quantities (such as ρ_0) apply in the absence of sound, first-order quantities (such as ρ_1) are contributions defined by linear acoustics, and second-order quantities (such as ρ_2) are additional contributions obtained from nonlinear theory. We consider the field to emanate from a source-transducer generating continuous ultrasound of frequency f and characteristic amplitude A. Then, the characteristic magnitude of each contribution is proportional to A^n, where n is the order of the contribution. Thus, zero-order terms are, of course, independent of A (proportional to $A^0 = 1$), while first-order terms are proportional to A, and second-order terms are proportional to A^2.

4.3.1 Non-linear Intensity

The usual approximation for intensity is of second-order, given by the product of first-order pressure and first-order velocity. The instantaneous intensity, i, in Equation 4.3, has both a constant part and a second-harmonic component. However, it is the time-averaged intensity, I, given in Equation 4.4 , that is usually measured and cited for

continuous waves. Intensity is a measure of the rate at which energy is transmitted across unit area; it is also called the power density. The total power output from a transducer can be calculated, in principle, by integrating the (normal component of the) intensity over the transducer face. In practice, however, the total power output of the transducer is measured (e.g. by the radiation force method, as described below), and this is divided by the area of the transducer face to obtain the spatially averaged intensity.

4.3.2 Radiation Force

In a sound field, a body may respond as if acted on by a steady force; by definition, this is the radiation force. If the surface of the body is rigid and motionless, the radiation force can be calculated by integrating the radiation pressure over the surface. If the surface oscillates, this motion must be taken into account. These calculations are difficult, but relatively simple approximations apply in special situations. For example, for a body of material, whose particle velocity, "ρc", matches that of water, the radiation force is given by

$$F_{rad} = W / c \qquad (4.6)$$

where W is the acoustic power output of the device and c is the velocity of the beam in that medium. When an ultrasound beam impinges on any surface, a radiation force results.

4.3.2.1 Radiation Force Measurements

Figure 4.4 is a schematic of the set-up that can be used for measuring the acoustic power output that emanates from the face of a transducer. A block (Absorber) of very efficient absorbing material (e.g. polystrene rubber) is mounted on one arm of a sensitive analytical balance and is immersed in a tank of degassed water. The beam of

ultrasound from the transducer is directed at the absorber through an acoustically transparent screen which prevents the absorber being displaced by acoustic streaming (see below). Weights are added to the counterbalance pan (W) to compensate for the ultrasound force. From Equation 4.6, the weight registered on the pan for a known acoustic power can be calculated. For example, if the medium is water (in which ultrasound velocity ≈ 1500 m/sec), and an incident acoustic power of 1 W strikes a perfect absorber

$$\text{Frad} = \frac{1\ \text{W}}{1500\ \text{m/sec}}$$

$$= \frac{1\ \text{N-m/sec}}{1500\ \text{m/sec}}$$

$$= 6.7 \times 10^{-4}\ \text{Newtons}$$

which is equivalent to a measured weight of about 0.068g.

4.3.3 Acoustic Streaming

Radiation forces can also cause a body to undergo angular displacement. In a fluid, such a force can cause steady circulatory flows to be set up, which is called acoustic streaming. The effect can be very small with dimensions of the order of microns; it is then appropriately called "microstreaming". Microstreaming in the form of micro-scale eddying takes place in the vicinity of any small vibrating object. However, acoustic streaming in the SC does not appear plausible, because of the lack of free fluid bodies. In contrast, in the more aqueous epidermal and dermal tissue, this phenomenon may occur.

4.3.4 Cavitation

Cavitation, defined broadly, includes various kinds of sonically generated activity of highly compressible bodies composed of gas and/or vapor. This phenomenon will be discussed in detail (Section 6.4) when the mechanism of ultrasound-induced effects is discussed.

4.4 Generation and Propagation of Ultrasound

The design of high frequency ultrasound transducers is a science in itself. Since our objective was not to design these high frequency transducers, only a brief description of the transducers is presented.

4.4.1 Transducers for Generating Ultrasound

A transducer is a device that converts one form of energy into another. For example, a loudspeaker is a transducer, which converts electrical energy into mechanical energy (audible waves). Similarly, an ultrasound transducer converts electrical signals at frequencies greater than 20 kHz into ultrasound waves. Generally, a piezoelectric crystal is employed for this purpose. When a voltage difference is applied across a piezoelectric crystal, the crystal deforms. Thus, an alternating voltage across the face of the crystal causes an oscillating change in shape (Figure 4.5). Therefore, the application of an a.c. voltage at ultrasonic frequency results in the crystal oscillating at that same frequency. The crystal oscillates with maximum displacement amplitude (maximum efficiency) for any given input power at its resonant frequency. This is called the fundamental resonant frequency. As the driving frequency is increased, the ultrasonic output decreases to a minimum when the wavelength equals the thickness of the transducer. If the driving frequency is further increased, the ultrasonic output then

increases until another resonant condition is obtained at a frequency equal to three times the fundamental frequency. This frequency corresponds to 1.5 wavelengths within the transducer and is known as the third harmonic frequency. Yet another resonant condition occurs at the fifth harmonic when the driving frequency is five times the fundamental frequency, and the transducer is 2.5 wavelengths thick. A pictorial representation of the displacement amplitude of the transducer as a function of the driving frequency is shown in Figure 4.6. At resonant frequencies the transduction process is most efficient.

Commercially available transducers emanate more than one frequency at any instant (broad band transducers). Furthermore, their acoustic efficiencies (ratio of acoustic power output to electrical power input) are low (5 - 60%) even when driven at their fundamental frequency. These two conditions preclude the possibility of using these transducers at their harmonics, since at the harmonic frequencies the transducer efficiency is further reduced.

4.4.2 Propagation of Ultrasound

Acoustic energy is continuously lost from an ultrasonic beam through one or more of the following processes:

1. Direct conversion into heat (absorption).
2. Redirection of energy out of the beam by: (a) reflection, (b) refraction, and (c) a change in phase of a portion of the beam (scattering).

When a plane wave passes through a medium, in which the inhomogeneities are of small dimension compared to the width of the ultrasound beam (i.e., through a statistically homogeneous medium), the amplitude of the acoustic pressure, the particle velocity, and the intensity all decay exponentially as the wave progresses. Figure 4.7 shows a typical p versus z curve, showing how the particle pressure, p, varies along

the propagation direction at a given time. Also shown is a plot of $p_0 e^{-\alpha z}$ (the pressure amplitude) as a function of z; where α is a constant, the attenuation coefficient. The attenuation coefficient α, is, in general, the sum of an absorption coefficient, α, and a scattering coefficient, a_s. Attenuation is generally expressed in units of decibels or Nepers (Np). The attenuation in decibels between two points z and z' is given by Equation 4.7:

$$\text{attenuation (decibels)} = 10 \log_{10} (I/I') \tag{4.7}$$

where I and I' are the intensities at z and z' respectively.

The relation between decibel and Neper is given by

$$1 \text{ dB} = 8.86 \text{ Np} \tag{4.8}$$

4.4.2.1 Attenuation

Ultrasound waves which are travelling in a medium with a characteristic acoustic impedance (given by the ratio of p (Eqn. 4.1) and u (Eqn. 4.2)), ρc, and which encounter another medium with characteristic acoustic impedance, $\rho' c'$, can be reflected at the interface. The reflection coefficient, the square of the ratio of the intensity in the reflected wave to that in the incident wave, is given by Equation 4.9.

$$\text{reflection coefficient} = \left| \frac{\rho c - \rho' c'}{\rho c + \rho' c'} \right|^2 \tag{4.9}$$

The magnitude of the reflection coefficient, i.e., the degree of reflection of the incident waves, is governed by the impedance mismatch between the two media. If the impedances are equal, no reflection occurs. For example, the characteristic acoustic impedances of water and skin are ca. 1.56×10^5 and 1.59×10^5 g/cm^2/sec respectively

[Goss et al., 1980]. The reflection coefficient is, therefore, close to zero, which implies that the ultrasound intensity lost by reflection at the water-skin interface is negligible.

There is an extensive body of literature which documents the values of attenuation coefficient in different tissues. These data can be used for predicting the reduction in beam intensity with increasing distance from the source. It is difficult to assess the relative contributions to the attenuation coefficient due to scattering and absorption. The percentage of the attenuation coefficient due to scattering depends on the frequency and tissue. Scattering occurs when a beam encounters an interface bounded by different acoustic impedances. If the dimensions of the reflector are smaller than the wavelength, then the reflector acts as a point source and radiates a spherical wave. However, in the case of skin, due to the complex nature of this tissue, the relative contribution of scattering to the attenuation coefficient is unknown.

4.5 Effects of Ultrasound

Acoustic energy directed into any biological material can result in either (a) thermal, and/or (b) non-thermal effects.

4.5.1 Thermal Effects

Tissues exposed to ultrasound cannot transmit all of the incident acoustic energy. Some of the transmitted energy is, therefore, removed from the ultrasound beam as heat. If sufficient heat is generated, it can lead to a detectable change in the normal tissue. The absorption coefficient is a measure of the amount of energy removed from an ultrasound wave as it propagates through a given tissue. This energy can appear as heat and, if not transported by diffusion or conduction, can cause an increase in the temperature of that tissue. (Note: Skin serves as a thermoregulatory organ and,

therefore, is supplied with a rich supply of bloodvessels. Any rise in skin temperature is immediately countered with increased blood flow and consequent heat transport. This minimizes heat build-up and, therefore, the temperature rise. This will be of significant relevance, when we discuss the thermal effects of ultrasound on skin). Knowing the absorption coefficient, the rate of heat production within the tissue can be calculated. Using this value, a heat balance can be placed on the volume of tissue, and the temperature gradient achieved in the tissue can be determined. The following calculations illustrate this strategy.

Attenuation = A dB/cm/MHz

Incident energy = I W/cm^2

Transmitted energy = I' W/cm^2

$$A\ dB = 10 \log_{10} (I/I') \qquad (4.10)$$

Therefore,

$$I' = \frac{I}{10^{Af\Delta x/10}} \qquad (4.11)$$

where,

f = frequency in MHz

Δx = tissue thickness in cm

Energy loss

$$Q = (I - I')$$

$$= I \left(1 - \frac{1}{10^{Af\Delta x/10}}\right)$$

4.5.1.1 Transient Heat Flow

Assuming that all the energy that is absorbed in the tissue is converted to heat and that there is no heat loss (by conduction, convection or radiation) - admittedly, highly unlikely events - the rate of temperature change (ΔT) can be calculated by heat balance.

$$Q = m\, c_p\, \Delta T$$

where,

m = mass of tissue being heated (g)

c_p = specific heat of tissue (cal/g/°C)

ΔT = temperature difference (°C)

The following numerical example shows the utility of the above equations:

A for skin ≈ 1 dB/cm/MHz

Assume that the density and specific heat of skin are 1 g/cm^3 and 1cal/g/°C respectively *[Stoll and Green, 1959]*.

Δx = 1cm

f = 10 MHz

I = 0.2 W/cm^2

$$Q = 0.2\,(1 - \frac{1}{10^{(1 \times 10 \times 1)/10}})$$

$$= 0.18 \text{ W/cm}^2$$

$$\frac{d(\Delta T)}{dt} = \frac{Q}{m\, c_p}$$

$$= \frac{0.18 \text{ cal}}{4.2 \text{ sec.cm}^3} \frac{\text{cm}^3}{1 \text{ g}} \frac{\text{g °C}}{1 \text{ cal}}$$

$$= 0.04 \text{ °C/sec}$$

4.5.1.2 Steady-state Heat Flow

At steady state, all the heat supplied is conducted away. The heat flux per unit area (Q) normal to the direction of propagation is proportional to the temperature gradient, $(\frac{dT}{dx})$, or:

$$Q = k\frac{dT}{dx} \qquad (4.12)$$

where k (cal/cm/°C/sec) is the thermal conductivity. The thermal conductivity of skin is reported to be $5x10^{-2}$ and $9x10^{-4}$ cal/cm/°C/sec *[Barbnel, 1988]* with and without blood circulation present respectively. The above equation (4.12) can be integrated to yield

$$Q = k\frac{\Delta T}{\Delta x}$$

If Δx is 1 cm, Q = 0.18 W/cm^2, and k = 5 x 10^{-2} cal/cm/°C/sec (assuming that the blood circulation is in effect *in vivo*)

$$\Delta T = Q\frac{\Delta x}{k}$$

$$= \frac{0.18}{4.2} \times \frac{1}{5x10^{-2}}$$

$$= 0.86\ ^\circ C$$

The above calculation reveals that a temperature gradient of 0.86°C exists in 1 cm of the skin under consideration. It should be noted that in both transient and steady-state analyses, the heat source was characterized to be a point source. If a distributed source is assumed, which is a closer approximation to reality, a lower temperature gradient will result, because of the proximity of the sink to some of the heat generation points.

4.5.2 Mechanical and Cavitational Effects (Non-thermal Effects)

When ultrasound impinges on a particle, each particle is initially displaced from its equilibrium (resting) position and overshoots this position on its return journey so that it oscillates back and forth about this point with gradually decreasing amplitude, until it is eventually stationary in its original position after the wave has departed. The

maximum displacement amplitude of each particle is determined by the amount of energy contained within the wave at that site and is proportional to the square root of the incident intensity at any given frequency. The frequency is important, because the particles vibrate faster at high frequencies and will therefore require the input of more energy to achieve the same maximum displacement amplitude as the frequency is raised. Thus, at any given intensity, the maximum displacement amplitude (A) of the particles of the medium decreases with increasing frequency (i.e. $A \propto 1/f$). For a wave of frequency of 1 MHz and intensity 1 W/cm^2, $A \approx 0.018$ μm.

The oscillatory motion of each particle means that it must be accelerated from its stationary position (i.e., its position of maximum displacement amplitude) until it attains its maximum velocity. It must then be decelerated at the same rate until its velocity is again zero when it reaches its opposite maximum displacement amplitude. The maximum value of this acceleration is also proportional to the square root of the intensity at that site. As the frequency of the wave increases, each particle has to undergo more cycles of acceleration and deceleration per second; hence, the maximum values developed have to be increased. These instantaneous acceleration forces are very large compared with the forces we normally encounter; for example, a 1 MHz wave at an intensity of 1 W/cm^2 develops a maximum particle acceleration equal to 71,000 times the acceleration due to gravity on earth. Thus, a "typical" ultrasound beam used in diagnostics or therapy might produce minute particle displacements with small particle velocities, but is associated with enormously large values of instantaneous particle accelerations.

As can be inferred from the above, adjacent portions of the same membraneous structure may be vibrating with different displacement amplitudes and may be subjected to considerable stress, which may cause "fatigue" and rupture.

However, the largest and potentially more serious mechanical forces, which are generated by an ultrasonic wave, are the fluid shear forces and/or shock waves produced by the oscillatory behavior of minute gas bubbles: i.e., cavitation, which is discussed in Chapter 6.

The third major class of mechanical forces generated by ultrasonic waves are the radiation pressure forces which effectively push or pull cells and gas bodies to different portions of an inhomogeneous acoustic field.

The crucial questions are: "how large are the forces generated by a given ultrasonic beam?", and "how are these forces distributed within the irradiated tissues?" Damage usually results when different portions of the same structure are subjected to different forces so that it is twisted or torn. The strains that act on these structures are governed by the relation between the size of the structures and the ultrasound wavelength (frequency). If the particle size is much smaller than the wavelength of the impinging beam, the probability of unequal stress and strain distribution is very low. Ultrasound with a frequency of 10 MHz (velocity ca. 1500m/sec, and $\lambda = 0.15$ mm) results in regions of maximum opposite motion at one half wavelength or 75 μm. Thus, structures having dimensions of this order or larger will be subjected to cylindrical strains equal to twice the maximum particle displacement amplitude. In the case of SC, the corneocytes are smaller than 75 μm and the intercellular lipid bilayers are of even smaller dimension. Therefore, it is unlikely that these structures are affected by cylindrical strains.

However, the effects of ultrasound on skin remain unclear, because this tissue has not been the organ of primary interest for ultrasound specialists. Inferences, based on the existing literature describing the effects of ultrasound on other tissues, are possible but remain largely unproven.

4.6 Conclusion

We have discussed the generation and propagation of ultrasound, and it has been shown that higher frequencies deposit more energy in a given volume of tissue than lower frequencies. This energy deposition is unlikely to result in significant temperature increase in tissue such as the SC. However, non-thermal effects, such as cavitation, can alter the tissue significantly.

Table 4.1 Acoustic Quantities

Symbol	Quantity	Units (SI; cgs)
u	Particle velocity	m/s
u_0	Velocity amplitude	Applicable when u(t) is sinusoidal
p	Acoustic pressure	Pa; dyn/cm^2
p_0	Pressure amplitude	Applicable when p(t) is sinusoidal
W	Acoustic pressure averaged over one or more cycles of a continuous wave	W; mW
I	Intensity or power averaged over one or more cycles of a continuous wave	W/m^2; mW/cm^2.
i	instantaneous intensity	W/m^2; mW/cm^2
f	frequency	Hz; MHz
ρ	density of the medium	kg/m^3; g/cm^3
c	speed of sound	m/s; cm/s
ρc	characteristic acoustic impedance	N s/m^3; dyn s/m^3
λ	wavelength	m; cm
k	propagation constant	$2\pi/l$
α	attenuation coefficient	Np/m; Np/cm (db/cm/MHz)
α	absorption coefficient	Np/m; Np/cm (db/cm/MHz)

References

Barbnel, J.C., 1988, The Thermal Properties of Skin, in **The Physical Nature of the Skin,** eds. Marks, R.M., Barton, S.P., and Edwards, C.; MTP Press Ltd., Boston, pp. 191-200.

Goss, S.A., Johnston, R.L., and Dunn, F., 1980, Compilation of Empirical Ultrasonic Properties of Mammalian Tissues:II, **Journal of the Acoustic Society of America,** 68: 93-110.

Stoll, A.M., and Green, L.C., 1959, Relationship Between Pain and Tissue Damage due to Thermal Radiation, **Journal of Applied Physiology,** 14: 373-387.

Williams, A.R., 1983, **Ultrasound: Biological Effects and Potential Hazards,** Academic Press, San Francisco.

Biological Effects of Ultrasound, *eds. Nyborg, W.L., and Ziskin, M.C.,* Churchill Livingstone, New York, 1985.

Biological Effects of Ultrasound: Mechanisms and Clinical Implications, National Council of Radiation Protection and Measurements Report No. 74, Bethesda, Maryland, 1983.

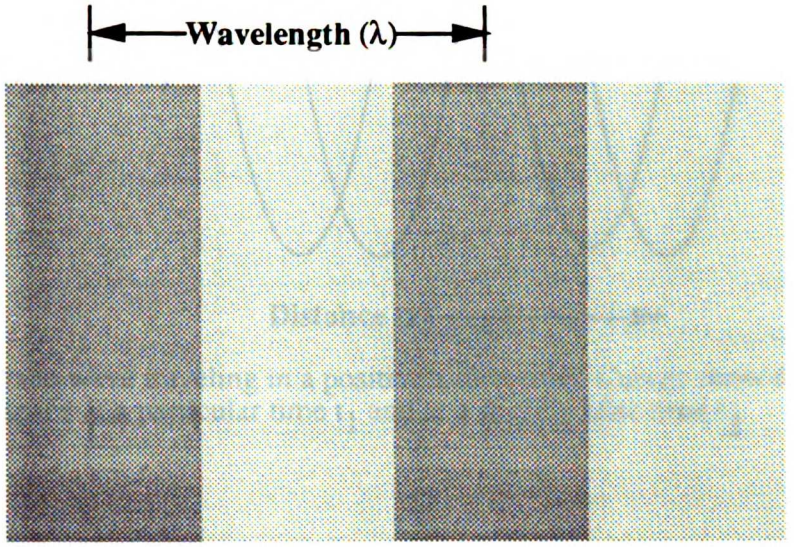

Figure 4.1. Alternating regions of compression and rarefaction as they exist at any instant in a plane wave of ultrasound. The wavelength is the distance between consecutive compressions (or consecutive rarefactions).

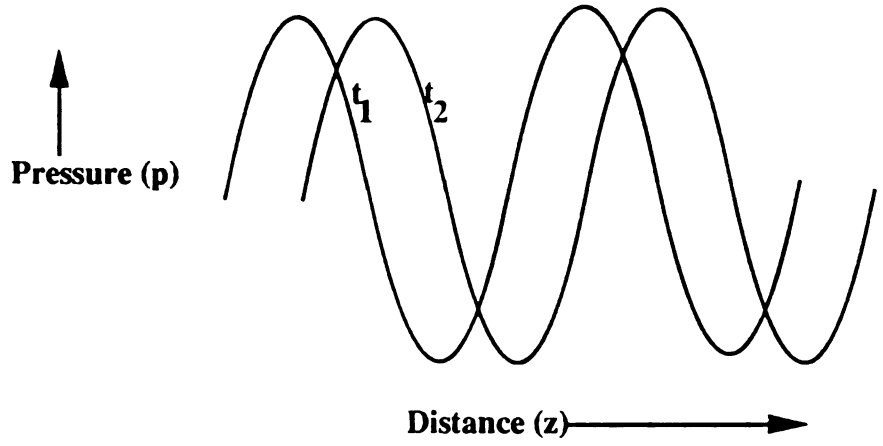

Figure 4.2. Plane wave traveling in a positive z direction. Curves show the pressure as it varies in space at a particular time t_1 and at a slightly later time t_2.

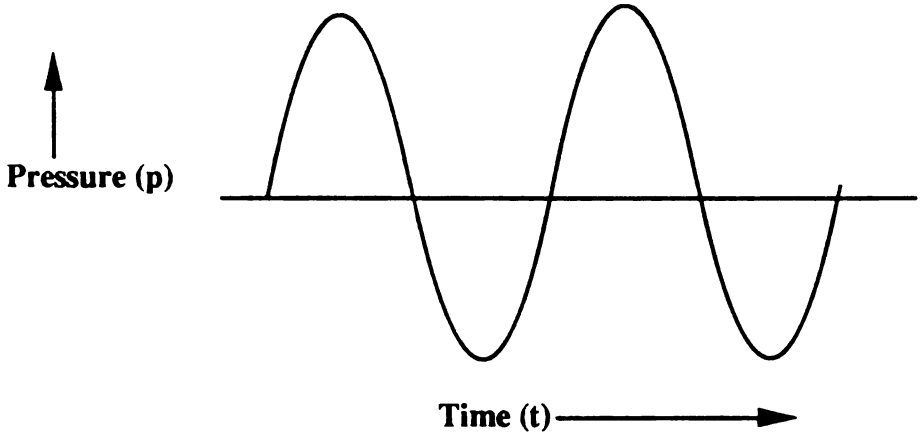

Figure 4.3. Variation of pressure with time in a continuous single-frequency ultrasonic field.

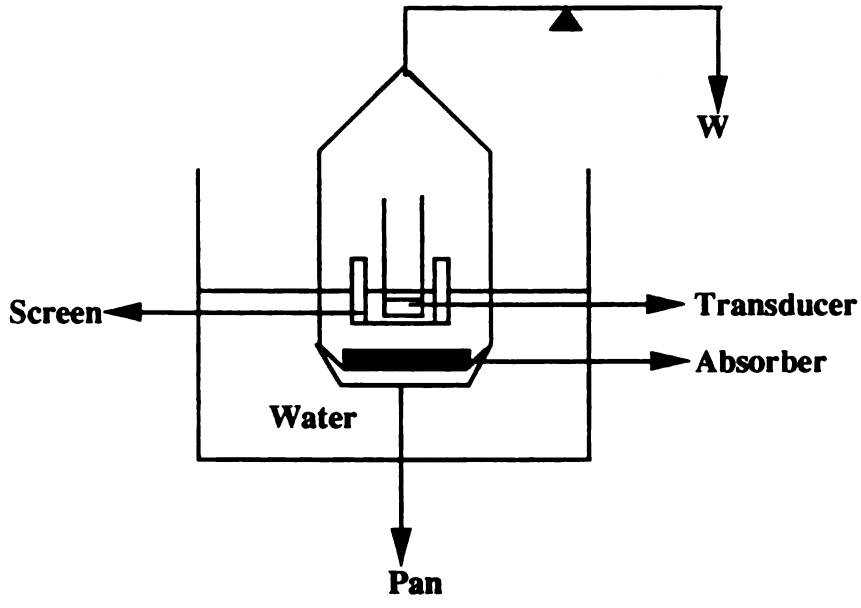

Figure 4.4. Experimental apparatus used for the measurement of acoustic power output. The ultrasound emitted by the transdurcer passes through the acoustically transparent screen (to eliminate acoustic streaming) before being absorbed by the "perfect absorber." The resulting force displaces the balance pan within the waterbath so that weight (W) has to be added to the counterbalance to restore the pan to its original position.

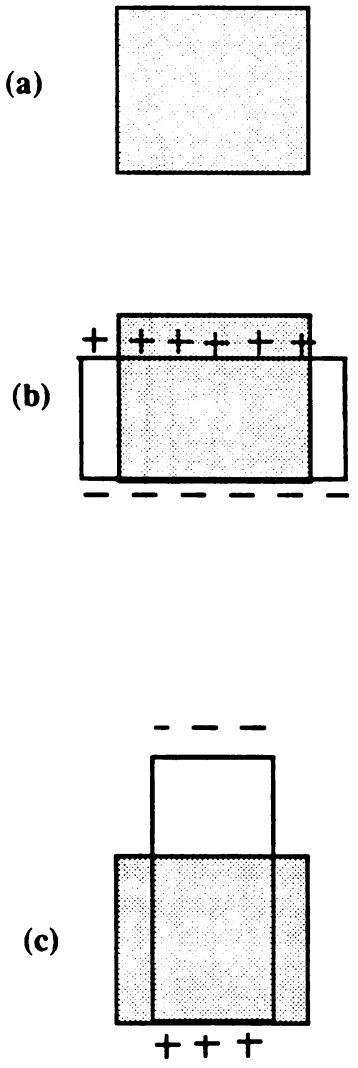

Figure 4.5 A schematic of the change in dimensions of a piezoelectric material. The undeformed crystal (a) is flattened by one polarity of an applied voltage (b) and stretched by the reverse polarity (c). Thus, the application of a sinusoidal (AC) voltage would cause the body to oscillate between the two extreme shapes shown in (b) and (c).

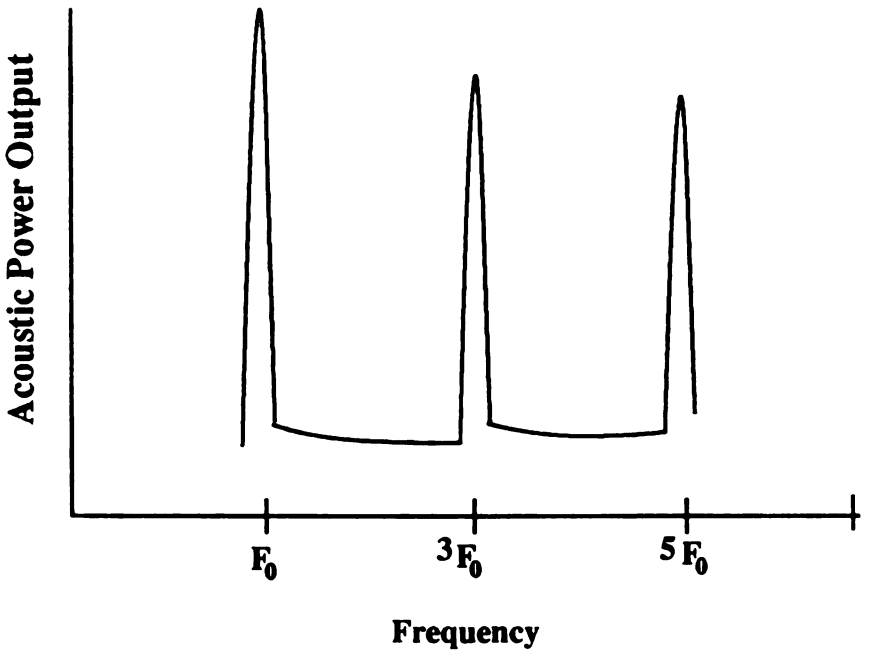

Figure 4.6 The displacement amplitude of a transducer as a function of the driving frequency. At resonance (e.g. F_0, $3F_0$ and $5F_0$) the acoustic power output is maximum.

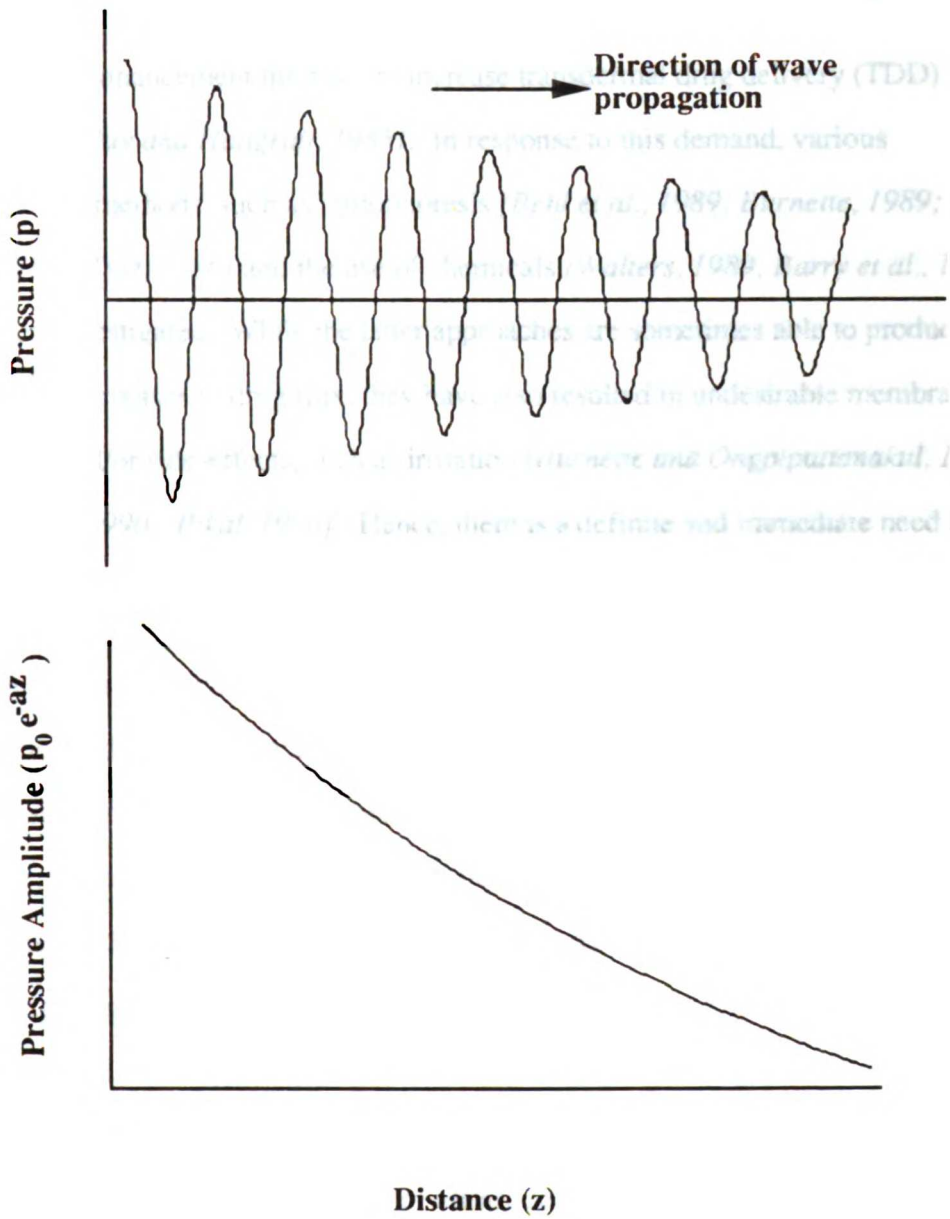

Figure 4.7. Acoustic pressure p (top) and pressure amplitude $p_0 e^{-\alpha z}$ (bottom) versus distance at a given instant in a strongly attenuated plane wave.

5. Sonophoresis: I. The Use of Ultrasound to Enhance Transdermal Drug Delivery

5.1 Introduction

The need for enhancement methods to increase transdermal drug delivery (TDD) is well established *[Guy and Hadgraft, 1985]*. In response to this demand, various enhancement methods, such as iontophoresis *[Behl et al., 1989; Burnette, 1989; Chien et al., 1989; Tyle, 1986]* and the use of chemicals *[Walters, 1989; Barry et al., 1989]* have been investigated. While the latter approaches are sometimes able to produce appreciable increases in drug flux, they have also resulted in undesirable membrane alterations and/or side-effects, such as irritation *[Burnette and Ongpipattanakul, 1988; Green et al., 1990; Pikal, 1990]*. Hence, there is a definite and immediate need for an effective enhancement method, which has minimal "toxicological" drawbacks.

Ultrasound has been used extensively over the last three decades for medical diagnostics and physical therapy. For such applications, the technique has been deemed safe with no long or short-term side effects *[NCRP report, 1983]*. Ultrasound, therefore, appears to satisfy at least one major criterion of an ideal approach to enhance TDD (see Section 1.3). The first published report on the use of ultrasound for increasing drug flux across the skin, so-called sonophoresis, appeared in 1954 *[Fellinger and Schmid, 1954]*. Since then, there have been numerous further studies, primarily *in vivo [Skauen and Zentner, 1984; Tyle and Agrawala, 1989]*. However, there is no consensus on the efficacy of ultrasound for increasing drug flux across the skin. While some studies report the successful employment of sonophoresis *[Davick et al., 1988; Griffin and Touchstone, 1963; Griffin et al., 1965; Griffin et al., 1967; Levy et al., 1989]*, others have reported negative results *[Benson et al., 1989; McElnay et al., 1985; Pratzel et al., 1986]*. Although these different investigations

have involved compounds (such as hydrocortisone, cortisol, salicylic acid, lidocaine, etc.) of various physicochemical characteristics, incorporated in a range of formulations (i.e., gels, creams and lotions), no consistent pattern of behavior has evolved. The common features of this earlier research were that the ultrasound used (1) was in the frequency range 1-3 MHz and (2) had an intensity between 1 and 3 W/cm^2.

An understanding of the physics of ultrasound propagation in tissue, and knowledge of the barrier properties of skin, permit us to identify those ultrasound parameters which should improve the efficacy of sonophoresis. It is established that stratum corneum (SC), the outermost, 15-25 μm of the skin, is the rate-limiting barrier for percutaneous absorption *[Scheuplein, 1976; Elias, 1983]*. Consequently, efforts to enhance percutaneous absorption must focus primarily on this barrier. Energy deposited within the SC can result in membrane alterations. Therefore, we, address the questions: "how is ultrasound transmitted through the skin?", and "in what way is the mechanical energy of ultrasound deposited in the different layers of the membrane?"

Ultrasound waves are sound waves above the audible limit (above 20 kHz). The properties of ultrasound are identical to those of audible sound. For example, ultrasound also requires a medium for transmission. Two parameters, the amplitude (A), and the frequency (f) fully describe ultrasound waves (Figure 5.1). They are longitudinal waves with periodic peaks and troughs. The particles in a medium, through which ultrasound passes, are subjected to periodic oscillations about their resting positions. The maximum displacement of a particle is proportional to the intensity (i.e., the energy content) of the ultrasound beam. As expected, the number of ultrasound-induced oscillations is proportional to the frequency of the ultrasound waves. Similar to audible sound, ultrasound waves can undergo reflection, refraction and/or absorption when they encounter another medium with dissimilar properties *[Williams, 1983]*. If the properties of the encountered medium are significantly

different from those of the transmitting medium, the acoustic energy of the transmitted ultrasound beam is attenuated by the above process(es). The attenuation of ultrasound in tissue, which limits its depth of penetration, is a function of the frequency, and of the properties of the absorbing tissue *[Williams, 1983]*. An empirical relationship between energy loss and frequency is given by *[Williams, 1983; NCRP report, 1983; Nyborg, 1985]*

$$\text{energy loss} = 1 \text{ decibel/cm/MHz}$$

where,

$$1 \text{ decibel} = 10 \log_{10} I/I'$$

and I and I' are the energy intensities of the beam at two points z and z'.

The preceding equation predicts that higher frequency waves undergo greater energy loss in a tissue, and lead to increased energy concentration in the tissue. This is illustrated in Figure 5.2 where the percentage of the applied energy which is lost in a 1mm thick tissue is plotted as a function of frequency. The absorbed ultrasound energy can cause tissue heating. In addition, since ultrasound waves are mechanical waves, they can also induce localized shear stresses within the conducting medium. This local effect may lead to structural alterations in the tissue. These effects can (singly or in combination) render the tissue more permeable.

When using ultrasound to increase drug flux across the skin, the SC is the rate-limiting membrane which has to be perturbed. Furthermore, since higher frequency ultrasound will increase the energy deposition within the SC (which is rather thin), use of high frequency ultrasound may result in a more permeable membrane. The objective of this work was to test this hypothesis. We have examined the skin penetration enhancement induced by ultrasound at 2, 10 and 16 MHz frequencies *in vivo* using hairless guinea

pigs. We have observed that the higher frequencies (1) increased drug flux across the skin, and (2) reduced the lag time typically associated with TDD.

5.2 Materials and Methods

High frequency continuous wave ultrasound was generated using a set-up consisting of a signal generator (Model 8116A, Hewlett Packard, Palo Alto, CA), a power amplifier (325LA, ENI Co., Santa Clara, CA), and a set of ultrasound transducers (Precision Acoustic Devices, Fremont, CA, and Panametrics, Waldham, MA). The resonant frequencies of the transducers were confirmed using a network analyzer, and the transducers were driven at their fundamental resonant frequencies in all the experiments. The electrical energy content of the amplified high frequency electrical signals was measured using a power meter (Model 4421-101, Bird electronics, Ojai, CA). The transducers converted these electrical signals into ultrasound waves. The experimental set-up is shown in Figure 5.3. To evaluate the acoustic efficiency of the transducers (efficiency of converting the electrical energy to mechanical (ultrasound) energy) radiation force measurements were made. These are described in detail elsewhere *[Carson et al., 1978; Lunt and Ashley, 1979]*. Briefly, the acoustic power output of the ultrasound waves can be measured by the weight they register on a sensitive balance. By measuring the weights which different transducers register on the balance for the same electrical energy input, the acoustic efficiency of these transducers can be compared. These radiation force measurements were made by using the equipment shown in Figure 4.4.

Hairless guinea pigs (8 - 16 weeks old) were obtained from Charles River (Boston, MA). Salicylic acid was obtained from Aldrich Chemicals (St. Louis, Missouri). Carbopol™ was a gift from BF Goodrich & Co (Akron, OH). The gel formulation, which acts as both coupling agent and drug reservoir, was prepared as follows: 0.5 gm

of salicylic acid (including trace amounts of ^{14}C labelled salicylic acid - NEN, Delaware) was dissolved in 97 ml of water to produce a saturated solution of salicylic acid. 0.5 gm of Carbopol™ (polyacrylic acid polymer) was added to this solution which was then thoroughly mixed using a vortex mixer. The formulation was left to stand overnight. After 24 hours, 0.5 gm of NaOH was added so that the polymer network would extend and the gel swell. The addition of NaOH also resulted in the formulation pH being equal to 5.5. Since the pKa of salicylic acid is 2.97, the drug was completely ionized and dissolved in the gel. To study the effect of ultrasound on the transdermal delivery of the unionized form of the drug, we formulated another gel without NaOH. This resulted in a gel pH of 1.5. At this pH, Carbopol™ is in a completely random coil form (as opposed to the extended network conformation at pH 5.5). The acidic formulation had a different consistency, therefore, from that of the pH 5.5 gel.

At least three animals were used for each experiment and, to reduce errors due to inter-animal variability, each animal served as its own control.

5.2.1 Tape-stripping and Urinary Excretion

Enough gel was spread on the face of the transducer to cover it completely as a thin film. (Based on the amount of drug penetrated, the amount of drug applied was an infinite dose). The transducer was placed in contact with the skin on one flank of the animal and was activated for 5 or 20 minutes. The intensity of the input energy was set to be 0.2 W/cm^2. At the end of the treatment period, the skin surface was cleaned of all residual gel by wiping with wet cotton swabs, followed by a water wash. The control experiments were carried out in an identical fashion on the contralateral flank of the animal. The only difference between control and treatment protocol was that the transducer was not activated during the control procedure. The efficacy of the treatment

was determined by comparing the amount of drug penetrated into the animal with and without ultrasound. There was at least a two week difference between the control and treatment procedures, and the procedures were conducted in random sequence.

The amount of drug that had penetrated into the animal was quantified in two ways: (1) Sequential tape-strips of the SC were removed using Scotch™ tape and the amount of radioactivity, which was recovered in each strip, was determined. (2) The animals were housed in metabolic cages, and urine was collected periodically and monitored for radioactivity until there was no further detectable amounts of ^{14}C-labelled material. To 0.5 ml of urine, 0.5 ml of 1 N HCl and 4.5 ml of scintillation fluid (Readygel™, Beckman, Irvine, CA) were added. The vials were kept in the dark for at least 12 hours so that the radioactivity measured by the scintillation counter was the result of true radioactive disintegration, rather than artifactual chemiluminescence. Subsequently, the amount of radioactivity was measured using a Beckman LS4000 liquid scintillation counter (Beckman, Irvine, CA). All radioactivity data were corrected for background radioactivity and, in the case of urine, quenching due to coloration.

5.2.2 Urinary Excretion

Excluding the tape-stripping step, a protocol identical to that described above, in Section 5.2.1, was followed.

5.2.3 Pre-treatment Experiments

The selected site was pre-treated with ultrasound for 10 minutes using water as the coupling medium. Thereafter, the skin was exposed to the drug-loaded gel for 5 minutes. Subsequently, tape-stripping and urinary analysis were performed as described in Section 5.2.1. The control procedure employed an identical protocol on the contralateral flank without the transducer being activated.

5.2.4 Skin Temperature Measurements

Skin temperature was monitored using a digital thermometer with an ultrasound transparent probe head (BAT-12, Sensortek, Clifton, NJ). The probe head was positioned between the transducer and the skin, and the local temperature was recorded at periodic intervals.

5.2.5 Data Analysis

Knowing the amount of radioactivity added to the gel, the recovered radioactivity (from tape-stripping the SC and urine) was converted to micrograms of drug. The amount of drug that was measured in the tape-strips and urine indicated the amount that had penetrated into the animals. The transducers used had different cross-sectional areas. In order to compare the results obtained using different transducers, the amount (in micrograms) of drug recovered was divided by the cross-sectional area of the transducer employed.

To quantify the effect of ultrasound on the drug flux, we defined the percentage enhancement, E, as

$$E = \frac{\text{radiolabel (drug) recovered post-sonophoresis}}{\text{radiolabel (drug) recovered after passive diffusion}} \times 100$$

5.3 Results

The results of the radiation force measurements are in Figure 5.5. The 2 and 16 MHz transducers (received from the same manufacturer) had the same acoustic efficiency. The 10 MHz transducer (obtained from a different manufacturer) had a relatively higher efficiency.

Figure 5.6 compares the amount of salicylic acid, which penetrated hairless guinea pig skin in 20 minutes, (a) by passive diffusion and (b) with sonophoresis using 2, 10 and 16 MHz frequencies at 0.2 W/cm^2. The hatched bars represent drug present in the SC, which was recovered by tape-stripping. The unfilled segments above the hatched rectangles indicate drug recovered in the urine. The results obtained for each animal after sonophoresis (T) and passive diffusion (C) are presented side-by-side to facilitate direct comparison. Sonophoresis at 2 MHz did not significantly increase the total drug flux compared to passive diffusion. However, sonophoresis using 10 and 16 MHz frequencies resulted in a significantly enhanced amount of TDD (E_{10MHz} = 415±89 %, $p \leq 0.03$; E_{16MHz} = 253±42 %, $p \leq 0.05$).

In the next series of experiments, to assess the effect of shorter ultrasound exposure, sonophoresis was carried out for only 5 minutes. The results of these experiments are shown in Figure 5.7. Similar to the results obtained following 20 minutes of sonophoresis, the shorter exposure at 10 and 16 MHz enhanced the flux of salicylic acid through the skin for all the animals used (E_{10MHz} = 160±24 %, $p \leq 0.02$; E_{16MHz} = 177±21 %, $p \leq 0.04$). As expected, due to the reduced contact time between the formulation and skin, TDD overall was lower.

Figure 5.8 shows the results of the experiments, in which drug penetration was assessed from urine analysis alone, and tape-stripping was not performed. (Section 5.2.2 of Materials and Methods). Sonophoresis for 5 and 20 minutes increased the amount of radioactivity eliminated in the urine of all animals tested, indicating again that more drug entered the systemic circulation under the influence of ultrasound ($E_{5min.}$ = 226±106 %; $E_{20min.}$ = 211±29%; $p \leq 0.08$). To assess the effect of ultrasound on diffusional lag-time, temporal evolution of the data in Figure 5.8 are plotted in Figures 5.9a and 5.9b. Two conspicuous and significant features are: (1) The area under the treatment curve (indicating the total amount of radioactivity eliminated) is larger than the

corresponding control. (2) Radioactivity is detected in the urine much sooner following sonophoresis indicating that the lag-time for diffusion is reduced. Ultrasound did not appear to influence the volume of urine excreted: there was no significant difference between the volumes of urine excreted with and without ultrasound.

Figure 5.10 shows the effect of pre-treating the skin with ultrasound followed by application of the drug-containing gel without ultrasound (Section 5.2.3). As observed above, salicylic acid absorption through ultrasound-pretreated skin is greater than that through the corresponding control. These data suggest that that pre-treating the skin with ultrasound makes the SC more permeable.

Figure 5.11 shows the effect of sonophoresis on the percutaneous transport of unionized salicylic acid (gel pH = 1.5). Compared to the results using the pH 5.5 gel (Figure 5.6), there are two significant differences: (1) The total amount of the drug penetrating (both with and without ultrasound) is about an order of magnitude greater. (2) The enhancement effects are smaller (E_{10MHz} = 130±7 %; E_{16MHz} = 156±21 %). Nevertheless, sonophoresis increased drug flux relative to passive diffusion.

5.4 Discussion

As stated earlier, previous attempts to enhance percutaneous absorption using ultrasound have been unsuccessful or unimpressive, despite the use of high intensities (≥1 W/cm^2). We hypothesized that this poor performance was due to the use of relatively low ultrasound frequencies (1-3 MHz) which would produce very little energy dissipation within the SC. Thus, in this study, we have used frequencies of 2, 10 and 16 MHz. The intensity of 0.2 W/cm^2, a value much lower than that previously used, falls in the range of diagnostic applications of ultrasound; the higher levels employed before are characteristic of those considered beneficial in physical therapy. Our preference for avoiding high intensity was based on the fact that continuous and/or

repeated application of high intensity ultrasound, as may be needed for TDD enhancement, can lead to significant, and often intolerable, heating. To minimize heating, physical therapists either use pulsed waves and/or move the transducer around the treatment area, while minimizing direct contact with the skin. Obviously, appreciable local heating may be expected to lead to poor patient compliance. Under our experimental conditions, no significant increase in skin temperature (i.e., less than 1°C) was observed, presumably because of the low intensities employed. We can, therefore, discount local heating of the skin as a mechanism by which the observed enhancement is induced. Parenthetically, we note that, for water, a 10°C increase in temperature is necessary for a doubling of skin permeability *[Potts and Francoeur, 1990]*.

Although the biological effects of diagnostic intensities have been well documented, the same cannot be said of high ultrasound intensities *[Williams, 1983]*. The acceptability of sonophoresis, therefore, will be greater if it is shown to be effective at low intensities. A comment should also be made about the use of high frequency ultrasound. Because the attenuation of ultrasound is directly proportional to the frequency, the depth of penetration of ultrasound varies inversely with frequency. The combination of low intensity and high frequency, therefore, should concentrate the effect of the ultrasound beam to the superficial skin layers, and minimize any negative effects of ultrasound on deeper tissue. In the next chapter, this issue is addressed by examining the impact of ultrasound on epidermal tissue morphology.

The results presented in this chapter demonstrate that high frequency ultrasound, at a diagnostic intensity (0.2 W/cm^2), can enhance the TDD of salicylic acid. Ultrasound requires a coupling medium for efficient energy transmission to the skin; an aqueous gel is a suitable coupling medium between the transducer and skin. Furthermore, the gel can also serve as a drug reservoir and salicylic acid was chosen for this study, at

least in part, because of its solubility in water. Although it had been reported earlier that ultrasound can facilitate the release of molecules from polymeric matrices *[Kost et al., 1989]*, we found that ultrasound did not alter the efflux of salicylic acid into an aqueous reservoir from the gel employed (see Figure 6.1 and the discussion in Chapter 6). The acoustic impedance mismatch between the transducer and the polymer matrix may explain the enhanced drug release observed in the experiments of Kost *et al. (1989)*. Conversely, the acoustic impedance values of water (gel) and skin do not differ significantly. Confirmation that ultrasound acts on the SC barrier (and not on the release of drug from the formulation) is provided by the pre-treatment experiments. As no drug-containing gel is involved in the pre-treatment of the skin with ultrasound, the enhanced drug delivery that is measured on subsequent application of the formulation must result from ultrasound-induced changes in the skin during the pre-treatment process. The duration and reversibility of this effect, and the possible mechanism(s) of action, are discussed in the next chapter.

The majority of the experiments described were performed with the pH 5.5 gel formulation, in which salicylic acid (pKa = 2.97) is essentially completely ionized. To study the effect of ultrasound on the transport of unionized drug, some experiments were also conducted using a gel formulation at pH 1.5. Although the delivery of radiolabel in this case was higher (for both ultrasound-treated and control experiments), the enhancement achieved by ultrasound was lower than that observed when the pH 5.5 formulation was used. We note that the two formulations had different physical properties. The pH 5.5 gel was more viscous and clearly recognizable as a conventional gel; the low pH formulation, on the other hand, was more a viscous solution than a gel. At present, it is not known whether the observed difference in the effects of ultrasound on the permeation of ionized and unionized species are formulation-related or a consequence of the inherent mechanism of action of

ultrasound. Furthermore, the strongly acidic formulation (pH 1.5) could also have an effect on skin and influence the permeation of salicylic acid.

Two major impediments to the more widespread use of TDD are the limited permeability of molecules through the skin and the unacceptably long lag-times associated with the attainment of a therapeutically useful flux. The data presented here suggest that ultrasound can, to some extent, counter both of these problems (see Figures 5.9a and 5.9b). Figure 5.9a shows that the extent of TDD is increased using sonophoresis. Figure 5.9b indicates that the lag-time can be reduced compared to that associated with passive diffusion. These advantages may be particularly significant, for example, in the delivery of local anesthetics.

A comment upon the characteristics of the transducers is warranted at this point. High frequency transducers (>2 MHz) are not commonly available. The transducers used in this study were custom-made, therefore. The transducers were supplied by two different manufacturers (2 and 16 MHz from one, and 10 MHz from another), and they possessed different performance efficiencies (Figure 5.5). For different input electrical energies, the 10 MHz transducer operated at a much higher efficiency, compared to the other two transducers, in converting the electrical signals to mechanical waves. The increased enhancements we observed using the 10 MHz transducer (compared to the 16 MHz), which is contrary to our initial hypothesis are, we believe, due to its higher efficiency. To account for the lower acoustic efficiency of the 16 MHz transducer, attempts were made to use higher intensities (≈ 0.35 W/cm^2). Unfortunately, the transducer heated up significantly. Since we were unable to distinguish between enhancement due to ultrasound effects and that due to skin heating, we had to abandon this approach.

The exposure of the skin to ultrasound in the experiments reported here was of much shorter duration than those previously described in the literature. In general, studies of the effects of different enhancers or enhancement methods have typically involved treating the skin for periods longer than one hour. The earlier work on sonophoresis (which has produced equivocal results) is no exception to this rule. In contrast, the treatment times of 20 and 5 minutes, which we have used here, have yielded significantly enhanced transport of the test molecule compared to its passive diffusion. Although the increase in TDD is modest (maximally about 4-fold), the results support the hypothesis that higher frequency ultrasound is more effective for sonophoresis. Furthermore, it is efficacious with relatively short treatment times, a potentially desirable feature from the standpoint of patient acceptability and compliance. One may also speculate that the combination of sonophoresis with other enhancement methods, such as chemical enhancement and/or iontophoresis, may result in a synergistic response in which the result exceeds the sum of individual parts. This may simply take the form of reducing the "severity" of the conditions employed in the different promotion methods. For example, the use of a lower current density in iontophoresis when used in conjunction with sonophoresis. As a variation on this theme, one might envisage sonophoretic pre-treatment of the skin prior to the application of an iontophoresis device, which would now be able to operate at a much lower power.

Having established that high frequency ultrasound can cause significant increase in TDD, it is now necessary to address a number of key mechanistic questions, including: Where is ultrasound eliciting its action? On which route of penetration? What membrane (i.e., epidermal) alterations are induced by ultrasound? To what extent are these effects reversible? Investigations designed to respond to these issues are presented in the next chapter.

5.5 Conclusions

Based on the theory of ultrasound propagation in tissue, we postulated that high frequency ultrasound would improve the efficacy of sonophoresis. From experiments performed in hairless guinea pigs *in vivo* , we have shown that: (1) The TDD of salicylic acid is significantly increased by ultrasound application for 5 or 20 minutes, when compared to passive diffusion. (2) The lag-time associated with passive diffusion through the skin is significantly reduced with sonophoresis. In Chapter 6, we describe attempts to probe the enhancement mechanism underlying sonophoresis, the reversibility of the effect, and the impact of ultrasound on epidermal morphology.

References

Barry, B.W., 1983, **Dermatological Formulations,** Marcel Dekker, New York.

Behl, C.R., Kumar, S., Malick, A.W., DelTerezo, S., Higuchi, W.I., and Nash, R.A., 1989, Iontophoretic Drug Delivery: Effects of Physicochemical Factors on the Skin Uptake of Nonpeptide Drugs, **Journal of Pharmaceutical Sciences,** 78: 355-360.

Benson, H.A., McElnay, J.C., and Harland, R., 1989, Use of Ultrasound to Enhance Percutaneous Penetration of benzydamine, **Physical Therapy,** 69: 113-118.

Burnette, R.R., 1989, Iontophoresis, in **Transdermal Drug Delivery: Developmental Issues and Research Initiatives,** eds. Hadgraft, J., and Guy, R.H., Marcel Dekker, Inc., New York, pp. 247-291.

Burnette, R.R., and Ongpipattanakul, B., 1988, Characterization of the Pore Transport Properties of Excised Human Skin During Iontophoresis, **Journal of Pharmaceutical Sciences,** 77: 132 -138.

Carson, P.L., Fischella P.R. and Oughton, T.V., 1978, Ultrasonic Power and Intensities Produced by Diagnostic Ultrasound Equipment, **Ultrasound in Medicine and Biology,** 3: 341-350.

Chien, Y.W., Siddiqui, O., Shi, W., Lelawongs, P., and Liu, J., 1989, Direct Current Iontophoretic Transdermal Delivery of Peptide and Protein Drugs, **Journal of Pharmaceutical Sciences,** 78: 376-383.

Davick, J.P., Martin, R.K., and Albright, J.P., 1988, Distribution and Deposition of Tritiated Cortisol Using Phonophoresis, **Physical Therapy,** 68: 1672-1675.

Elias, P.M., 1983, Epidermal Lipids, Barrier Function and Desquamation, **Journal of Investigative Dermatology,** 80: 44s-49s.

Fellinger, K., and Schmid, J., 1956, Klinik und Therapie des Chronishen, **Gelenkreumatismus,** Maudrich, Vienna, pp. 549-554.

Green, P.G., Hinz, R.S., Kim A., Szoka, Jr., F.C., and Guy, R.H., 1990, Iontophoretic Delivery of a Series of Tripeptides Across the Skin *in vitro,* **Pharmaceutical Research,** submitted.

Griffin, J.E., Echternach, J.L., Price, R.E., and Touchstone, J.C., 1967, Patients Treated with Ultrasonic Driven Hydrocortisone and with Ultrasound Alone, **Physical Therapy,** 47: 594-601.

Griffin, J.E., and Touchstone, J.C., 1963, Ultrasonic Movement of Cortisol into Pig Tissues, I. Movement into Skeletal Muscle, **American Journal of Physical Medicine,** 42: 77-85.

Griffin, J.E., Touchstone, J.C., and Liu, A. C-Y., 1965, Ultrasonic Movement of Cortisol into Pig Tissues, I. Movement into Paravertebral Nerve, **American Journal of Physical Medicine,** 44: 20-25.

Guy, R.H., and Hadgraft, J., 1985, Transdermal Drug Delivery: The Ground Rules are Emerging, **Pharmaceutics International,** 6: 112-116.

Kost, J., Lenog, K., and Langer, R.,1989, Ultrasound-enhanced Polymer Degradation and Release of Incorporated Substances, **Proceedings of the National Academy of Sciences of the United States of America,** 86: 7663-7666.

Levy, D., Kost, J., Meshulam, Y., and Langer, R., 1989, Effect of Ultrasound on Transdermal Drug Delivery to Rats and Guinea Pigs, **Journal of Clinical Investigation,** 83: 2074-2078.

Lunt M.J., and Ashley, B., 1979, A Simple Balance For Measuring Ultrasonic Power, **Journal of Medical Engineering and Technology,** 3: 194-196.

McElnay, J.C., Matthews, M.P., Harland, R., and McCafferty, D.F, 1985, The Effect of Ultrasound on the Percutaneous Absorption of Lignocaine, **British Journal of Clinical Pharmacology,** 20: 421-424.

NCRP report, 1983, **Biological Effects of Ultrasound: Mechanisms and Clinical Implications,** National Council of Radiation Protection and Measurements Report No. 74, Bethesda, Maryland.

Nyborg, W.L., 1985, Mechanisms, in **Biological Effects of Ultrasound,** eds. Nyborg, W.L., and Ziskin, M.C., Churchill Livingstone, New York, pp. 23-33.

Pikal, M.J., 1990, Transport Mechanisms in Iontophoresis. I. A Theoretical Model for the Effect of Electroosmotic Flow on Flux Enhancement in Transdermal Iontophoresis, **Pharmaceutical Research,** 7:118-26.

Pikal, M.J., and Shah, S., 1990, Transport Mechanisms in Iontophoresis. III. An Experimental Study of the Contributions of Electroosmotic Flow and Permeability Change in Transport of Low and High Molecular Weight Solutes, **Pharmaceutical Research,** 7 :222-9.

Potts, R. O., and Francoeur, M. L., 1990, Lipid Biophysics of Water Loss through the Skin, **Proceedings of the National Academy of Science,** 87: 3871-3873.

Pratzel, H., Dittrich, P., Kukovetz, W., 1986, Spontaneous and forced cutaneous absorption of indomethacin in pigs and humans, **Journal of Rheumatology,** 13:1122-1125.

Scheuplein, R. J., 1976, Permeability of the Skin: A Review of Major Concepts, **Current Problems in Dermatology,** 7: 172-186.

Skauen, D.M., and Zentner, G.M., 1984, Phonophoresis, **International Journal of Pharmaceutics,** 20: 235-245.

Stoughton, R.B., 1989, Percutaneous Absorption of Drugs, **Annual Review of Pharmacology and Toxicology,** 29: 55-69.

Tyle, P., 1986, Iontophoretic Devices for Drug Delivery, **Pharmaceutical Research,** 3: 318-326.

Tyle, P., and Agrawala, P., 1989, Drug Delivery of Phonophoresis, **Pharmaceutical Research,** 6: 355: 361.

Walters, K.A., 1989, Penetration Enhancers and Their Use in **Transdermal Drug Delivery: Developmental Issues and Research Initiatives,** eds. Hadgraft, J., and Guy, R.H., Marcel Dekker, Inc., New York, pp. 197-246.

Williams, A.R., 1983, **Ultrasound: Biological Effects and Potential Hazards,** Academic Press, San Francisco.

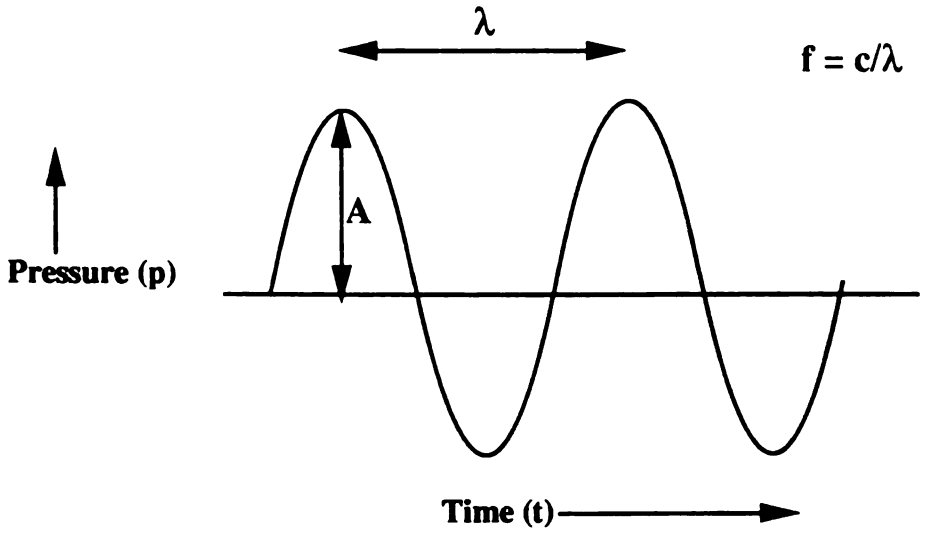

Figure 5.1 An ultrasound wave is described by its amplitude (A) and frequency (f).

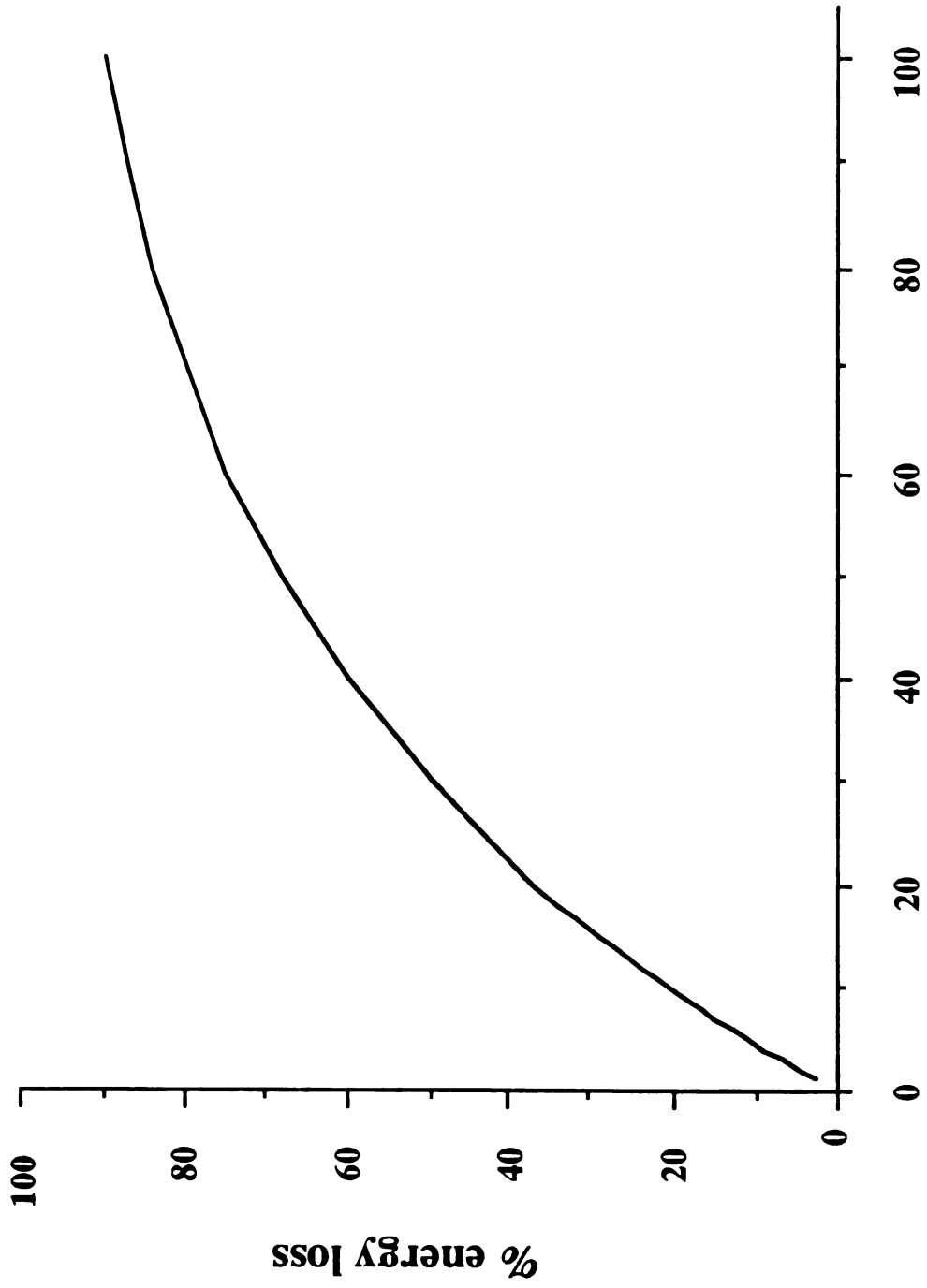

Figure 5.2 Percentage of the applied ultrasound energy lost in a 1 mm thick tissue (calculated assuming a loss of 1dB/cm/MHz).

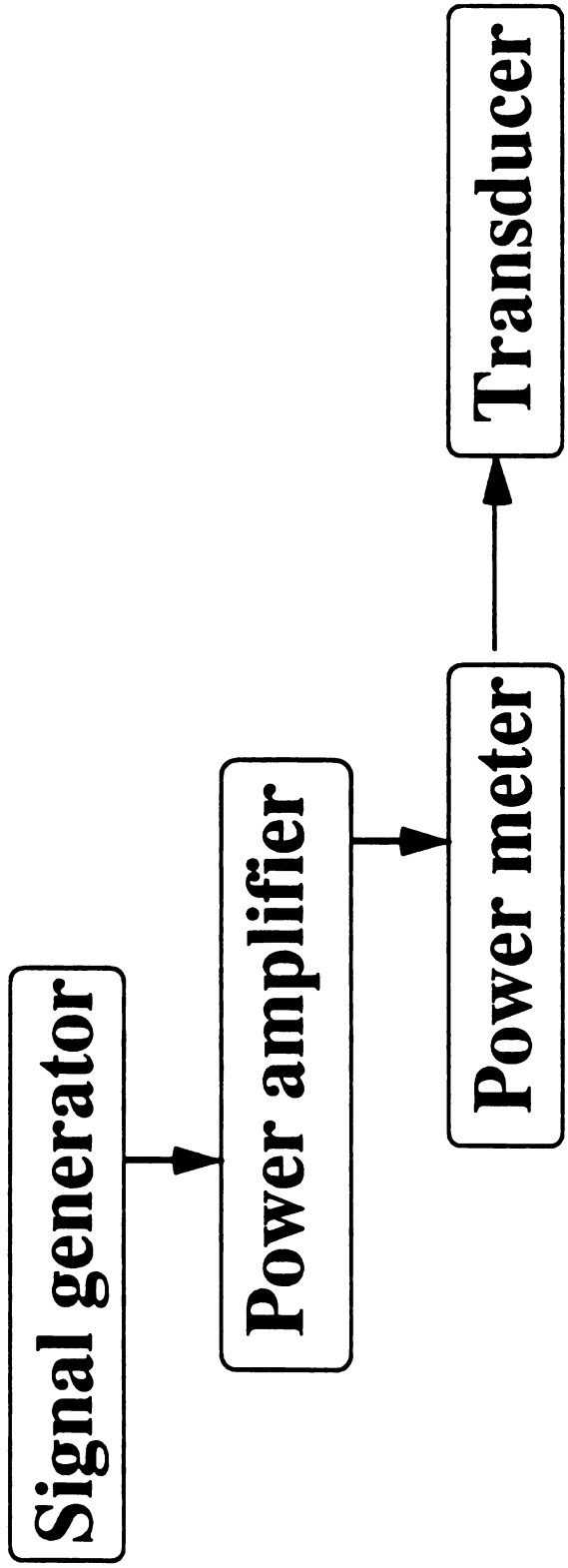

Figure 5.3 Experimental apparatus necessary for the generation of high frequency ultrasound.

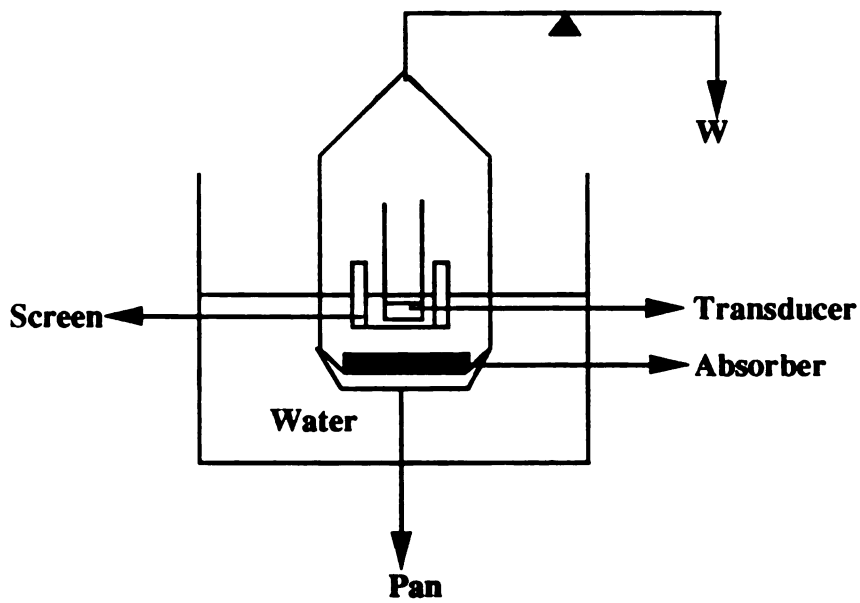

Figure 4.4. Experimental apparatus used for the measurement of acoustic power output. The ultrasound emitted by the transdurcer passes through the acoustically transparent screen (to eliminate acoustic streaming) before being absorbed by the "perfect absorber." The resulting force displaces the balance pan within the waterbath so that weight (W) has to be added to the counterbalance to restore the pan to its original position.

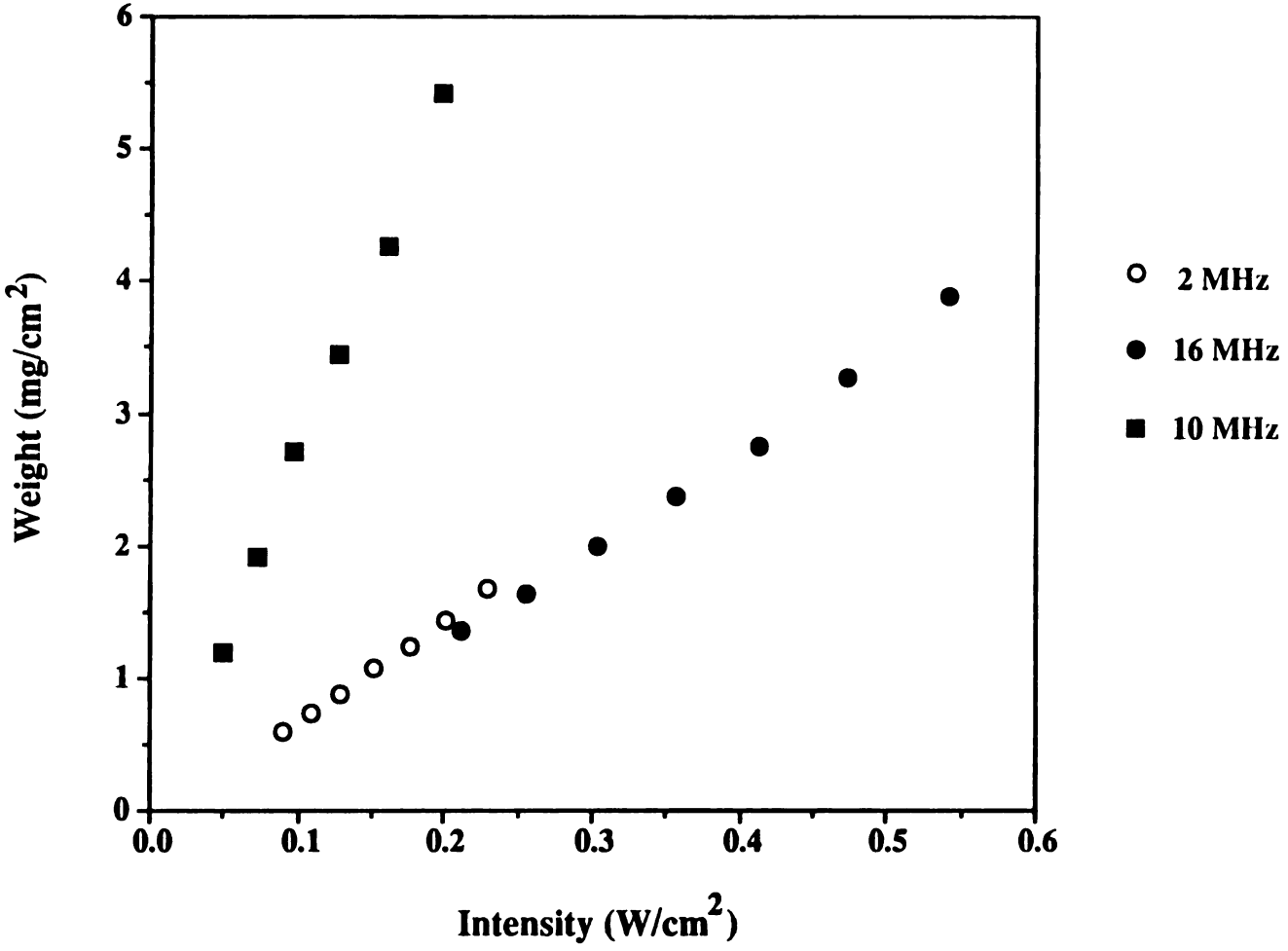

Figure 5.5 Radiation force measurements to determine the acoustic efficiency of the different transducers. The weight registered on the balance for a given electrical energy is plotted as a function of the input.

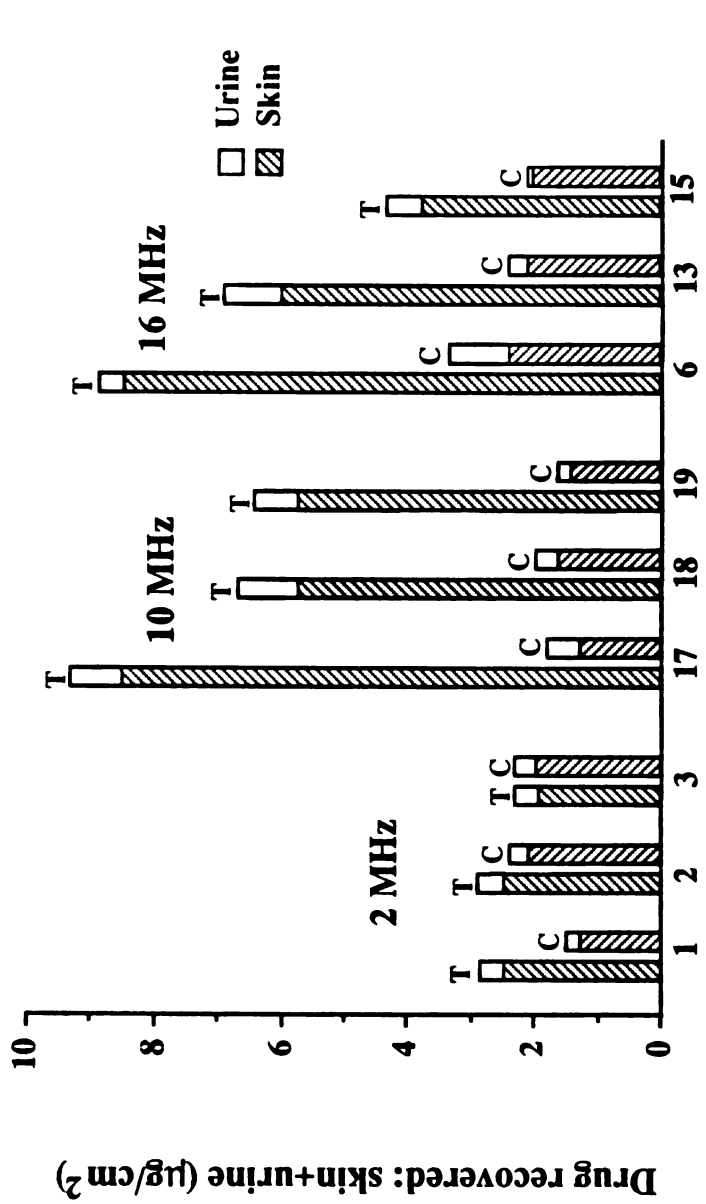

Figure 5.6 TDD of salicylic acid following 20 minutes of sonophoresis (T), using 2, 10 and 16 MHz frequencies, and passive diffusion (C). Paired t-test reveals that there is no significant difference between T and C when 2 MHz is used. However, there is a significant difference between T and C after sonophoresis using 10 MHz ($p \leq 0.03$) and 16 MHz ($p \leq 0.05$).

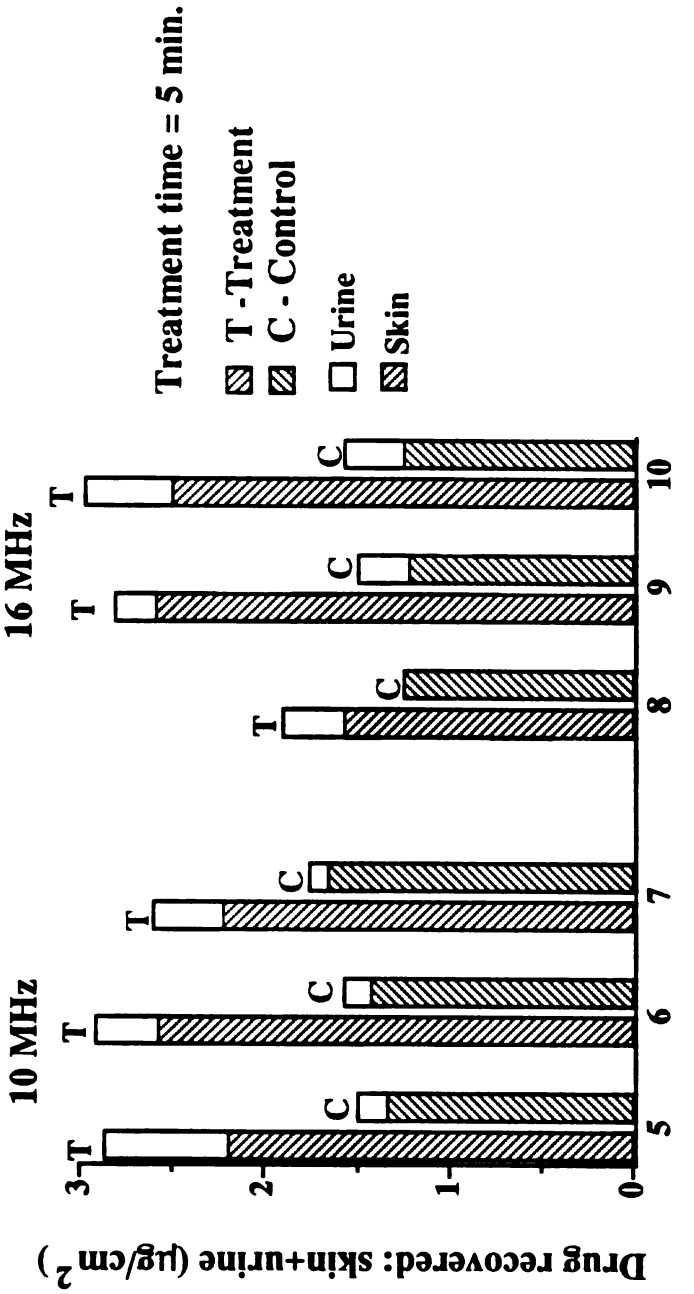

Figure 5.7 TDD of salicylic acid following (a) sonophoresis (at 10 and 16 MHz) for 5 minutes (T), and (b) passive diffusion (C). There is a significant difference between T and C for both the frequencies used (10 MHz, $p \leq 0.02$ and 16 MHz, $p \leq 0.04$). The effect of sonophoresis exposure time can be assessed by comparison with data in Figure 5.5.

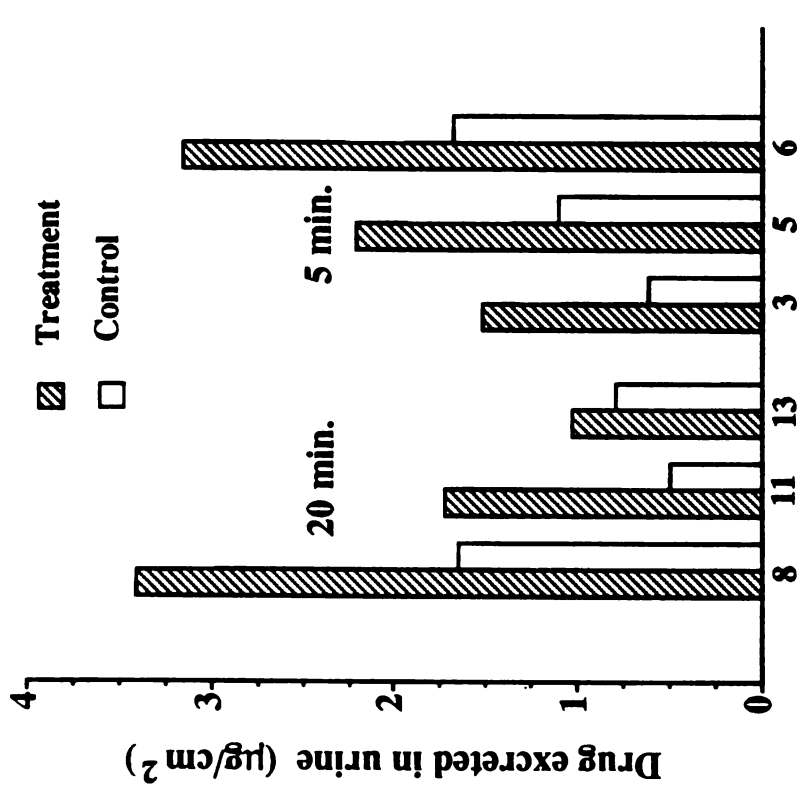

Figure 5.8 Total amount of salicylic acid absorbed transdermally (calculated from the radiaoactivity eliminated in the urine) following 20 and 5 minutes of sonophoresis at 16 MHz. A paired t-test reveals that there is a significant difference between treatment and control ($p \leq 0.08$).

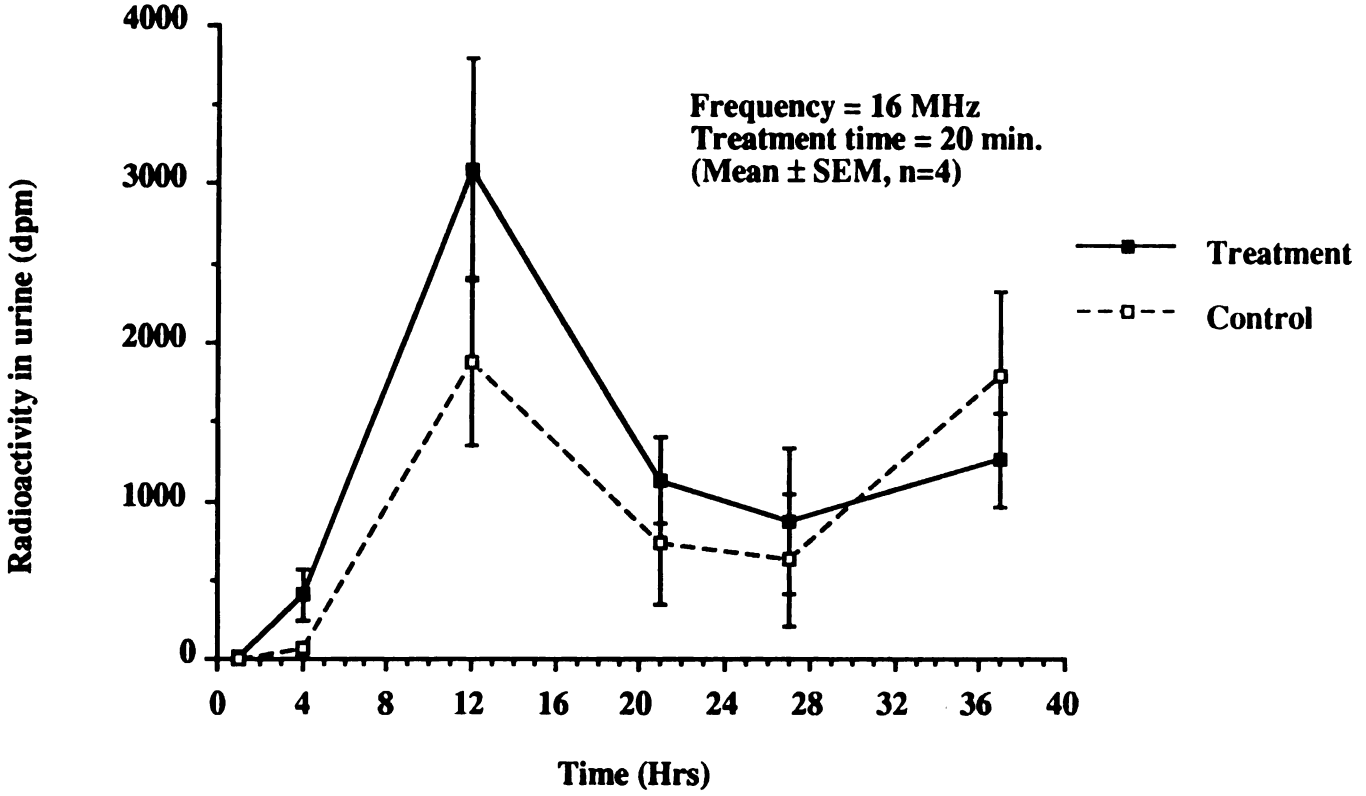

Figure 5.9a Radioactivity (mean ± SEM, n=3) eliminated in the urine, as a function of time, after sonophoresis at 16 MHz for 20 minutes (Fig. 5.8a) and 5 minutes (Fig. 5.8b). Different amounts of radiolabelled tracer were administered in the two experiments making direct, quantitative comparison inappropriate. However, in both cases, the total amount of radioactivity eleiminated post-sonophoresis is significantly greater ($p \leq 0.02$ for 5 min. treatment and $p \leq 0.05$ for the 20 min. treatment) than the control. Furthermore, the value at each time point is significantly different from the corresponding time point after passive diffusion ($p \leq 0.01$ for 5 min., and $p \leq 0.2$ for 20 min.)

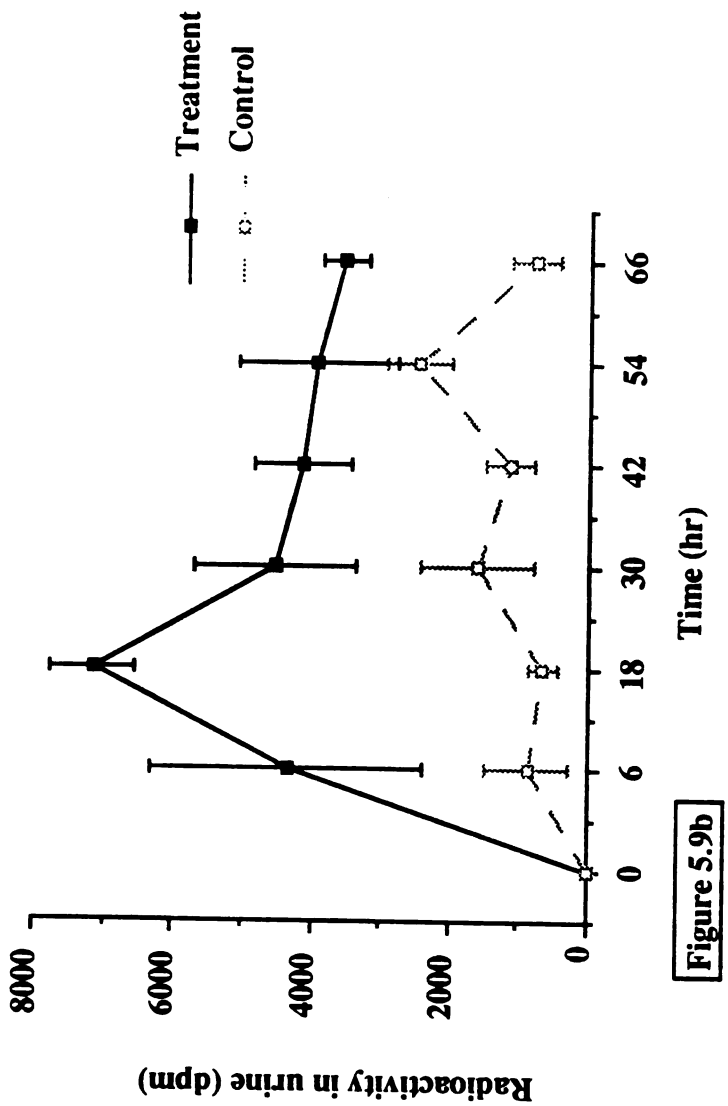
Treatment
Control
Radioactivity in urine (dpm)
8000
6000
4000
2000
0
0
6
18
30
42
54
66
Time (hr)

Figure 5.9b

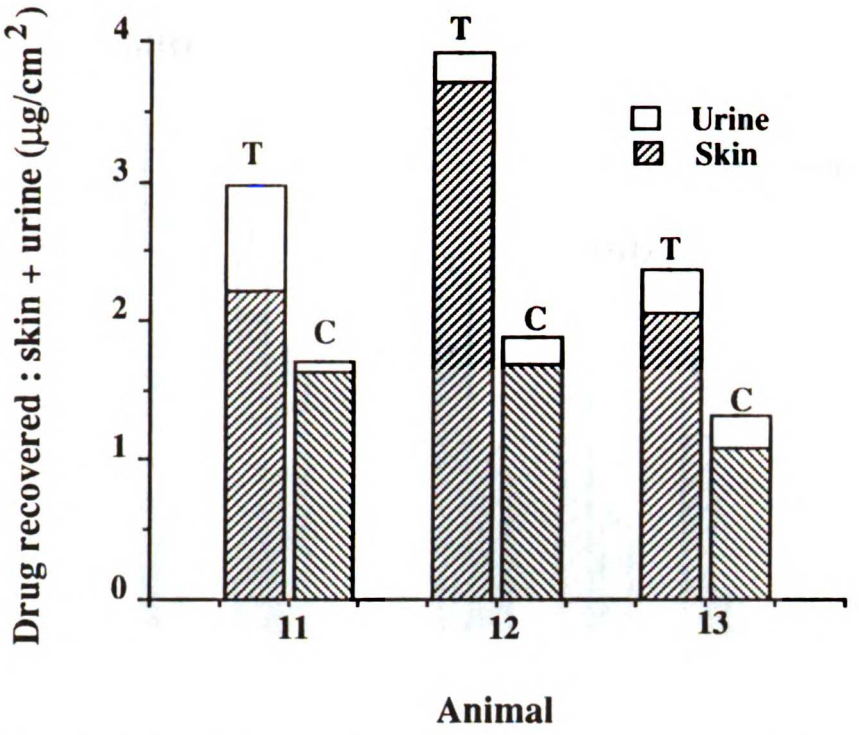

Figure 5.10 TDD of salicylic acid following (a) pre-treatment of the skin with ultrasound (16 MHz, 10 minutes) and then a 5 minute application of drug-containing gel (**T**), and (b) a 5 minute application of the same gel without ultrasound pre-treatment (**C**). Significantly more drug was delivered when the ultrasound pre-treatement was used ($p \leq 0.04$).

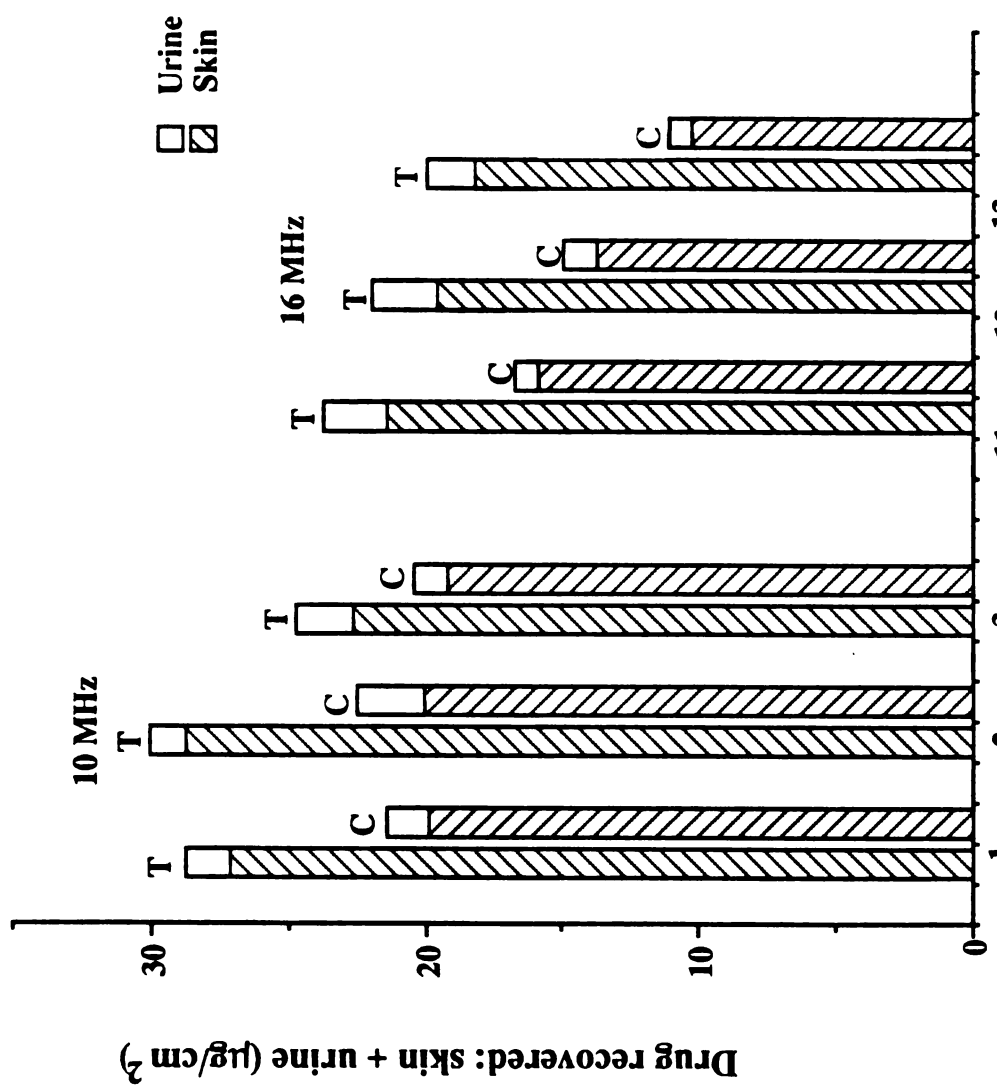

Figure 5.11 TDD of salicylic acid, delivered in its unionized form, following (a) sonophoresis (at 10 and 16 MHz) for 5 minutes (T), and (b) passive diffusion (C).

6. Sonophoresis: II. Examination of the Mechanism(s)

In Chapter 5, we showed that high frequency ultrasound, at low intensity (0.2 W/cm^2), can (1) increase transdermal drug flux, and (2) decrease percutaneous diffusional lag-times. In this chapter, we describe investigations to decipher the mechanism(s) that underlies the observed effects.

6.1 Ultrasound Effects on Skin

To comprehend the mechanism of sonophoresis, it was first necessary to demonstrate that ultrasound acted on the skin and not on the drug release process from the gel formulation used. We, therefore, measured drug efflux from the gel in the presence and absence of ultrasound and confirmed that ultrasound was not facilitating release of the drug from the gel (Figure 6.1). Furthermore, we also pre-treated the skin with ultrasound and evaluated TDD. In this case, prior exposure to ultrasound led to enhanced salicylic acid transport supporting the assumption that ultrasound was acting on the skin and not on the gel. Subsequent to these control experiments, we used transmission electron microscopy (EM) to track the skin permeation of an electron dense tracer (lanthanum nitrate (LN)). This allowed us to address two issues: (1) the permeation pathway of the diffusing molecule (LN) under the influence of ultrasound, and (2) the effect of ultrasound on skin morphology.

6.2 Thermal and Non-thermal Effects of Sonophoresis

The effects of ultrasound can be broadly classified into two categories: (1) thermal and (2) non-thermal. Thermal effects are easy to monitor, because they cause an increase in the temperature of the tissue under consideration. In contrast, non-thermal effects are difficult to assess and almost impossible to quantify. We have found that, under the conditions of our experiments, significant skin heating (>1°C) does not occur (Section

5.4). Theoretical calculations were consistent with these observations (see Section 4.5.1). Furthermore, the literature reports that temperature changes of more than 5°C are necessary to cause reasonable increases in skin permeability*[Potts and Francoeur, 1990; Knutson et al., 1988]*.

As described in Section 4.5.2, mechanical and cavitational phenomena constitute the major non-thermal effects. Mechanical effects become significant, if the cellular structures are of comparable dimensions to, or larger than, the wavelength of the ultrasound beam. Under these circumstances, the cells simultaneously undergo variable stresses and strains leading to mechanical fatigue. However, in the frequency range which we have used, the corneocyte dimensions are much smaller than the wavelength of the ultrasound beam. For example, the wavelength of a 10 MHz beam in water equals 0.01 cm (100 μm), whereas the thickness of a typical corneocyte is about one μm. It is highly unlikely, therefore, that the cellular structures of the SC, (nor, indeed, the rest of the skin) are subject to uneven mechanical stresses, which could lead to "fatigue" and cell rupture. We then considered the possibility that cavitational effects play a role in sonophoresis.

Cavitation is the oscillatory behavior of highly compressible bodies, such as gas, vapor-filled "bubbles", or "cavities", (so-called micronuclei) which are powered by and, therefore, extract energy from the incident acoustic field. Some of this energy (about 10%) is re-radiated as an acoustic wave; the remainder, however, is transformed into other forms of energy and may appear as heat (resulting in the production of highly energetic, short-lived chemical species), or as shock waves or hydrodynamic shear fields which can easily disrupt biological tissues. The occurrence of cavitation in a medium is crucially dependent upon the number and availability of these micronuclei, the intensity and frequency of the ultrasound wave and a number of additional variables. Furthermore, cavitation occurs randomly, and is more difficult to

study, therefore. There are a few *in vitro* studies which report the effects of ultrasound in the MHz range on human platelets. Miller and co-workers *[Miller et al., 1978, 1979a]*, for example, showed that these cells aggregate when exposed to ultrasound at intensities < 100 mW/cm^2. However, the cavitational effects on skin caused by high frequency ultrasound have not been examined. Even in the case of diagnostic ultrasound, which has been used for decades, the possible adverse effects of cavitation remain unclear *[American Institute of Ultrasound in Medicine. Bioeffects Report, 1988]*. To our knowledge, we present here the first examination of non-thermal (cavitational) effects caused by high frequency ultrasound on skin *in vivo*.

We have used EM to address the issues discussed above. It has been found that: (1) The tracer (LN) does not permeate the skin by passive diffusion; whereas, under the influence of ultrasound, it traverses the skin along the intercellular route. (2) Tracer is delivered through the epidermis to the dermis, even after only 5 minutes of ultrasound treatment. (3) The SC and the cells of the epidermis do not appear to be adversely affected by either 5 and 20 minutes of ultrasound treatment at 10 MHz frequency, or 5 minutes of sonophoresis at 16 MHz. However, 20 minutes treatment with ultrasound at 16 MHz resulted in altered cellular morphology compared to the no-sonophoresis control.

6.3 Methods

For all studies, control experiments were conducted in a manner identical to the treatment protocol, except that the transducer was not activated.

6.3.1 Release Experiments

The gel (preparation described in Section 5.2) was applied as a thin film onto the transducer surface, which was then immersed in 20 ml of well-stirred water. Post-

immersion 0.2 ml samples were withdrawn periodically and assayed. Quadruplicate measurements were made in both treatment and control experiments.

6.3.2 Electron Microscopy *[Elias and Brown, 1980]*

Lanthanum nitrate (LN) solution at pH 7.6 was applied topically and the site was then immediately treated with 10 or 16 MHz ultrasound (at 0.2 W/cm^2 intensity) for 5 or 20 minutes. The LN solution was an adequate ultrasound coupling medium, and the penetrated lanthanum served as an electron dense tracer for microscopic visualization. Unlike the permeation experiments, in which control and treatment procedures were performed on the same animal to minimize inter-subject variability, for the EM work different animals were used for the treatment and control procedures. After the exposure period, full thickness skin was biopsied using a 5 mm diameter punch. The excised skin was then carefully cut into smaller pieces (< 0.5mm), which were fixed and processed for electron microscopy as follows :

(1) immersed in Karnovsky's fixative for 1 hr at 25°C;

(2) left overnight at 4°C;

(3) washed with 0.1M cacodylate buffer;

(4) post-fixed in buffered 1% OsO_4.

After fixation, samples were dehydrated in graded ethanol solutions and embedded in an Epon-epoxy mixture. Thin sections (600 - 800 nm), cut using an MT2B ultra microtome, were examined (either unstained or after double staining with uranyl acetate and lead citrate) with an electron microscope (model 10A; Carl Zeiss, Inc., Thornwood, NY) operated at 60kV .

6.4 Results

6.4.1 Effect of Ultrasound on Drug Release from the Gel.

Figure 6.1 shows the drug release profile from the gel with and without ultrasound. There is no statistically significant difference between the release profiles, showing that ultrasound is not facilitating drug release from the gel.

6.4.2 EM Observations

6.4.2.1 Controls

Controls show normal epidermal morphology and an intact permeability barrier, represented by a compact SC, with the secreted contents of lamellar bodies filling the intercellular domain at the stratum granulosum (SG) - SC junction (Figure 6.2). There is no evidence of tracer permeation into the intercellular domains of SC, or into the nucleated cell layers below (SG). Basal cells show abundant ribosomes, mitochondria (M), keratin filaments (KF), and hemidesmosomes (HD) at the zone of contact with the basement membrane (BM). Intercellular spaces are prominent between the adjacent cells of stratum basale (Figure 6.3). Superficial dermis shows collagen filaments in both longitudinal and cross sectional profile, and is devoid of any tracer particles.

6.4.2.2 Ultrasound-Exposed Skin

In animals treated with ultrasound for 5 minutes, abundant precipitates of the tracer appear within the superficial dermis in the zona lucida (above the dense zone) of the basement membrane, and in the intercellular spaces of stratum basale (Figures 6.4 and 6.5). The epicutaneously applied tracer permeates through the intercellular route (Figures 6.4-6.6). Thus, a short ultrasound-treatment of only 5 minutes results in considerable percutaneous delivery of LN with no obvious alterations in skin

morphology. However, longer exposure (20 minutes) results in damage of SG and basal cells (Figures 6.6-6.8). Changes are not apparent in the upper SC, though, where the corneocytes appear normal and undamaged. The tracer can be seen within the intercellular domains (Figure 6.6 insert). The tracer is clearly present in the superficial dermis; compared to the discrete distribution of electron dense material after ultrasound treatment for 5 minutes, the longer exposure to sonophoresis leads to an apparent aggregation of the tracer.

Ultrasound treatment at 10 MHz for 5 minutes also drives the tracer into the dermis (Figure 6.9). Furthermore, similar to the 16 MHz results, the tracer concentrates at the epidermal-dermal junction.

Figures 6.10 and 6.11 are unstained sections which confirm that the electron dense particles observed in Figures 6.4-6.10 are due to the tracer and are not the result of a staining artifact.

6.5 Discussion

Release experiments: Although the acoustic impedance of water (1.56×10^5 g/cm^2/sec) differs from that of skin (1.59×10^5 g/cm^2/sec), the values are sufficiently similar that the use of water as the receiver medium in the release experiments is a close approximation of the experimental situation *in vivo*. We believe, therefore, that the absence of effect of ultrasound on drug release is relevant to the animal studies. Furthermore, because pre-treatment of the skin with ultrasound increases TDD, the action of sonophoresis on the skin is unequivocal [see Section 5.2.3].

Tracer studies: While the EM experiments can reveal pathways and extent of permeation, the relevance of LN transport to the diffusion of therapeutically active molecules can be questioned. Nevertheless, the approach is justified because there are

few direct methods available to visualize permeation pathways in skin. Confocal microscopy is one approach of promise, but awaits complete validation *[Cullander et al., 1990]*. Autoradiography is an alternative *[Schaefer et al., 1978]*, and, similar to EM, involves mechanical sectioning of the skin post-treatment. However, autoradiographic sections are thicker than EM sections, complicating the quantification of the tracer in the different strata of the skin.

A significant observation is that the tracer penetrates to the dermis after only five minutes of sonophoresis. Lanthanum does not permeate by passive diffusion in the control experiments. Parenthetically, we also note that, in an unrelated study, it was found that iontophoresis of LN into hairless mouse skin *in vivo* drove the tracer only to the SG+. It is quite remarkable, therefore, that sonophoresis for 5 minutes can deliver LN into the dermal tissue. We believe that this observation is unique.

The EM studies locate the tracer in the intercellular spaces of the epidermis and the dermal-epidermal junction. This observation supports the hypothesis that the permeation pathway is primarily intercellular. Careful inspection of Figures 6.4 - 6.11 also reveals that the tracer is not uniformly distributed. Why this should be the case is unknown at this time.

The effect of ultrasound on the cellular structures of the skin requires comment. 5-minutes of sonophoresis, at either 10 or 16 MHz, did not appear to alter cellular morphology. However, 20 minutes of sonophoresis at 16 MHz resulted in significant effects. Cavitation (described under Section 6.2) may be involved in this adverse finding. This suggestion is based upon Figures 6.9 and 6.10, in which the tracer appears to be aggregated (compared to the discrete distribution of particles seen in Figure 6.4 (5 minutes, 16 MHz)). The aggregation of tracer following the extended

---

+ Personal communication with Dr. G. Menon

treatment at 16 MHz (in both micrographs, the tracer appears to line the surface of imaginary spheres) could be explained by a mechanism described as follows. Assume the presence of bubbles (micronuclei) in the intercellular spaces. It is plausible that 20 minutes of continuous wave ultrasound causes this bubble to grow (cavitation). The tracer in this region that is initially dispersed, can now be pushed towards adjoining cell structures by bubble expansion. Finally, when the bubble collapses, the tracer may be in close proximity to the surface of the adjacent structures (as suggested by Figures 6.7 and 6.8). Concomitantly, the repeated expansion and self-destruction of micronuclei in the skin due to cavitation may induce enhanced permeation of the permeant.

The above discussion leads us to questions of reversibility, and the adverse effects of different frequencies and exposure times. Are the changes induced by ultrasound reversible? If they are, for how long does the perturbation last? These issues remain unanswered and must form the basis of future work.

6.6 Conclusions

In this study, we have examined the effects of ultrasound on the permeation of the electron-dense tracer, lanthanum nitrate. The results reveal that 5 minutes of sonophoresis, at a frequency of 10 or 16 MHz, delivers the tracer through the epidermis into the dermis, a remarkable achievement. The penetration pathway of the tracer appears to be intercellular. Longer exposure of the skin to high frequency ultrasound (20 minutes, 16 MHz) resulted in structural alterations of the stratum granulosum and stratum basale cells.

References

American Institute of Ultrasound in Medicine. Bioeffects Report, 1988, **Journal of Ultrasound Medicine,** 7: S1-S38.

Cullander, C., Menon, G.K., Guy, R.H., and Elias, P.M.,1990, In situ Visualization of the Lamellar Body Secretory System by Confocal Microscopy, **Journal of Investigative Dermatology,** 94: 517.

Elias, P.M., and Brown, B.E., 1987, The Mammalian Cutaneous Permeability Barrier, **Laboratory Investigation,** 39: 574-583.

Knutson, K., Potts, R.O., Guzek, D.B., Golden, G.M., McKie, J.E., Lambert, W.J., and Higuchi, W.I., 1986, Macro- and Molecular Physical-chemical Considerations in Understanding Drug Transport in the Stratum Corneum, **Journal of Controlled Release,** 2: 67-87.

Miller, M.W., Kaufman, G.E., Cataldo, F.L., and Cartensen, E.L., 1976, Absence of Mitotic Reduction in Regenerating Rat Livers Exposed to Ultrasound, **Journal of Clinical Ultrasound,** 4: 169-172.

Miller , M.W., 1978, Comparison of Micronuclei Induction for X-ray and Ultrasound Exposures of *vicia fibia* Root Meristem Cells, **Ultrasound in Medicine and Biology,** 4: 263-267.

Miller, D.L., Nyborg, W.L., and Whitcomb, C.C., 1979, Platelet Aggregation Induced by Ultrasound Under Specialized Conditions *in vitro*, **Science,** 205: 505-507.

Potts, R.O., and Francoeur, M.L., 1990, Lipid Biophysics of Water Loss through the Skin, **Proceedings of the National Academy of Sciences,** 87: 3871-3873.

Schaefer, H., Stuttgen, G., Zesch, A., Schalla, W., and Gazith, J.,1978, Quantitative Determination of Percutaneous Absorption of Radiolabeled Drugs *In Vitro and In Vivo* by Human Skin, **Current Problems in Dermatology,** 7: 80-94.

Figure Legend

Figures 6.2: Electron micrographs of control skin, i.e., that which has not been exposed to ultrasound. Figure 6.2 shows the upper layers of the skin, the SC and the stratum granulosum (SG) cells below the SC-SG junction. In the SC, the dark structures are the corneocytes and the electron-lucent regions are the intercellular lipids between the corneocytes. The keratohyalin of the SG appears as patchy dark regions. Note the compact packing of the intercellular lipids and the unaltered cellular morphology. (x 16,000)

Figure 6.3: Electron micrograph showing the basal layer of the skin, the epidermal-dermal junction, and collagen bundles in the dermis. The collagen is arranged in bundles, which are seen in cross-section as uniform rods. (x 24,000)

Figures 6.4 and 6.5: Electron micrographs of the excised skin after 5 minute treatment with ultrasound at 16 MHz frequency. Figure 6.4 shows the tracer as discrete electron dense particles (i) between a basal cell (BC) and the basement membrane (BM) zone, and (ii) within the dermis (D) (x 20,000). Figures 6.5 (x 13,600) indicates that the tracer has traversed the epidermis and can be found in between the cells of the stratum basale. Furthermore, note that the tracer is more abundant in the epidermis than in the dermis (insert- x 30,000). The insert (x 28,000) in Figure 6.5 also helps us to distinguish between the appearance of collagen and lanthanum in an electron micrograph.

Figure 6.6: EM (x 38,000) showing alterations in the cellular morphology after a 20 minute treatment with 16 MHz ultrasound at 0.2 W/cm^2 intensity (compared to the unaltered cellular morphology (Figures 6.2 and 6.3- controls)). Again, the tracer is observed only between the cells. Insert shows unaltered morphology of the corneocytes.

Figure 6.7: EM showing the presence of the tracer in large aggregates past the basal lamina.

Figure 6.8: Electron micrograph of the dermal tissue below the basal lamina. Similar to Figure 6.7, dense aggregates of the tracer are observed in the expanded spaces between the basal cells and the collagen bundles in the dermis.

Figure 6.9: 10 MHz ultrasound treatment also drives the tracer deep into the dermis. However, the tracer is less abundant than that observed after 16 MHz treatment.

Figures 6.10 and 6.11: Electron micrographs of unstained specimens after 5 minutes of 16 MHz ultrasound treatment at $0.2W/cm^2$. This confirms that the observed electron dense material in the earlier micrographs is the tracer (lanthanum) and not a staining artifact.

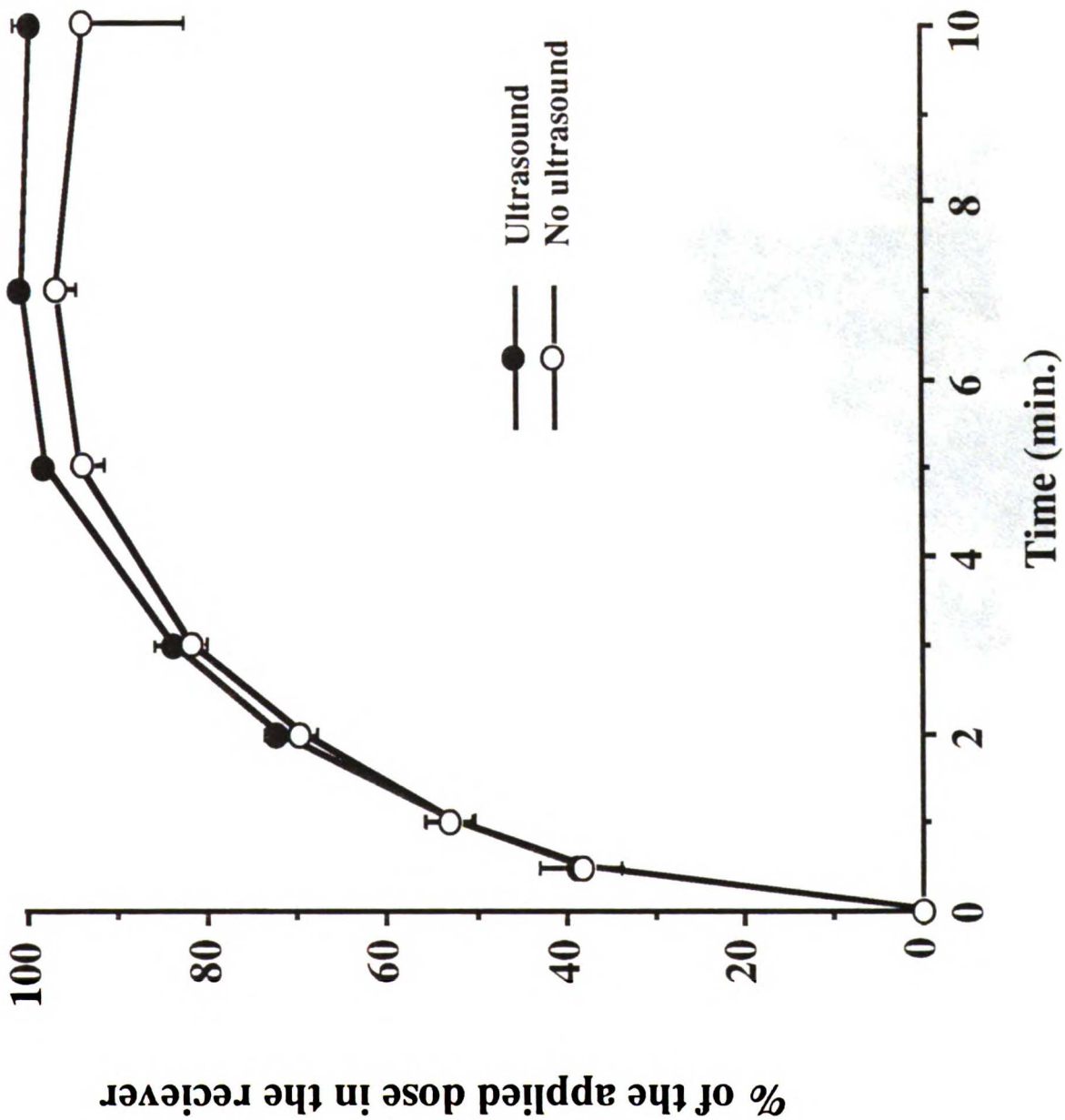
% of the applied dose in the reciever
100
80
60
40
20
0
0
2
4
6
8
10
Time (min.)
Ultrasound
No ultrasound

Figure 6.2

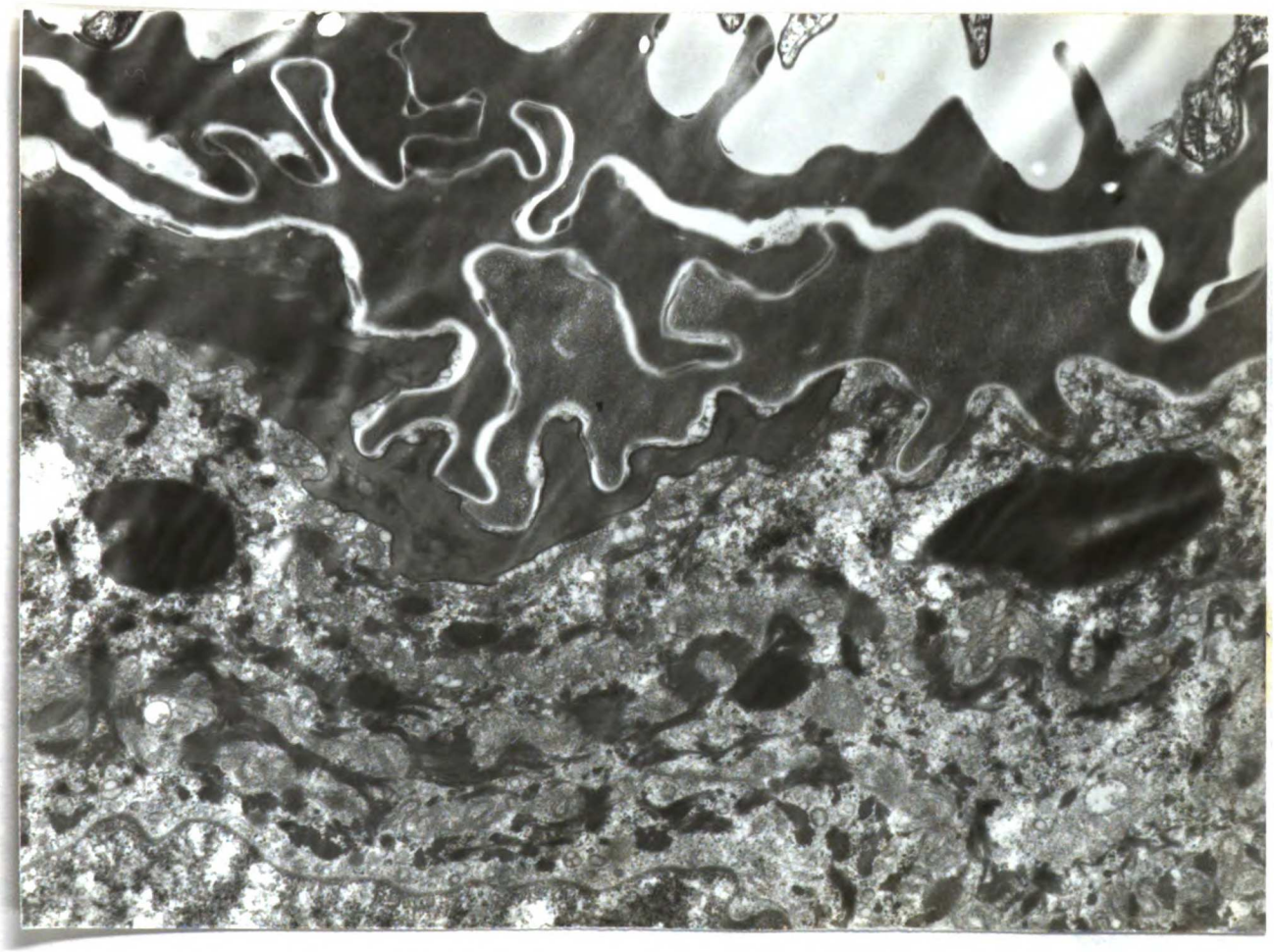

Figure 6.3

Figure 6.4

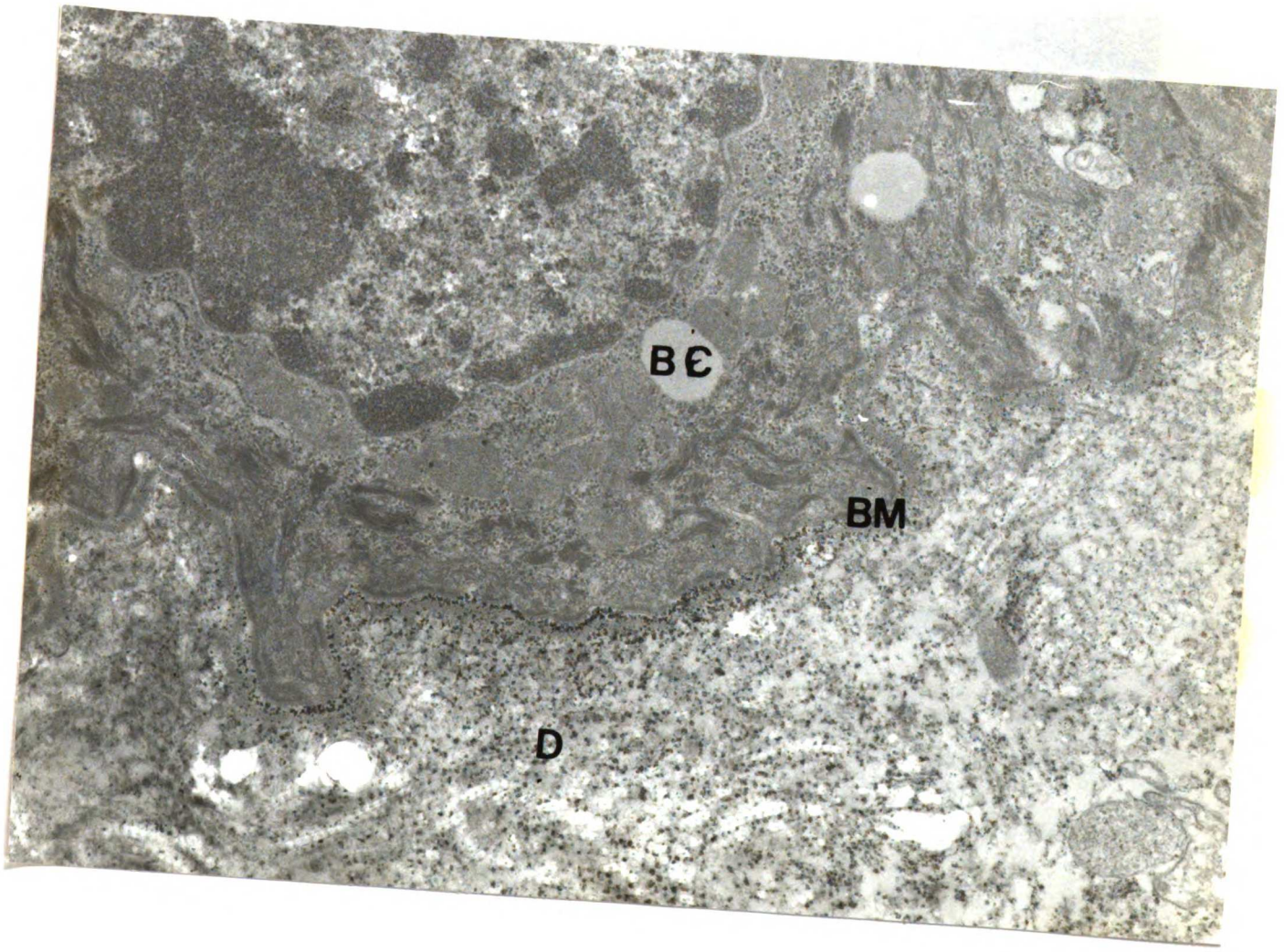

Figure 6.5

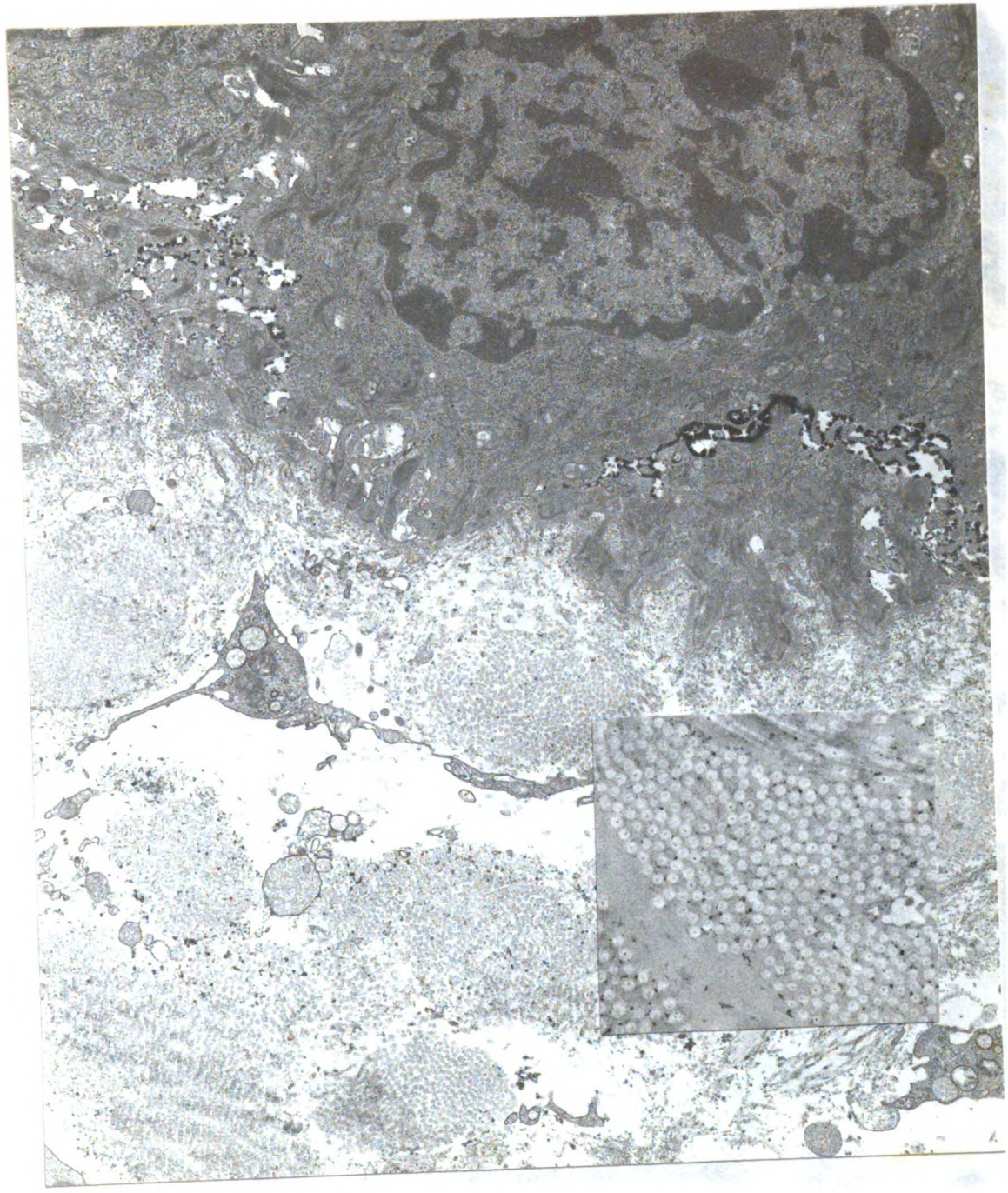

Figure 6.6

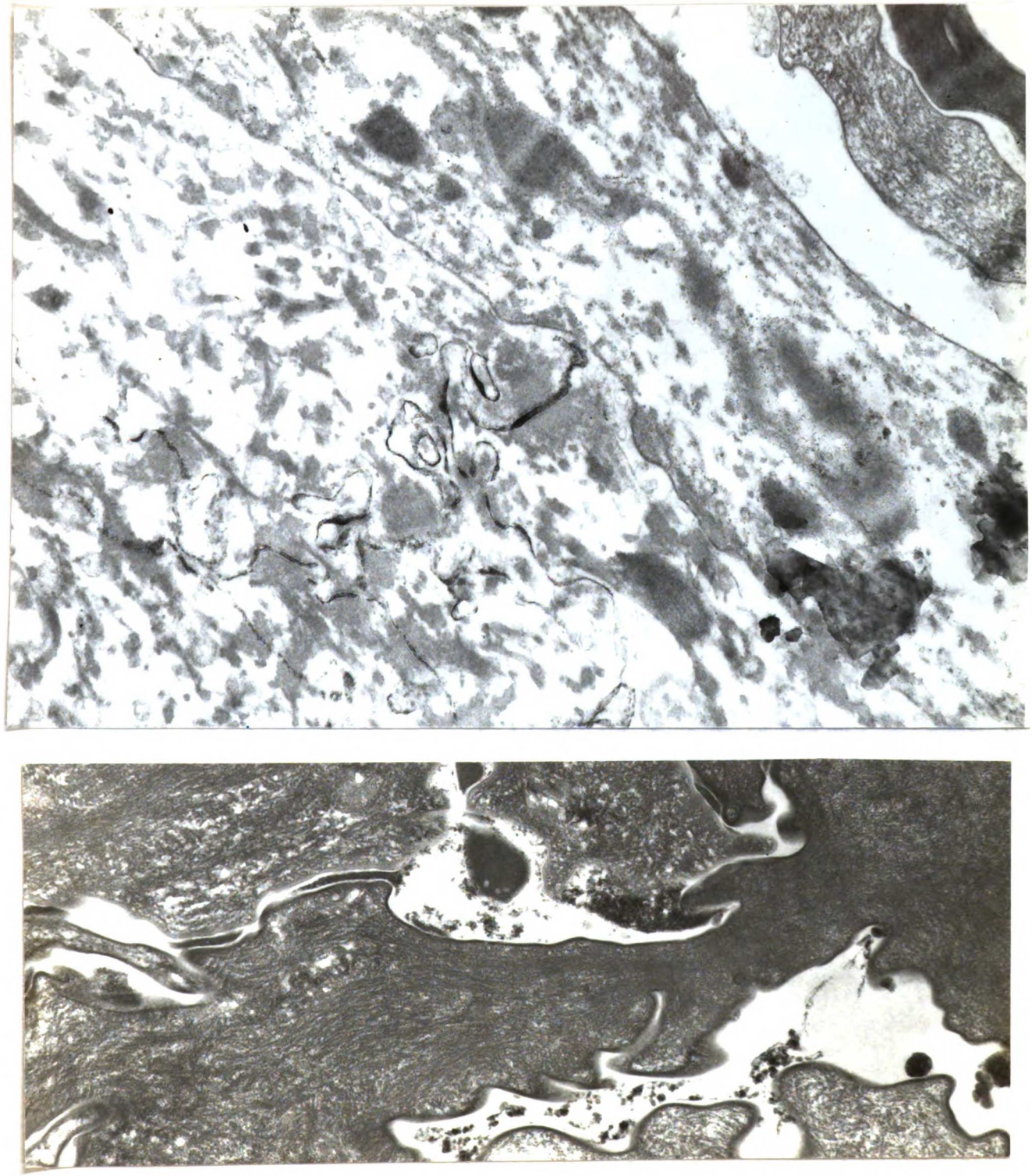

Figure 6.7

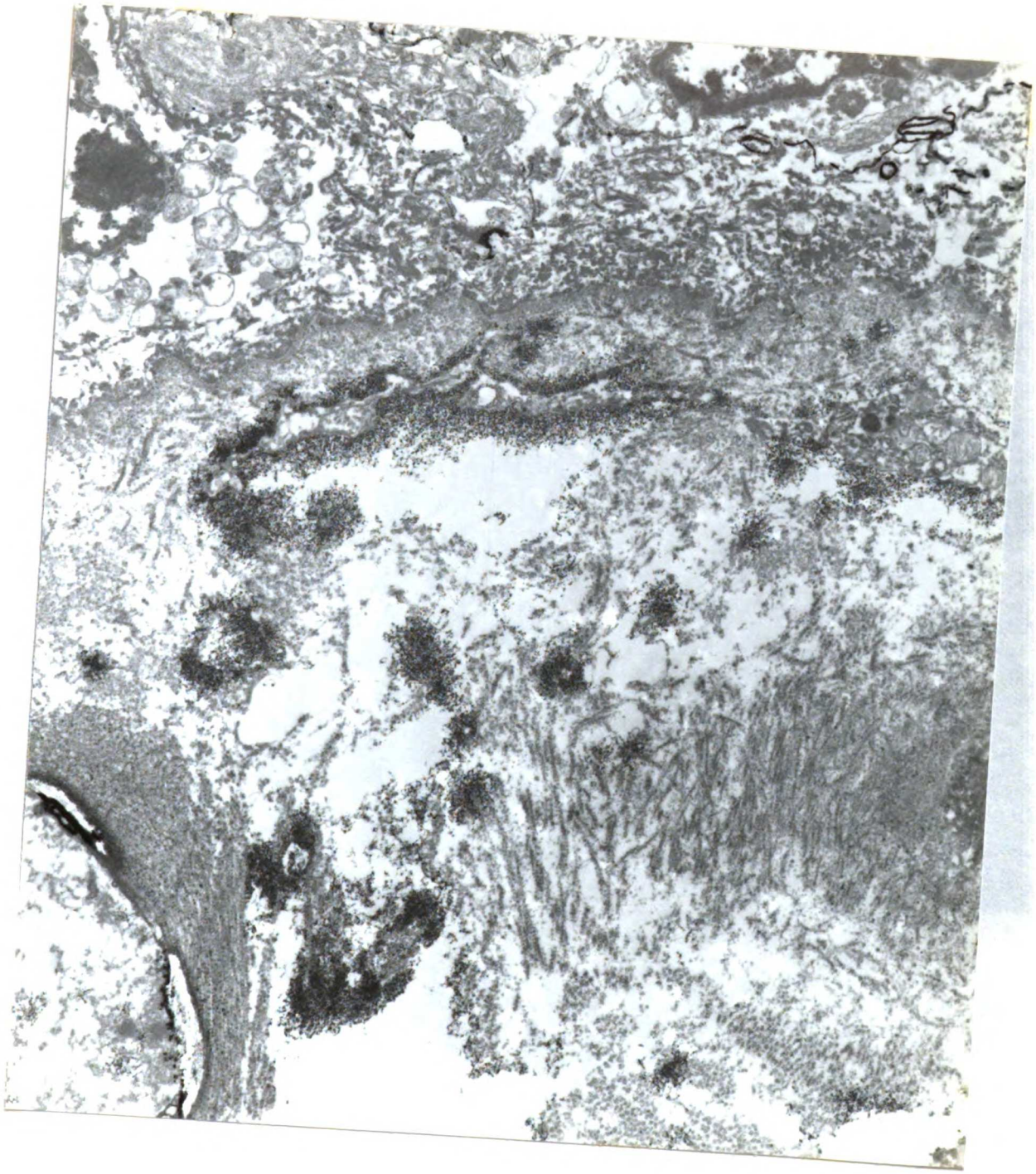

Figure 6.8

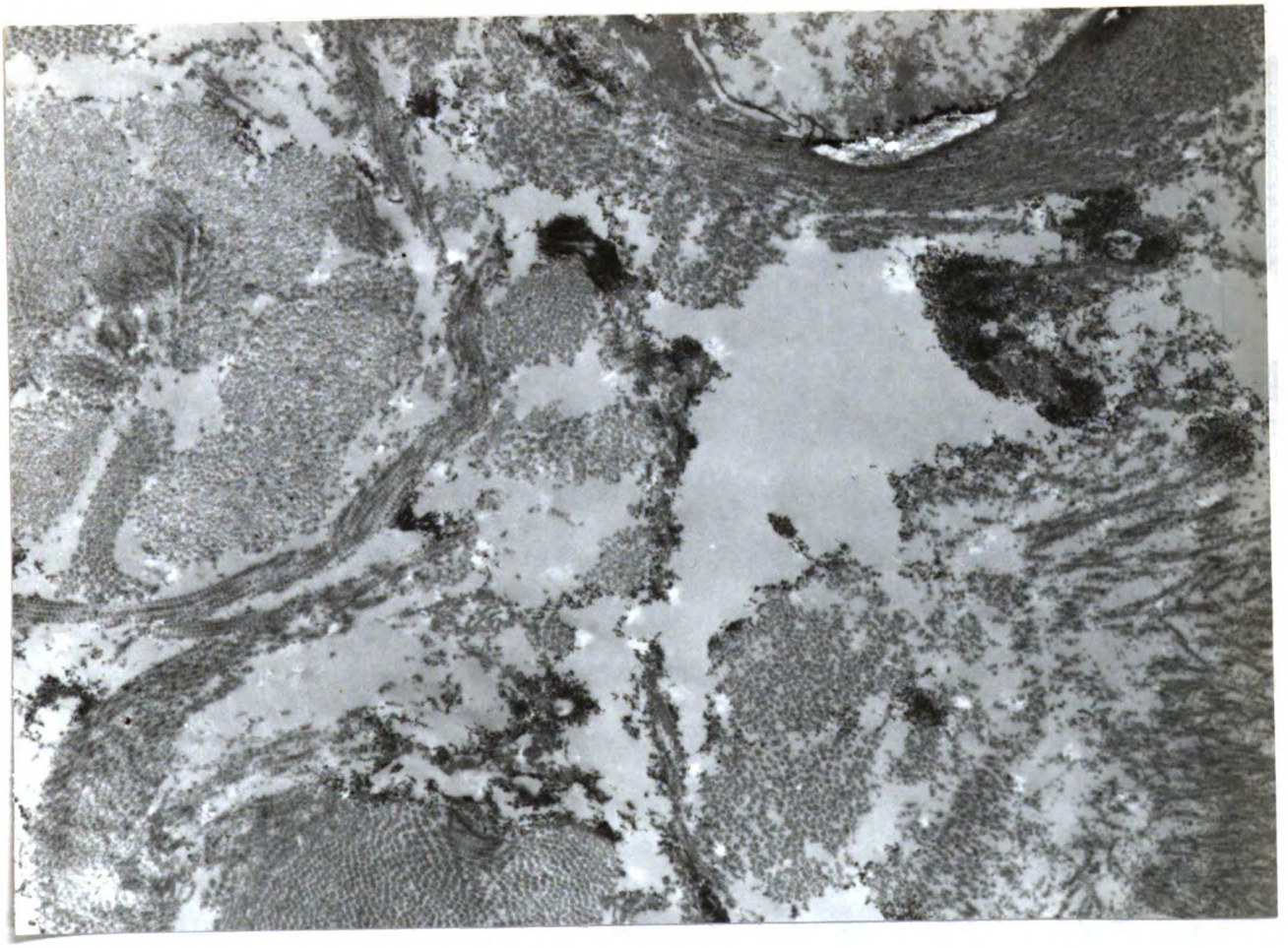

Figure 6.9

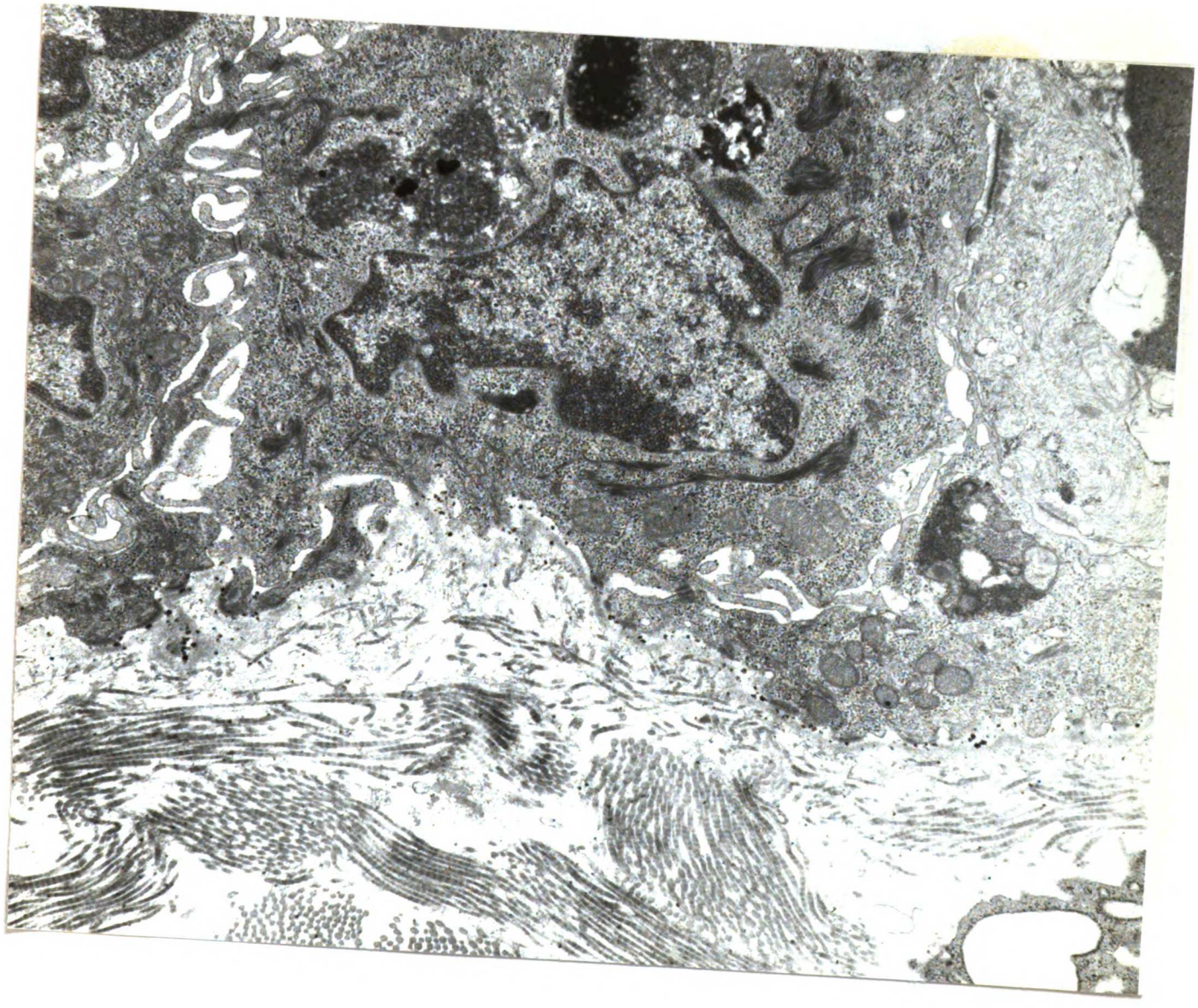

Figure 6.10

Figure 6.11

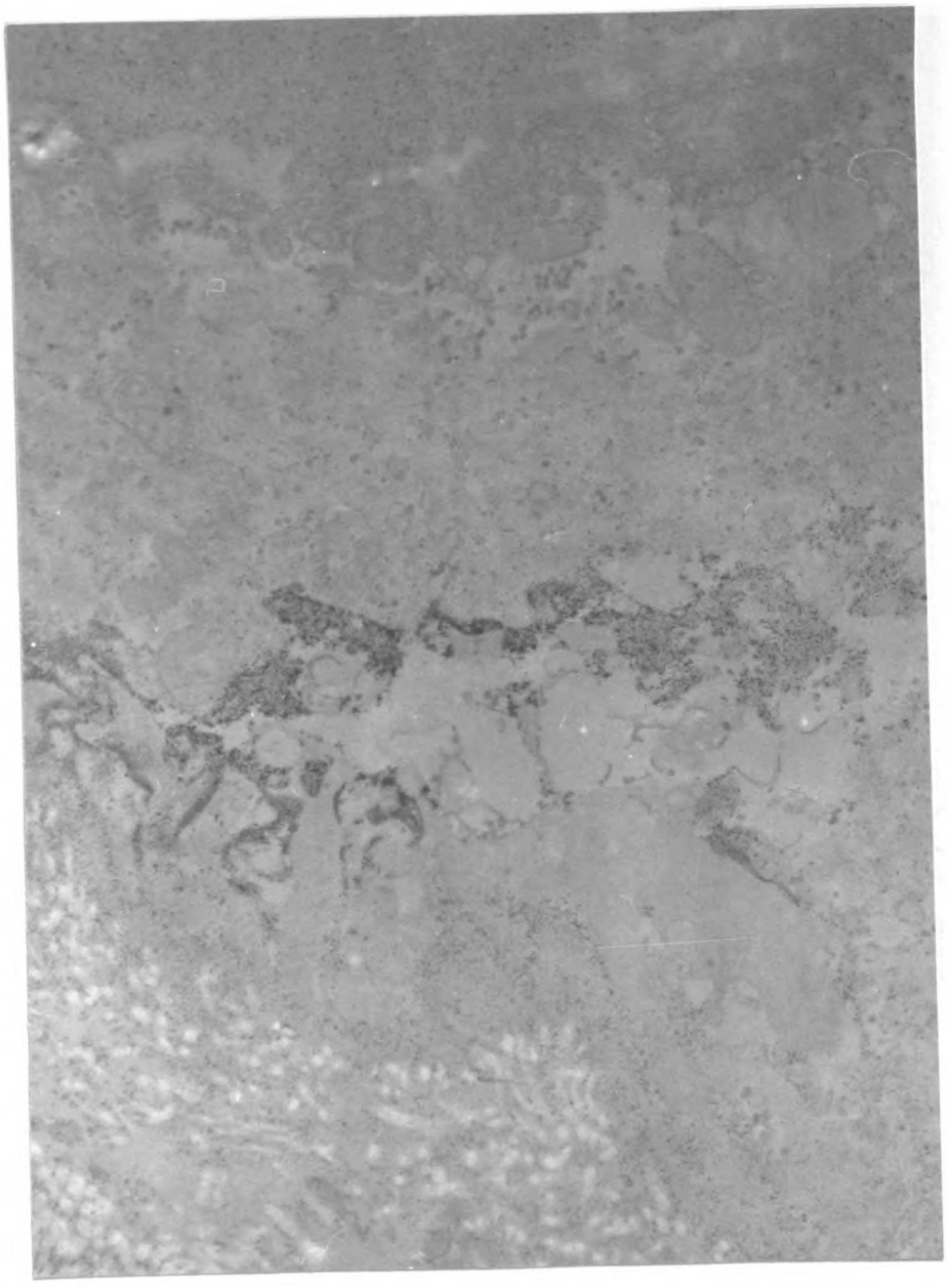

FOR REFERENCE

NOT TO BE TAKEN FROM THE ROOM

BRODART CAT. NO. 23 012

PRINTED IN U.S.A.